Electronic Supplementary Information

Copper(II) and Zn(II) Complexes of Mono- and Bis-(1,2,3-triazole)-substituted Heterocyclic Ligands

Natalija Pantalon Juraj,[a] Marko Krklec,[a,b] Tiana Novosel,[a,b] Berislav Perić,[a] Robert Vianello,[*,a] Silvana Raić-Malić[*,b] and Srećko I. Kirin[*,a]

[a]Ruđer Bošković Institute, Zagreb, Croatia

[b]Faculty of Chemical Engineering and Technology, University of Zagreb, Zagreb, Croatia

E-mail: Robert.Vianello@irb.hr, sraic@fkit.hr, Srecko.Kirin@irb.hr

Content:

Synthesis

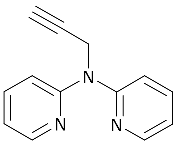

1

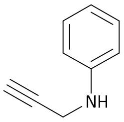

2

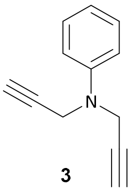

3

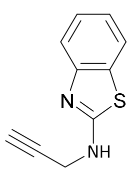

4

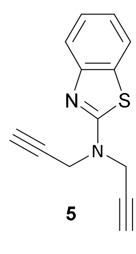

5

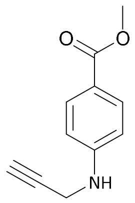

6

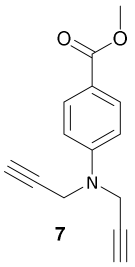

7

Figure S1. Prepared alkynes **1**-**7**.

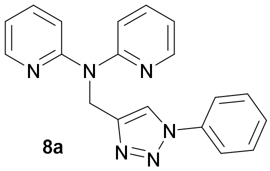

8a

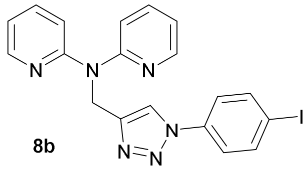

8b

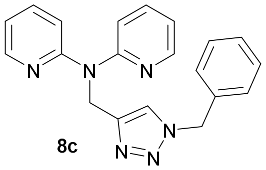

8c

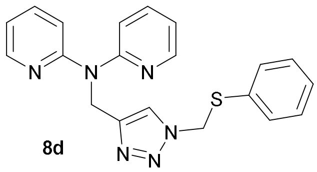

8d

Figure S2. Prepared mono-1,2,3-triazoles **8a**-**8d**.

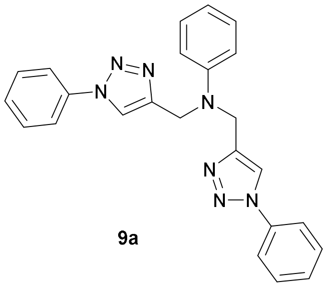

9a

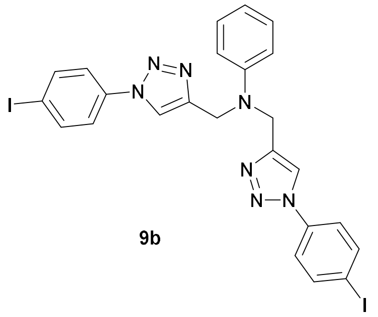

9b

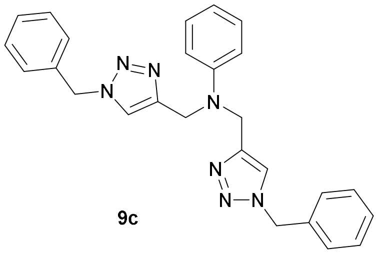

9c

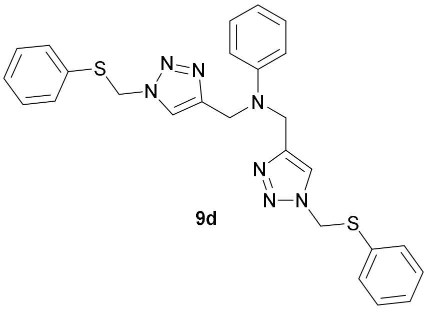

9d

Figure S3. Prepared bis-1,2,3-triazoles **9a**-**9d**.

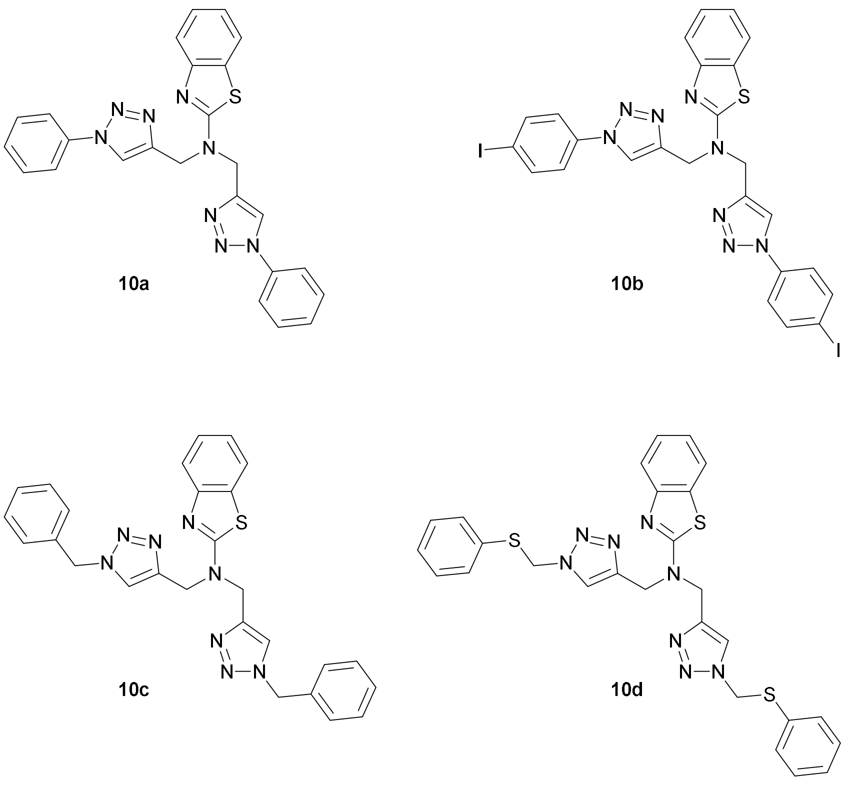

10a **10b** **10c** **10d**

Figure S4. Prepared bis-1,2,3-triazoles **10a**-**10d**.

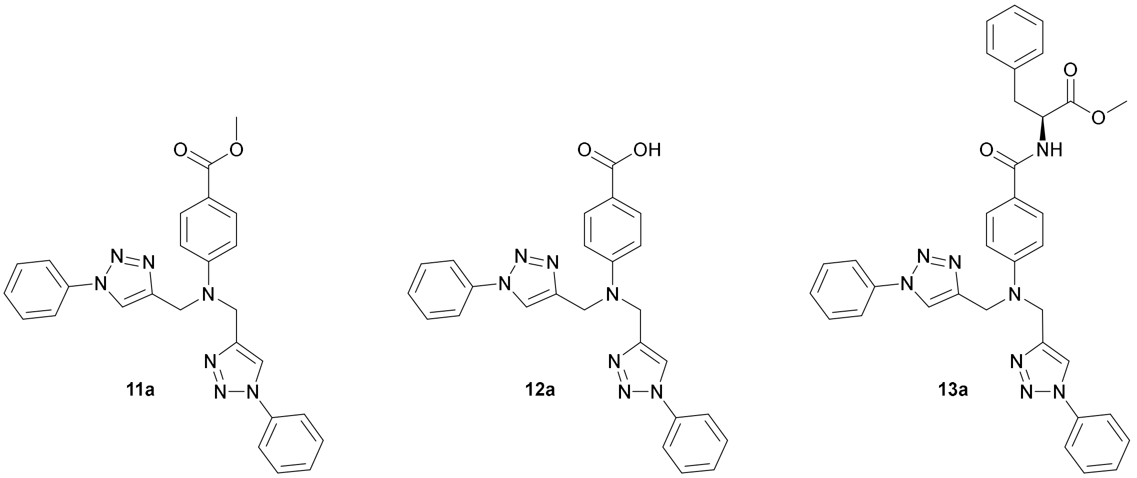

11a **12a** **13a**

Figure S5. Prepared ester **11a**, carboxylic acid **12a** and bioconjugate **13a**.

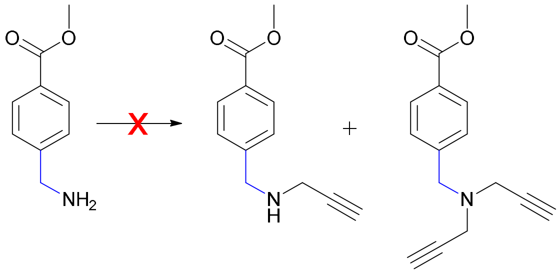

Figure S6. Propargylation reaction of aliphatic amine Methyl-4-(aminomethyl)benzoate gave a significantly lower yield than with the corresponding aromatic amine.

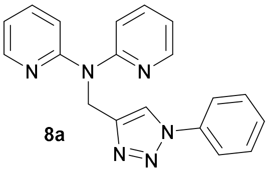

8a

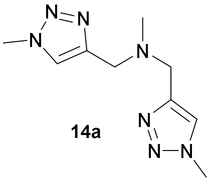

14a

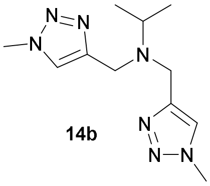

14b

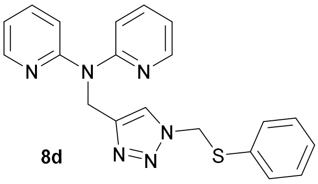

8d

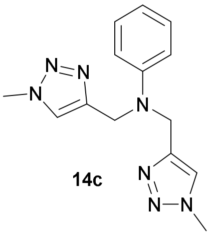

14c

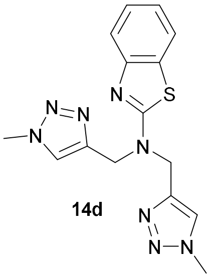

14d

Figure S7. Structures of ligands **8a**, **8d** and **14a**-**14d** used in calculations.

Crystallography

Table S1. Experimental data for X-ray diffraction studies (part 1).

	10a	**10c**	**8a$_{Cu}$**
Formula	$C_{25}H_{20}N_8S$	$C_{27}H_{24}N_8S$	$C_{38}H_{32}B_2CuF_8N_{12}$
F_w (g mol^{-1})	464.55	492.60	893.93
Temperature (K)	293(2)	129(7)	293(2)
Crystal size (mm)	0.3×0.1×0.05	0.3×0.1×0.05	0.2×0.03×0.02
Crystal colour	yellow	yellow	light-blue
Crystal system	orthorhombic	tetragonal	triclinic
Space group	*Pbca* (Nr. 61)	$I4_1/a$ (Nr. 88)	$P\bar{1}$ (Nr. 2)
a (Å)	15.1305(7)	41.5083(4)	8.7077(12)
b (Å)	10.1117(3)	41.5083(4)	10.2766(13)
c (Å)	29.9520(9)	5.58160(10)	11.6856(13)
α (°)	90	90	72.850(11)
β (°)	90	90	75.004(11)
γ (°)	90	90	86.999(11)
V (Å^3)	4582.5(3)	9616.8(3)	964.8(2)
Z	8	16	1
D_{calc}	1.347	1.361	1.539
F(000)	1936	4128	455
Reflns. collected	14281	11842	8434
Independ. reflns.	4701	4872	3958
R_{init}	0.0348	0.0480	0.0672
Reflns. observed [$I>2\sigma(I)$]	3298	4182	2381
Parameters	307	344	305
$R[I>2\sigma(I)]^a$	0.0790	0.0510	0.0804
wR_2 (all data)^b	0.2784	0.1366	0.2821
Goof, S^c	1.068	1.050	1.053
Max./Min. res. el. dens.	0.503/-0.503	0.213/-0.235	0.611/-0.751

^{a} $R = \Sigma||F_o|-|F_c||/\Sigma|F_o|$. ^{b} $wR_2 = \{\Sigma[w(F_o^2 - F_c^2)^2]/\Sigma[w(F_o^2)^2]\}^{1/2}$. ^{c} $S = \{\Sigma[w(F_o^2 - F_c^2)^2]/(n-p)\}^{1/2}$ where *n* is number of reflections and *p* is total number of parameters refined.

Table S1. Experimental data for X-ray diffraction studies (part 2).

	8d$_{\mathbf{Cu}}$	**9c**$_{\mathbf{Cu}}$	**10c**$_{\mathbf{Cu}}$
Formula	$C_{44}H_{56}CuF_6N_{12}O_6S_2Si$	$C_{52}H_{51.4}CuF_6N_{14}O_{0.7}Si$	$C_{54}H_{55.2}CuF_6N_{16}O_{3.6}S_2Si$
F_w (g mol^{-1})	1118.75	1089.39	1255.7
Temperature (K)	293(2)	293(2)	293(2)
Crystal size (mm)	0.2×0.08×0.03	0.3×0.2×0.1	0.3×0.2×0.1
Crystal colour	purple	brown	pink
Crystal system	triclinic	monoclinic	monoclinic
Space group	$P\bar{1}$ (Nr. 2)	$P2_1/c$ (Nr. 14)	$P2_1/c$ (Nr. 14)
a (Å)	8.4563(8)	10.6299(3)	11.5387(5)
b (Å)	10.9214(12)	16.4545(4)	16.3557(5)
c (Å)	15.1689(18)	16.1189(7)	16.1961(7)
α (°)	71.891(10)	90	90
β (°)	78.582(9)	110.830(3)	106.089(5)
γ (°)	71.330(9)	90	90
V (Å^3)	1253.9(3)	2635.08(16)	2936.9(2)
Z	1	2	2
D_{calc}	1.482	1.373	1.420
F(000)	581	1128	1298
Reflns. collected	1760	14816	8576
Independ. reflns.	1081	5390	4517
R_{init}	0.0388	0.0266	0.0424
Reflns. observed [$I>2\sigma(I)$]	729	4498	3263
Parameters	240	368	364
$R[I>2\sigma(I)]^a$	0.0401	0.0559	0.0586
wR_2 (all data)^b	0.0766	0.1829	0.1730
Goof, S^c	0.856	1.062	1.016
Max./Min. res. el. dens.	0.160/-0.189	1.010/-0.186	0.756/-0.311

[a] $R = \Sigma||F_o|-|F_c||/\Sigma|F_o|$. [b] $wR_2 = \{\Sigma[w(F_o^2 - F_c^2)^2]/\Sigma[w(F_o^2)^2]\}^{1/2}$. [c] $S = \{\Sigma[w(F_o^2 - F_c^2)^2]/(n-p)\}^{1/2}$ where n is number of reflections and p is total number of parameters refined.

ORTEP-III drawings and crystal packing of ligands **10a** and **10c** and complexes **8a**$_{\mathbf{Cu}}$, **8d**$_{\mathbf{Cu}}$, **9c**$_{\mathbf{Cu}}$ and **10c**$_{\mathbf{Cu}}$.

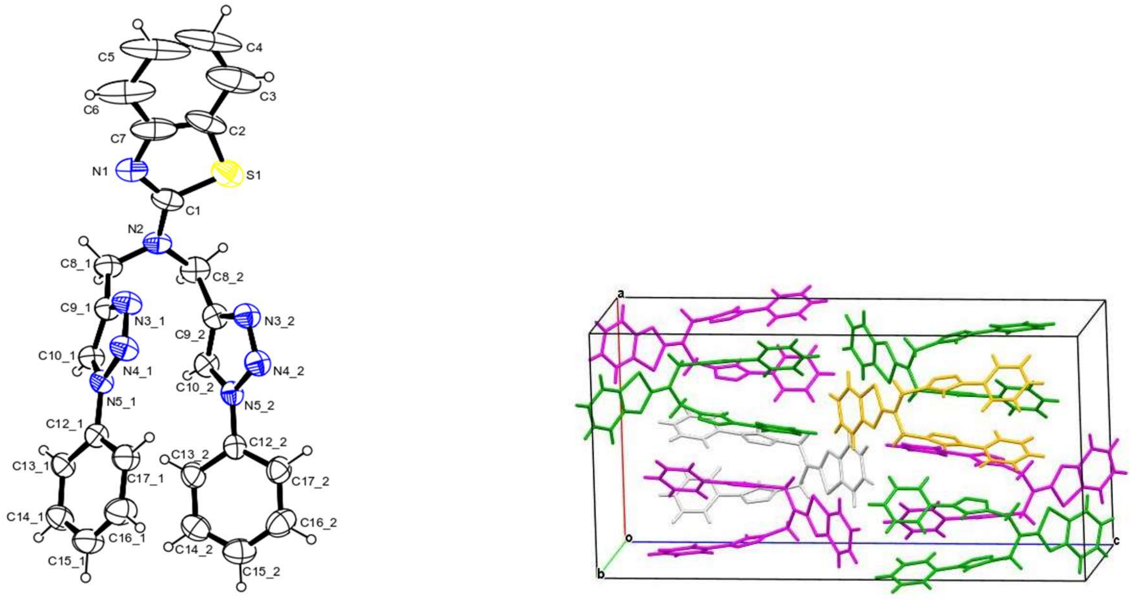

a) **b)**

Figure S8. (a) ORTEP-III[1] drawing with atom labelling scheme for ligand **10a**. All ellipsoids were drawn at the 30% probability level. (b) Packing of molecules in the crystal structure of **10a**.[2] Molecules related by different symmetry operations are coloured in different colours.

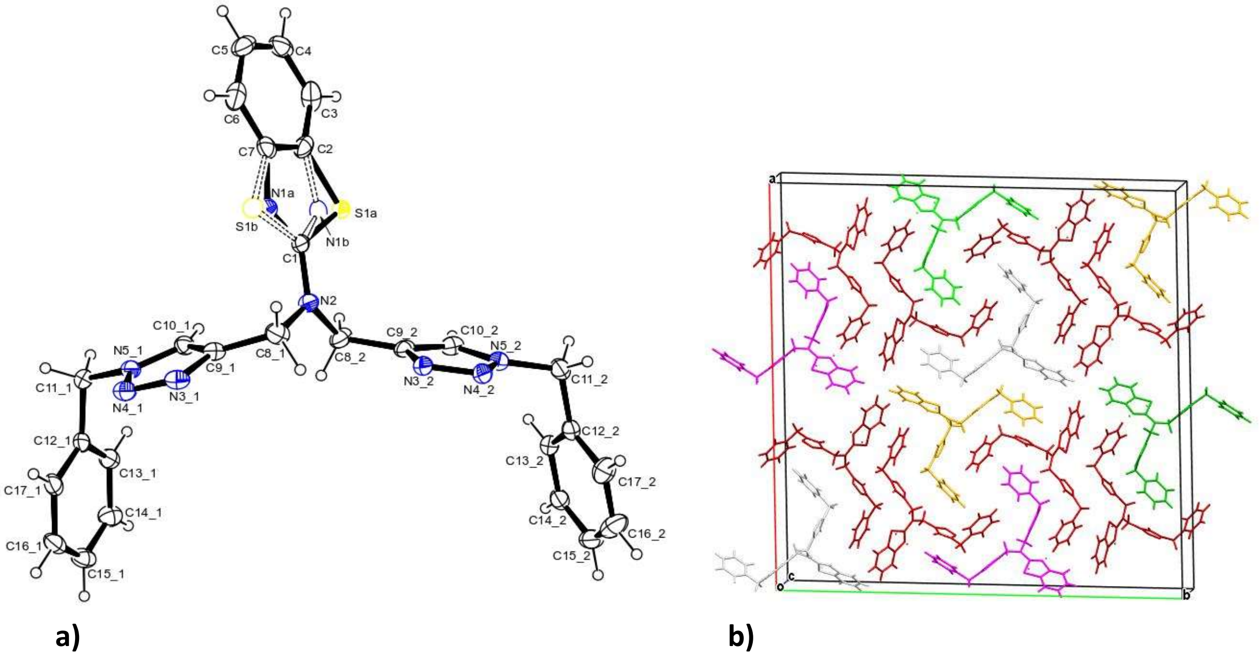

a) **b)**

Figure S9. (a) ORTEP-III[1] drawing with atom labelling scheme for ligand **10c**. All ellipsoids were drawn at the 30% probability level. Positions of disordered atoms with lower occupancy (N1b and S1b) are shown as empty ellipsoids and their bonds are shown as dashed lines. (b) Packing of molecules in the crystal structure of **10c**.[2] Molecules related by different symmetry operations are coloured in different colours.

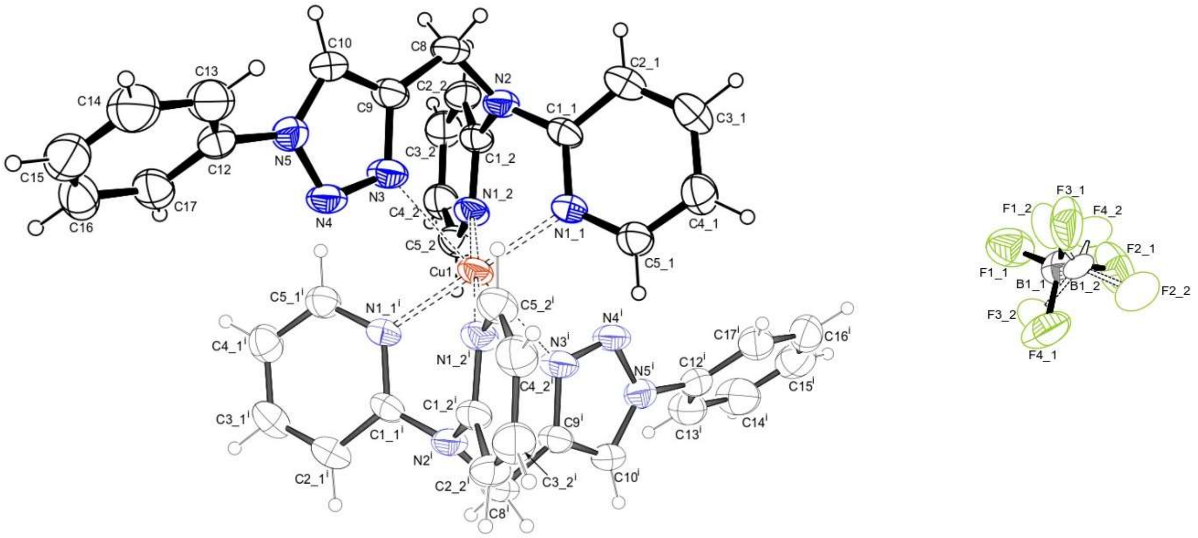

Figure S10. ORTEP-III[1] drawing with atom labelling scheme for complex **$8a_{Cu}$**. All ellipsoids were drawn at the 30% probability level. The complex cation is located at the position with a centre of symmetry. One ligand is shown bold and the other one, which is related by the centre of symmetry is shown light [symmetry code (i): 1-*x*, 1-*y*, 1-*z*]. Coordination bonds in the cation are shown as dashed lines. The BF_4^- anion is located at a general crystallographic position. Positions of disordered atoms with lower occupancy (B1_2, F1_2, F2_2, F3_2 and F4_2) are shown as empty ellipsoids and their bonds are shown as dashed lines.

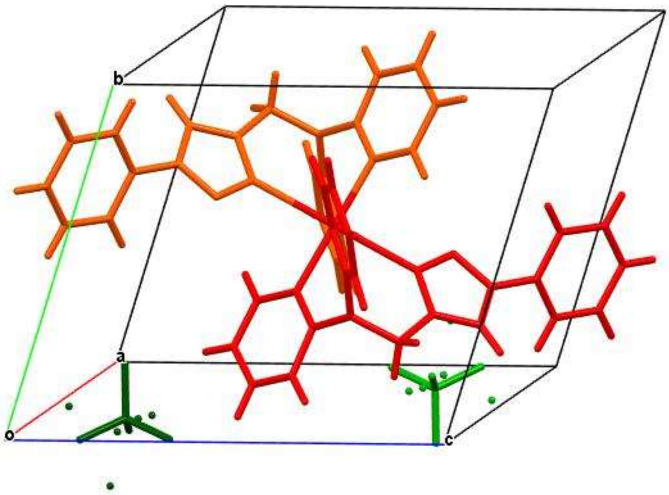

Figure S11. Packing of complex cation (red and orange) and two BF_4^- anions (dark and light green); in the crystal structure of **$8a_{Cu}$**.

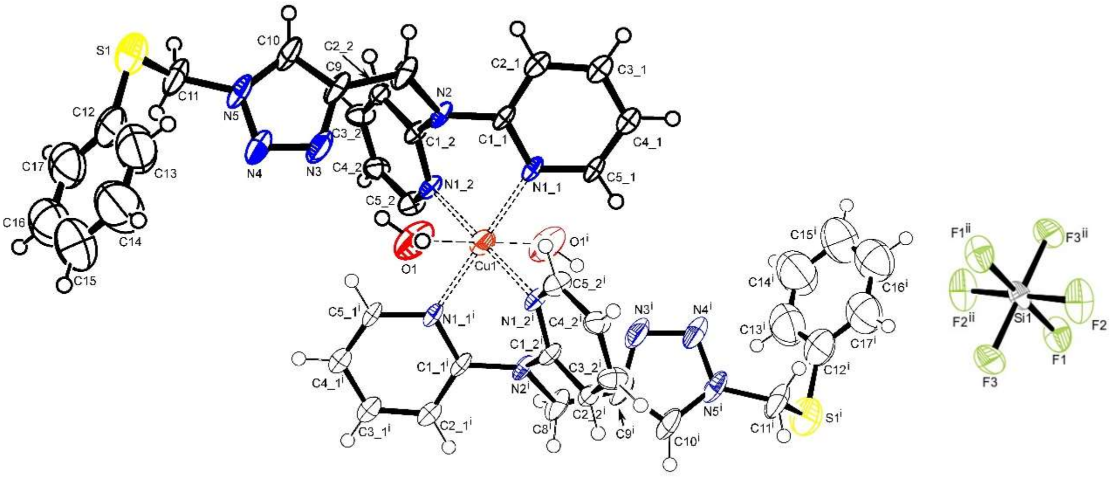

Figure S12. ORTEP-III[1] drawing with atom labelling scheme for complex **8d$_{Cu}$**. All ellipsoids were drawn at the 30% probability level. One ligand is shown bold and other one, which is related by the centre of symmetry in the Cu1 atom is shown light [symmetry code (i): 1-*x*, 1-*y*, 1-*z*]. Coordination bonds in the cation are shown as dashed lines. The SiF_6^{2-} anion is located at another centre of symmetry [symmetry code (ii): 2-*x*, -*y*, 1-*z*].

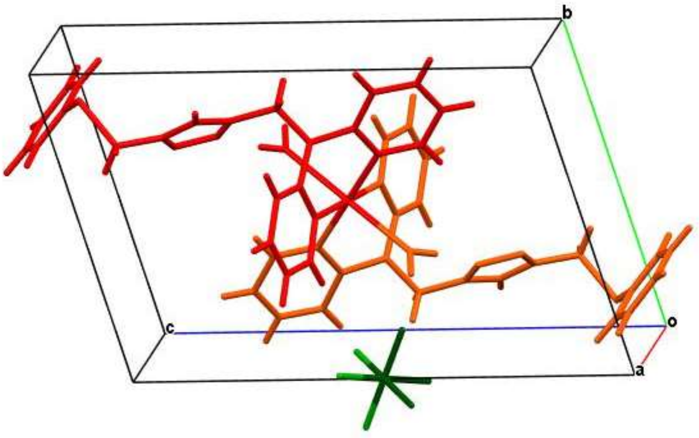

Figure S13. Packing of the complex cation (red and orange) and SiF_6^{2-} anions (dark and light green); in the crystal structure of **8d$_{Cu}$**.

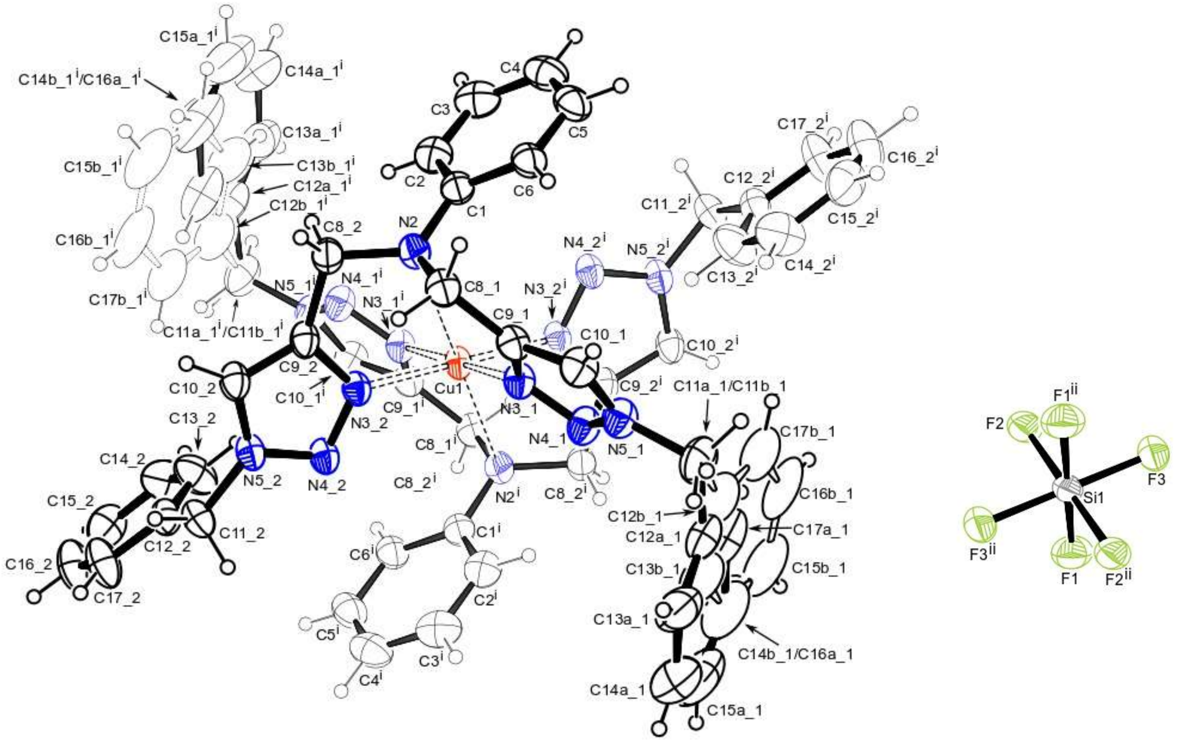

Figure S14. ORTEP-III[1] drawing with atom labelling scheme for complex **9c$_{Cu}$**. All ellipsoids were drawn at the 30% probability level. Positions of atoms of one phenyl ring having lower occupancy (C11b_1 – C17b_1) are shown as empty ellipsoids. One ligand is shown bold and other one, which is related by a centre of symmetry in the Cu1 atom is shown light [symmetry code (i): 1-*x*, 1-*y*, 1-*z*]. Coordination bonds in the cation are shown as dashed lines. The SiF$_6^{2-}$ anion is located at another centre of symmetry [Symmetry code (ii): 1-*x*, -*y*, 1-*z*].

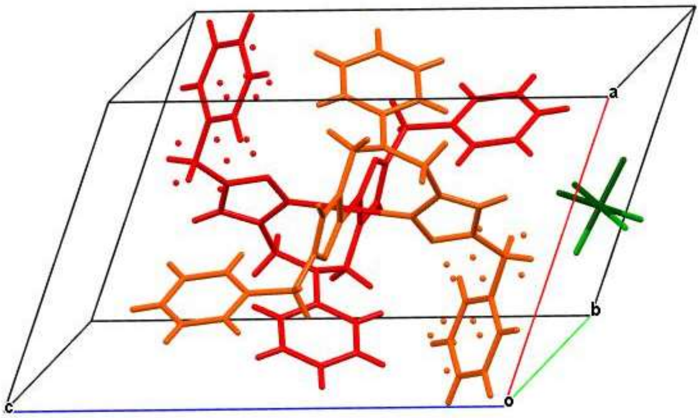

Figure S15. Packing of complex cation (red and orange) and SiF$_6^{2-}$ anions (dark and light green); in the crystal structure of **9c$_{Cu}$**.

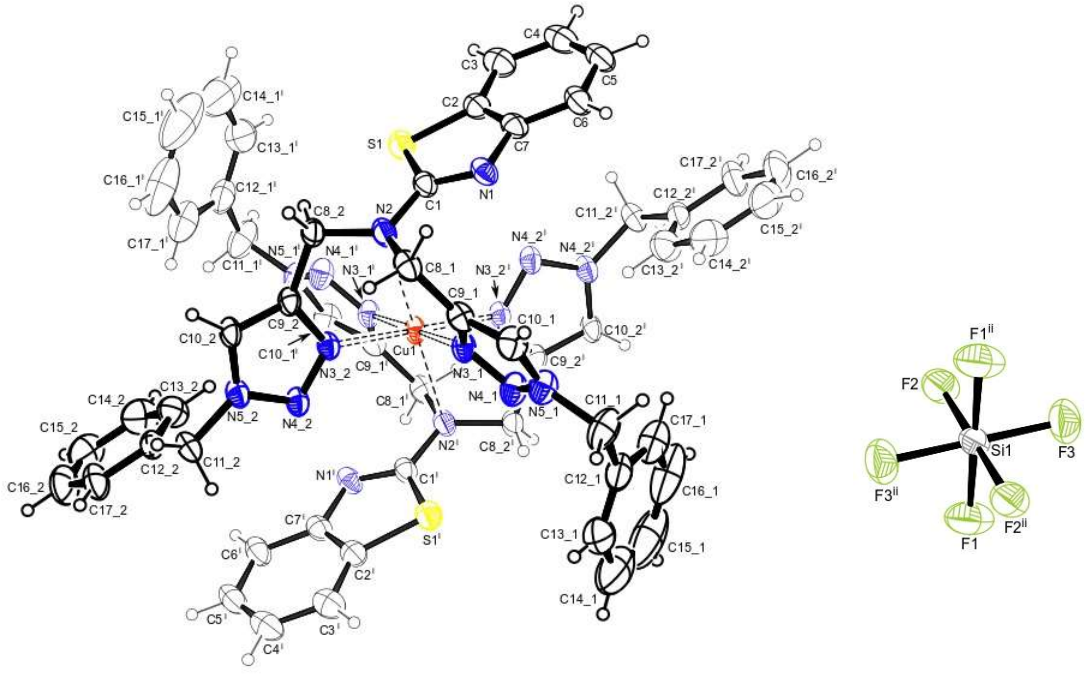

Figure S16. ORTEP-III[1] drawing with atom labelling scheme for complex $\mathbf{10c_{Cu}}$. All ellipsoids were drawn at the 30% probability level. One ligand is shown bold and other one, which is related by a centre of symmetry in the Cu1 atom is shown light [symmetry code (i): 1-*x*, 1-*y*, 1-*z*]. Coordination bonds in the cation are shown as dashed lines. The SiF_6^{2-} anion is located at another centre of symmetry [Symmetry code (ii): 1-*x*, -*y*, 1-*z*].

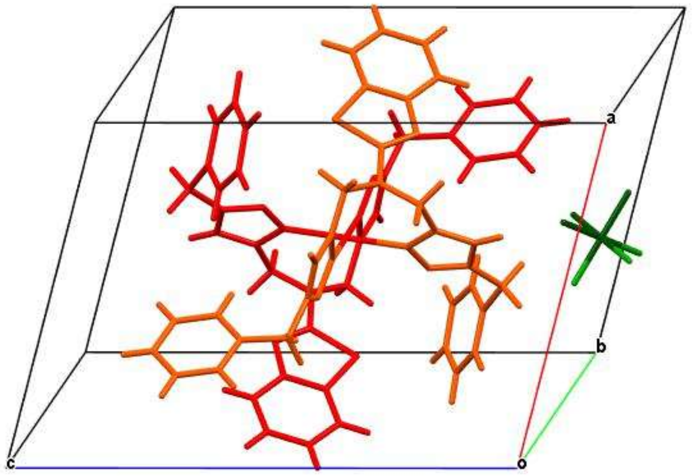

Figure S17. Packing of the complex cation (red and orange) and SiF_6^{2-} anions (dark and light green); in the crystal structure of $\mathbf{10c_{Cu}}$.

Table S2. CSD search of ML_2 complexes of tridentate nitrogen ligands with Cu(II).

	structure	octahedra: axial bond / Å	reference
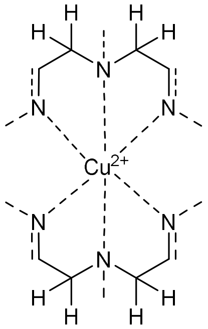 Di-(2-picolyl)amine ligands	JEPPAY	elongated: 2.364, 2.455	Yang Wang, Haixiong Liu, Xiaofeng Zhang, Zilong Zhang, Deguang Huang, *Org.Biomol.Chem.* (2017), **15**, 9164
	KAYQOQ	compressed: 2.010, 2.010	Gin-Song Huang, Jen-Kou Lai, Chuen-Her Ueng, Chan-Cheng Su, *Transition Met.Chem.* (2000), **25**, 84
	KAYQUW	compressed: 2.039, 2.053	
	ZOQCAJ	compressed: 2.035, 2.037	M.Palaniandavar, R.J.Butcher, A.W.Addison, *Inorg.Chem.* (1996), **35**, 467
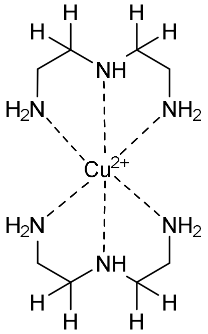 Diethylenetriamine ligands			
	AWUBEA	elongated: 2.296, 2.553	V.M.Nikitina, O.V.Nesterova, R.I.Zubatyuk, O.V.Shishkin, J.A.Rusanova, *Acta Crystallogr.,Sect.E:Struct.Rep.Online* (2011), **67**, m1023
	ETACUB	elongated: 2.459, 2.350	F.S.Stephens, *J.Chem.Soc.A* (1969), 2233
	ETAMCU	compressed: 2.001, 2.019	F.S.Stephens, *J.Chem.Soc.A* (1969), 883
	QAGCAD	elongated: 2.347, 2.634	C.A.Johns, K.M.A.Malik, *Polyhedron* (2002), **21**, 395
	QAGSUN	elongated: 2.467, 2.467	M.Gonzalez-Alvarez, G.Alzuet, J.Borras, B.Macias, J.M.Montejo-Bernardo, S.Garcia-Granda, *Z.Anorg.Allg.Chem.* (2003), **629**, 239
	SEZKOY	elongated: 2.339, 2.339	G.M.G.Hossain, A.J.Amoroso, *Acta Crystallogr.,Sect.E:Struct.Rep.Online* (2007), **63**, m759

	VAMTEL	elongated: 2.424, 2.456 elongated: 2.368, 2.607	Xiaodong Jin, R.P.Davies, *Cat.Sci.Tech.* (2017), **7**, 2110
	XAGWAE	compressed: 2.081, 2.088	Hui-Bo Zhou, Mao Liang, Li-Na Zhu, Wen Dong, Dai-Zheng Liao, Zong-Hui Jiang, Shi-Ping Yan, Peng Cheng, *J.Coord.Chem.* (2004), **57**, 865
	YAYREY	elongated: 2.541, 2.541	S.Kumar, R.P.Sharma, P.Venugopalan, Vijay Singh Gondil, S.Chhibber, T.Aree, M.Witwicki, V.Ferretti, *Inorg.Chim.Acta* (2018), **469**, 288
	ZIYHUM01	elongated: 2.352, 2.551	U.Florke, A.Begum, G.Henkel, *CSD Communication* (2016)

Table S3. Selected bond lengths and angles for experimental structures **8a$_{\mathrm{Cu}}$** and **8d$_{\mathrm{Cu}}$**.

Complex	denticity	Cu-N1_1 (Å)	Cu-N1_2 (Å)	Cu-X^{a} (Å)	N1_1-Cu-N1_2 (°)	X-Cu-X^{a} (°)	Coordination Geometry, RMSD / Å
8a$_{\mathrm{Cu}}$	3	2.022	2.025	2.486	86.37	180.00	Octahedron (regular), 0.092
8d$_{\mathrm{Cu}}$^{b}	2	2.000	2.015	2.583	86.83	180.00	Octahedron (regular), 0.175

^{a}X = N3 in **8a$_{\mathrm{Cu}}$** and X = O1 in **8d$_{\mathrm{Cu}}$**.

^{b}The large R-factor of **8d$_{\mathrm{Cu}}$** should be noted.

Table S4. Selected bond lengths and angles for experimental structures **9c$_{\mathrm{Cu}}$** and **10c$_{\mathrm{Cu}}$**.

Complex	Isomer	Cu-N31 Cu - N31^{i} (Å)	Cu - N32 Cu - N32^{i} (Å)	Cu - N2 Cu - N2^{i} (Å)	N31- Cu -N32 N31^{i}- Cu - N32^{i} (°)	N2- Cu - N2^{i} (°)	Coordination Geometry, RMSD / Å
9c$_{\mathrm{Cu}}$	*pseudo-trans-fac*	1.993	1.985	2.781	93.45	180.00	Octahedron (distorted), 0.678
10c$_{\mathrm{Cu}}$	*pseudo-trans-fac*	1.977	1.995	2.873	92.33	180.00	Square plane (regular), 0.062

^{i} symmetry related atom

Threshold coordination distance was set to 2.8 Å (default).

NMR spectroscopy

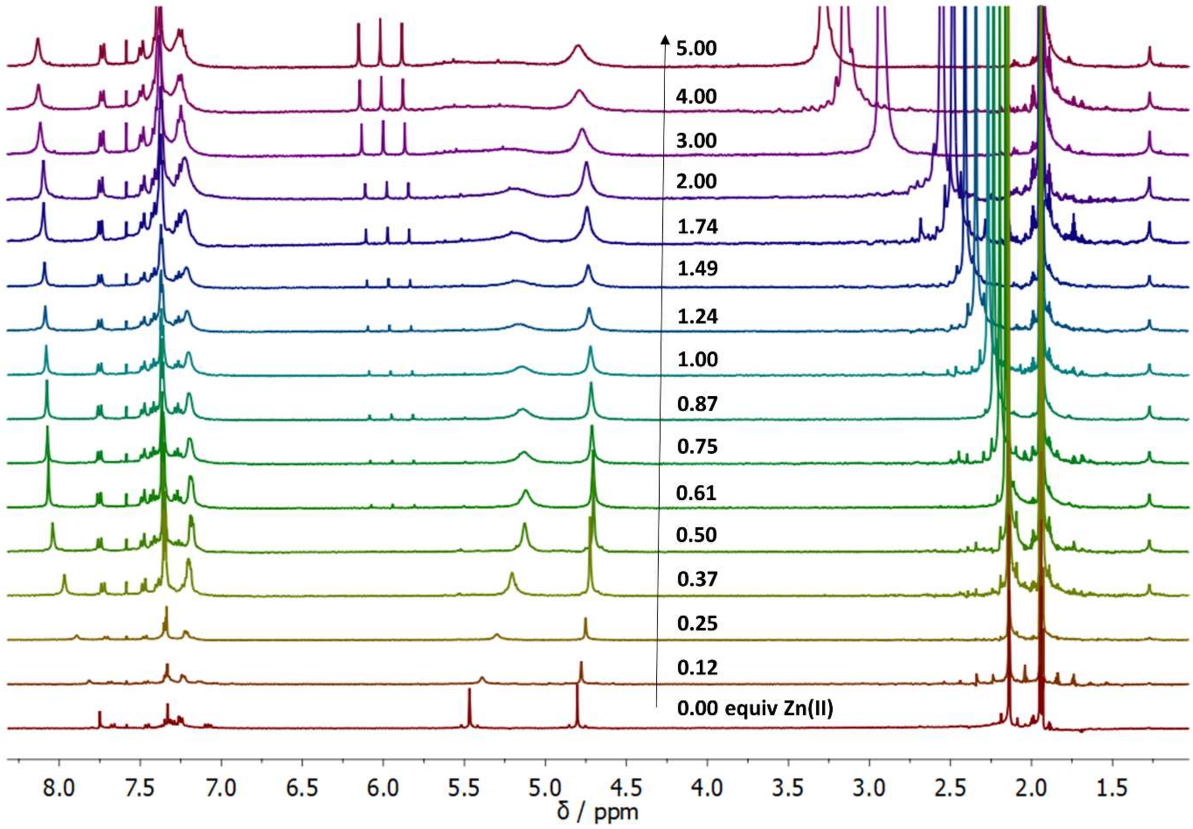

Figure S18. ^{1}H NMR titration of ligand **10c** with Zn(CF_3SO_3)$_2$.

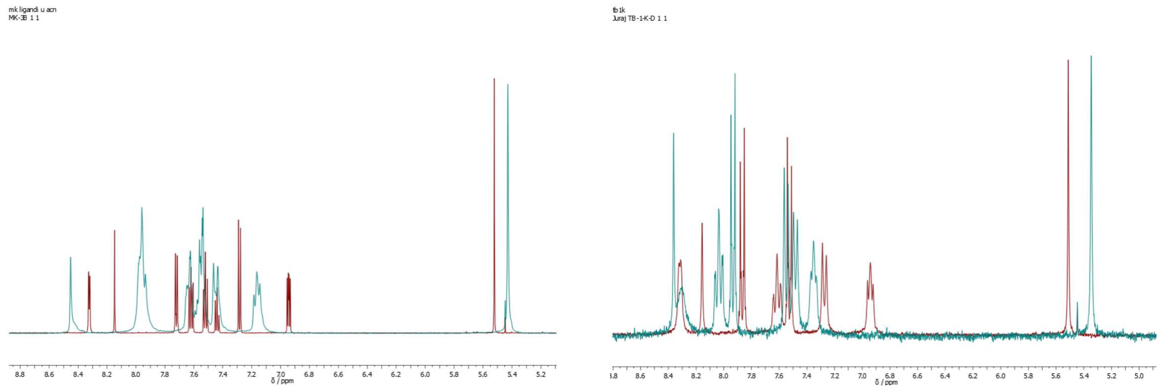

[Zn(**8a**)$_2$](BF$_4$)$_2$ [Zn(**8b**)$_2$](BF$_4$)$_2$

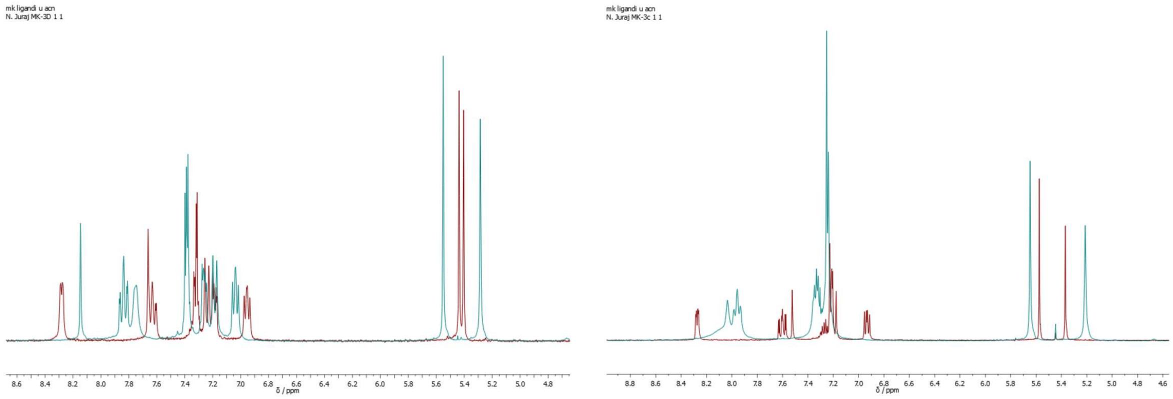

[Zn(**8c**)$_2$](BF$_4$)$_2$ [Zn(**8d**)$_2$](BF$_4$)$_2$

Figure S19. ^{1}H NMR (CD_3CN) spectra of complexes prepared at a 2 L to 1 Zn(II) ratio (blue) compared to the free ligands **8a**-**8d** (red).

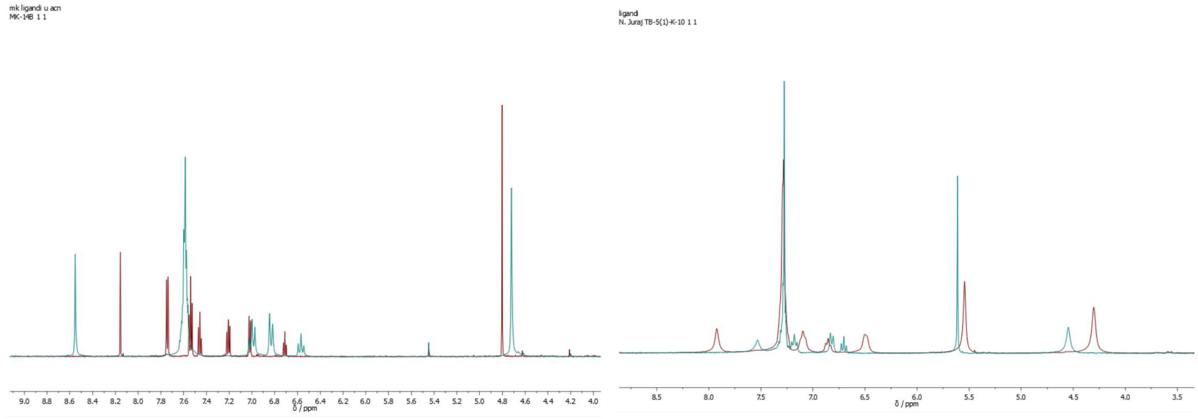

[Zn(**9a**)$_2$](BF$_4$)$_2$ [Zn(**9d**)$_2$](BF$_4$)$_2$

Figure S20. ^{1}H NMR (CD_3CN) spectra of complexes prepared at a 2 L to 1 Zn(II) ratio (blue) compared to the free ligands **9a**-**9d** (red). NMR spectra of ligands **9b** and **9c** and their complexes in acetonitrile are not shown due to limited solubility and/or peak broadening caused by intermediate ligand exchange.

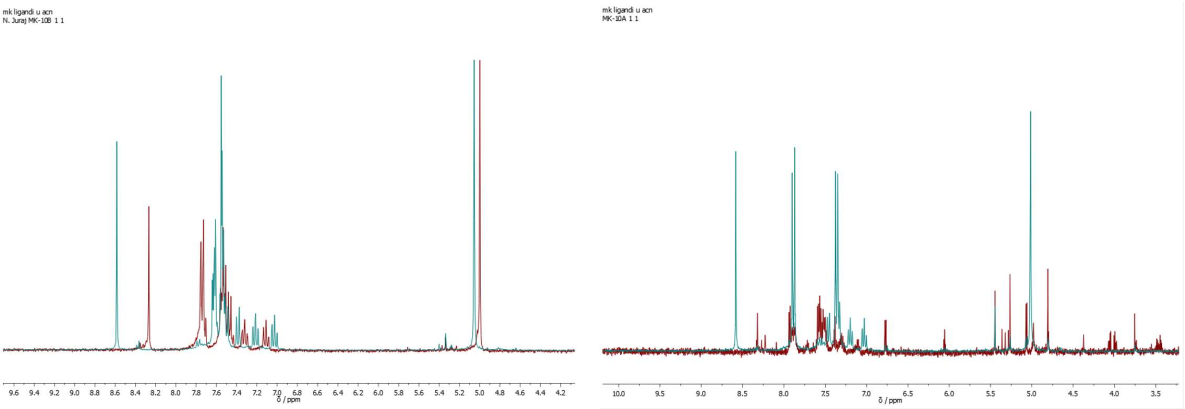

[Zn(**10a**)$_2$](BF$_4$)$_2$

[Zn(**10b**)$_2$](BF$_4$)$_2$

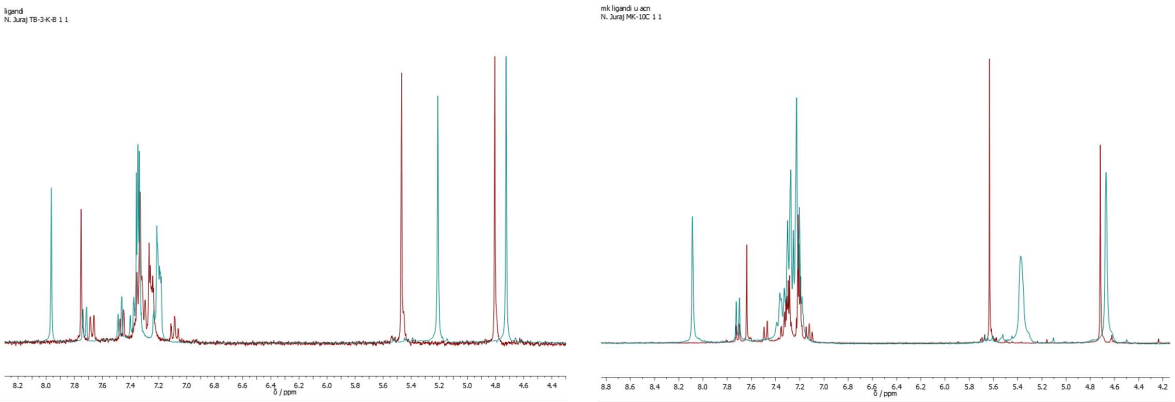

[Zn(**10c**)$_2$](BF$_4$)$_2$

[Zn(**10d**)$_2$](BF$_4$)$_2$

Figure S21. ^{1}H NMR (CD$_3$CN) spectra of complexes prepared at a 2 L to 1 Zn(II) ratio (blue) compared to the free ligands **10a**-**10d** (red).

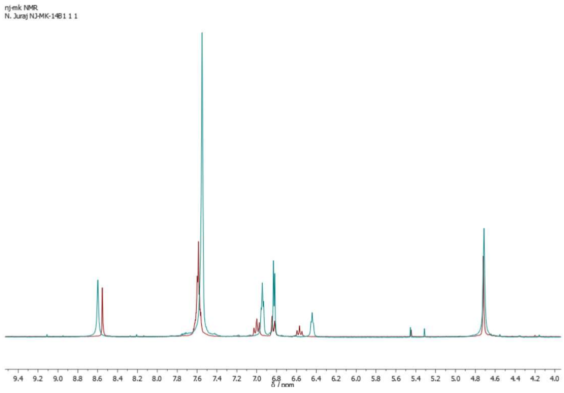

[Zn(**9a**)$_2$](BF$_4$)$_2$

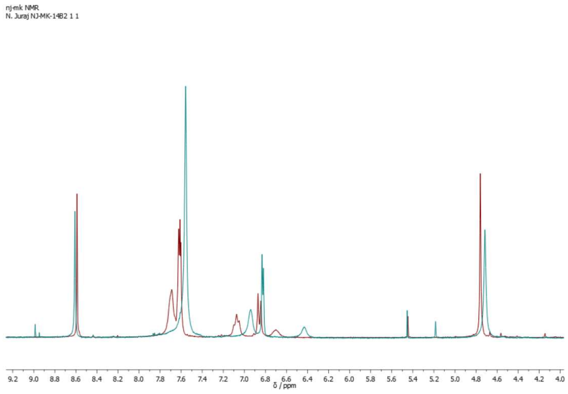

[Zn(**9a**)(CD$_3$CN)](BF$_4$)$_2$

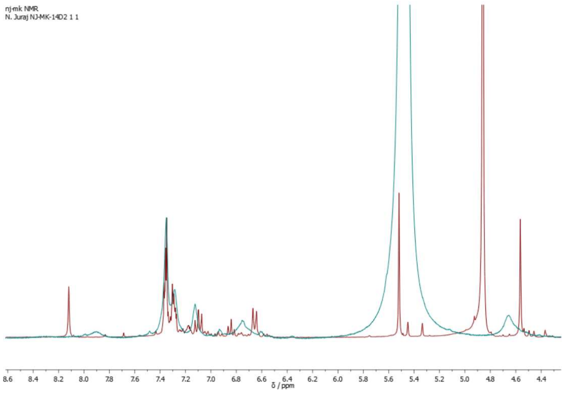

[Zn(**9c**)$_2$](BF$_4$)$_2$

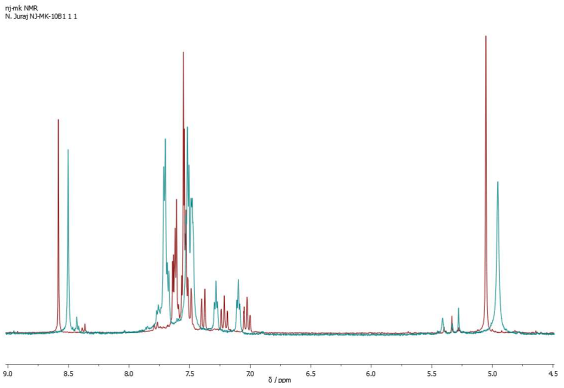

[Zn(**10a**)$_2$](BF$_4$)$_2$

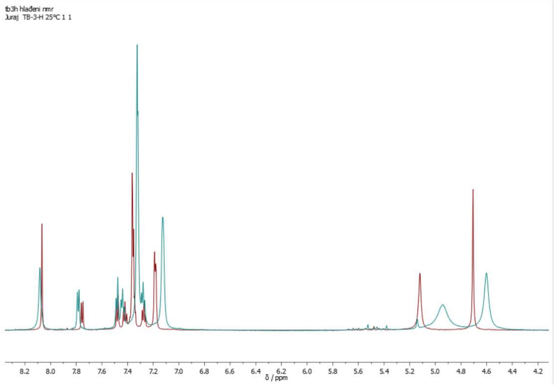

[Zn(**10c**)$_2$](BF$_4$)$_2$

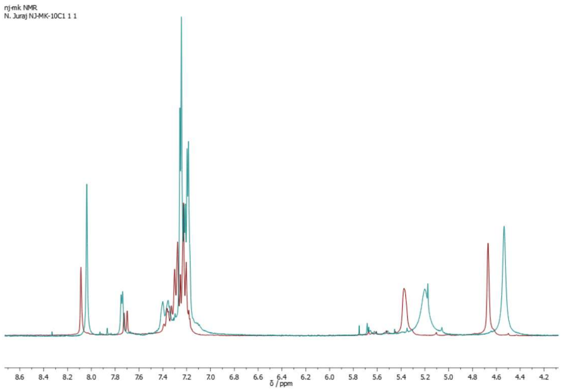

[Zn(**10d**)$_2$](BF$_4$)$_2$

Figure S22. ^{1}H NMR (CD$_3$CN) spectra at room temperature (red) and -40°C (blue). [Zn(**9c**)$_2$](BF$_4$)$_2$ and ligand **9c** were recorded in CD$_3$OD due to peak broadening observed in acetonitrile (see also Figure S25).

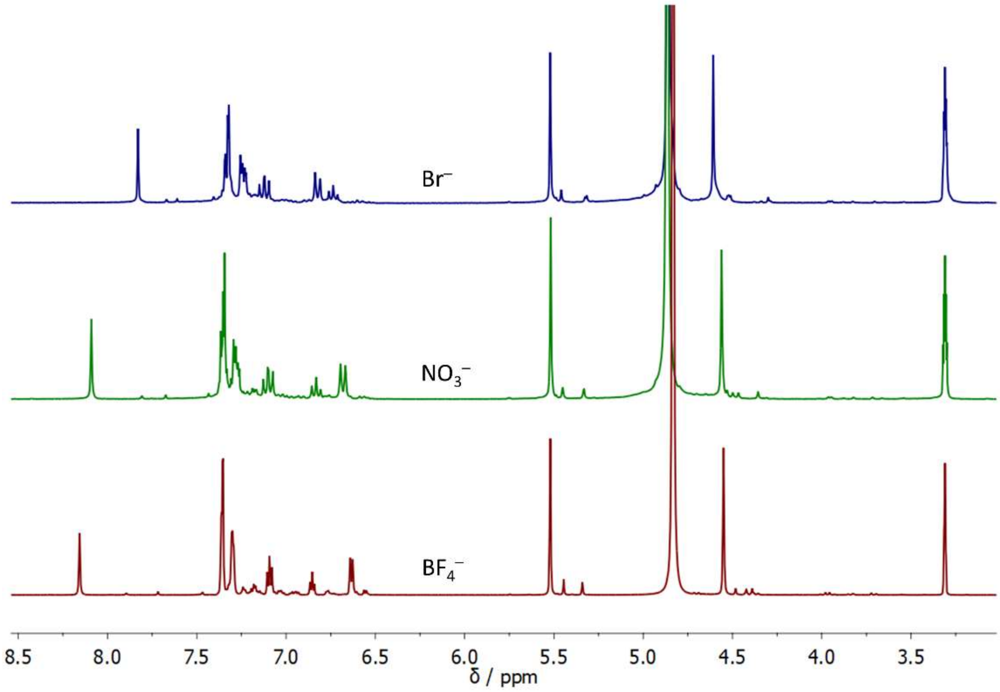

Figure S23. Complexes of ligand **9c** with $Zn(BF_4)_2$, $Zn(NO_3)_2$ and $ZnBr_2$ at a 2 L : 1 Zn ratio.

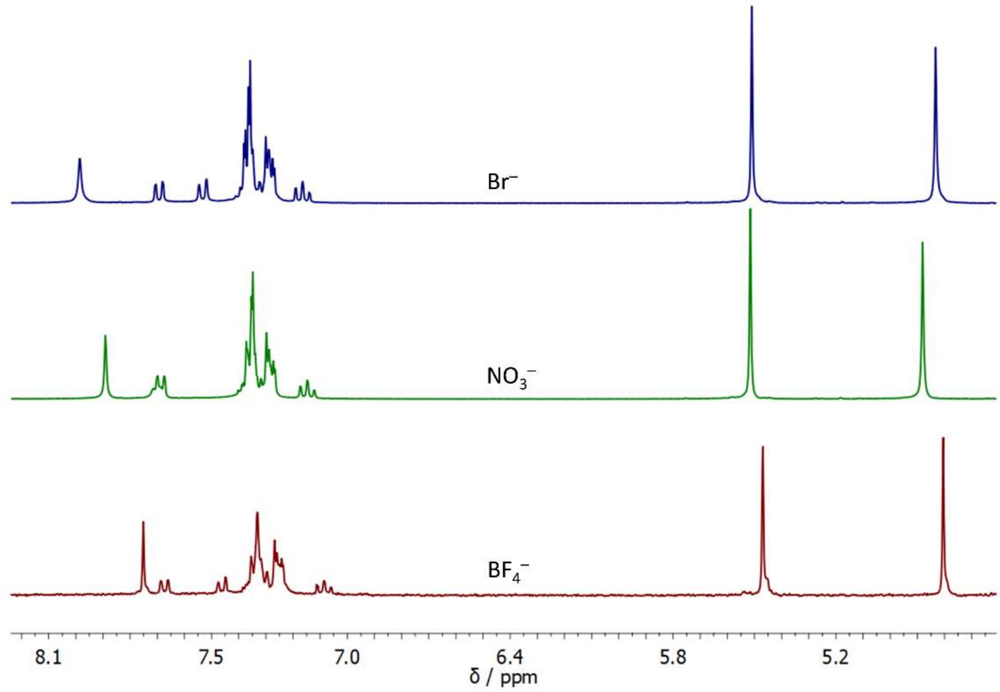

Figure S24. Complexes of ligand **10c** with $Zn(BF_4)_2$, $Zn(NO_3)_2$ and $ZnBr_2$ at a 2 L : 1 Zn ratio.

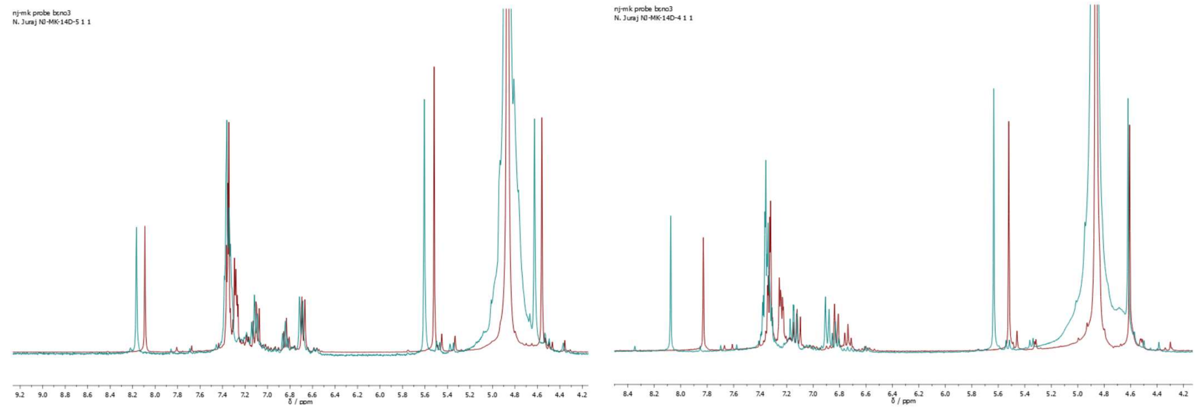

9c : Zn(NO$_3$)$_2$

9c : ZnBr$_2$

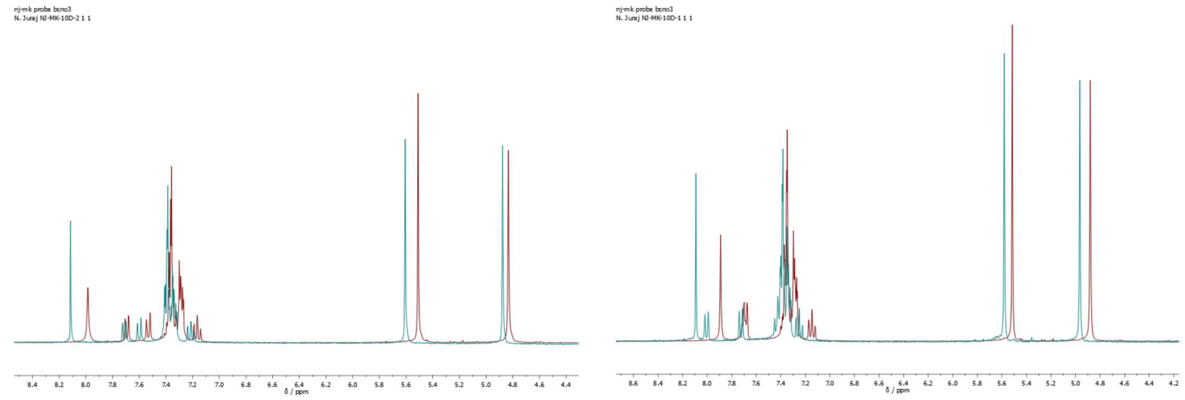

10c : Zn(NO$_3$)$_2$

10c : ZnBr$_2$

Figure S25. ^{1}H NMR spectra of **9c** and **10c** complexes with Zn(NO$_3$)$_2$ and ZnBr$_2$ prepared in a 2 L : 1 Zn(II) (red) and 1 L : 6 Zn(II) (blue) ratio. The spectra of **9c** were recorded in CD$_3$OD, and of **10c** in CD$_3$CN.

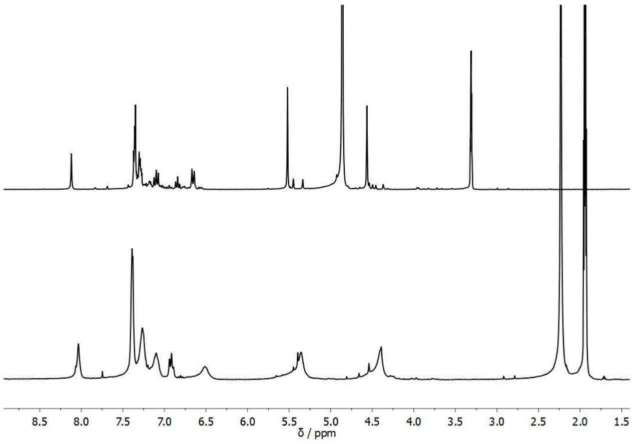

Figure S26. ^{1}H NMR spectra of complexes prepared at a 2 **9c** to 1 $Zn(BF_4)_2$ ratio in acetonitrile (bottom) and methanol (top). The ^{1}H NMR spectra show peak broadening in acetonitrile, indicating a ligand exchange intermediate compared to the NMR timescale, while the peaks are sharper in methanol, likely showing a fast exchange as observed in the titration of ligand **10c**.

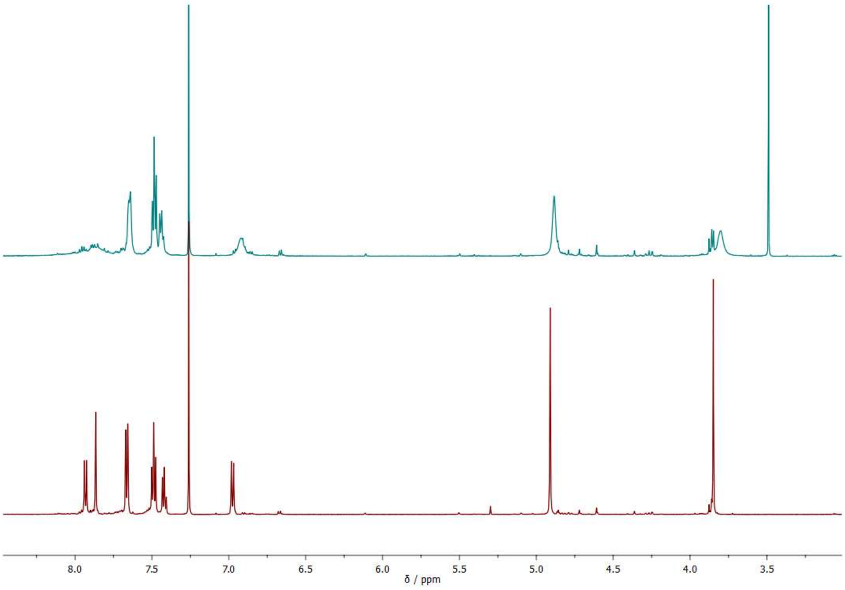

Figure S27. ^{1}H NMR spectra of ligand **11a** and complex $[Zn(\textbf{11a})_2](CF_3SO_3)_2$ in $CDCl_3$. Due to low solubility, the complex was first prepared in a mixture of dichloromethane and methanol, the solvent evaporated and the obtained solid dissolved in $CDCl_3$ for recording the NMR spectrum.

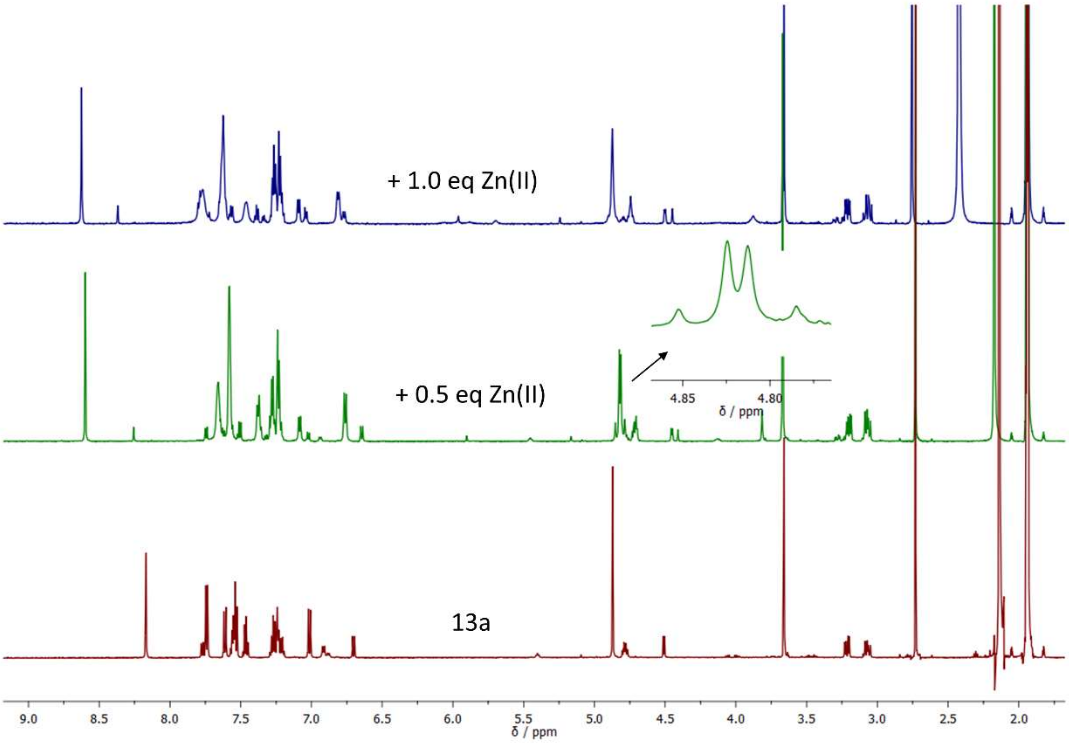

Figure S28. ^{1}H NMR spectra of ligand **13a** with 0.5 and 1.0 added equivalents of $Zn(CF_3SO_3)_2$ in CD_3CN.

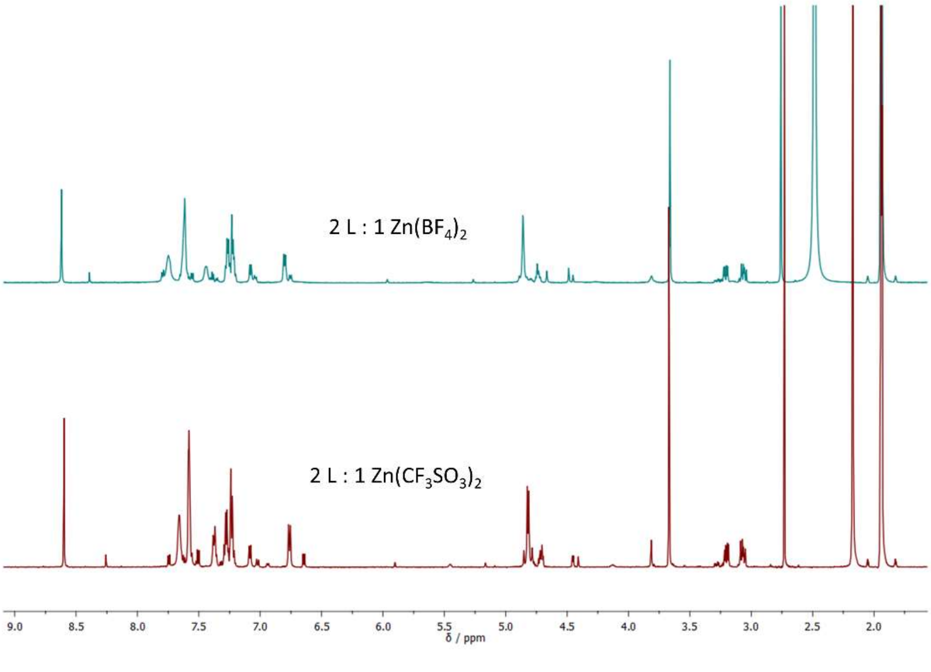

Figure S29. ^{1}H NMR spectra of ligand **13a** with 0.5 equivalents of $Zn(CF_3SO_3)_2$ or $Zn(BF_4)_2$.

Table S5. ^{1}H NMR (CD_3CN) shifts of triazole protons in ligands **8a**-**10d** and their Zn(II) complexes in acetonitrile at a 2 L to 1 Zn(II) ratio.

ligand	triazole H shift (ligand) / ppm	triazole H shift (complex) / ppm	Δ (complex-ligand)/ ppm
8a	8.15	8.45	0.30
8b	8.15	8.36	0.21
8c	7.66	8.14	0.48
8d	7.52	8.03	0.51
9a	8.16	8.55	0.39
9b	nd	8.56	-
9c	7.59	nd	-
9d	7.92	7.53	-0.39
10a	8.27	8.58	0.31
10b	nd	8.58	-
10c	7.75	7.96	0.21
10d	7.63	8.08	0.45
11a	-	nd	-
13a	8.17	8.60	0.43

nd = not dissolved

Table S6. ^{1}H NMR (CD_3CN) shifts of α-CH_2 protons in ligands **8a**-**10d** and their Zn(II) complexes in acetonitrile at a 2 L to 1 Zn(II) ratio.

ligand	α-CH_2 shift (ligand) / ppm	α-CH_2 shift (complex) / ppm	Δ (complex-ligand)/ ppm
8a	5.52	5.43	-0.09
8b	5.51	5.34	-0.17
8c	5.40	5.28	-0.12
8d	5.37	5.21	-0.16
9a	4.80	4.72	-0.08
9b	nd	4.74	-
9c	4.61	nd	-
9d	4.30	4.54	0.24
10a	4.99	5.05	0.06
10b	nd	5.01	-
10c	4.80	4.72	-0.08
10d	4.72	4.67	-0.05
11a	-	nd	-
13a	4.87	4.82	-0.05

Table S7. ^{1}H NMR (CD_3CN) shifts of benzyl-CH_2 protons in ligands **8c**, **9c** and **10c** and their Zn(II) complexes in acetonitrile at a 2 L to 1 Zn(II) ratio.

ligand	benzyl-CH_2 shift (ligand) / ppm	α-CH_2 shift (complex) / ppm	Δ / ppm
8c	5.44	5.55	0.11
9c	5.45	nd	-
10c	5.47	5.21	-0.26

Table S8. ^{1}H NMR (CD_3CN) shifts of S-CH_2 protons in ligands **8d**, **9d** and **10d** and their Zn(II) complexes in acetonitrile at a 2 L to 1 Zn(II) ratio.

ligand	S-CH_2 shift (ligand) / ppm	α-CH_2 shift (complex) / ppm	Δ / ppm
8d	5.57	5.65	0.08
9d	5.54	5.61	0.07
10d	5.63	5.37	-0.26

UV-Vis spectroscopy

Table S9. Binding constants of **CuL** and **CuL_2** complexes in the solvent mixture 1:1 CH_3OH:CH_2Cl_2 determined by HypSpec2014. $Cu(CF_3SO_3)_2$ was used as the metal salt.

	logβ(CuL)	**logβ(CuL_2)**
10c	3.53 ± 0.01	6.29 ± 0.01
11a	3.02 ± 0.02	5.25 ± 0.02
13a	3.45 ± 0.02	6.34 ± 0.01

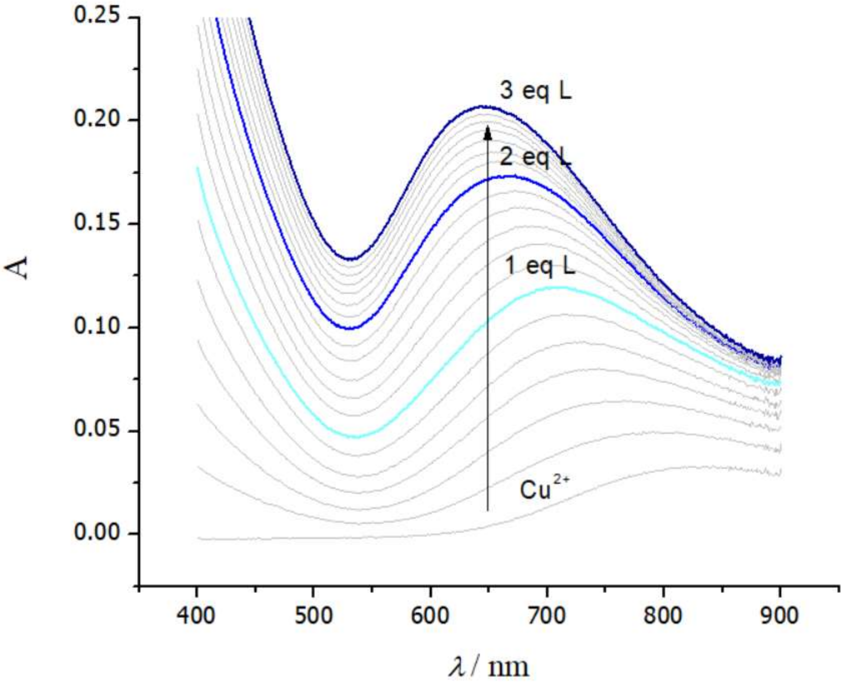

Figure S30. UV-Vis titration of Cu(II) with ligand **10c**.

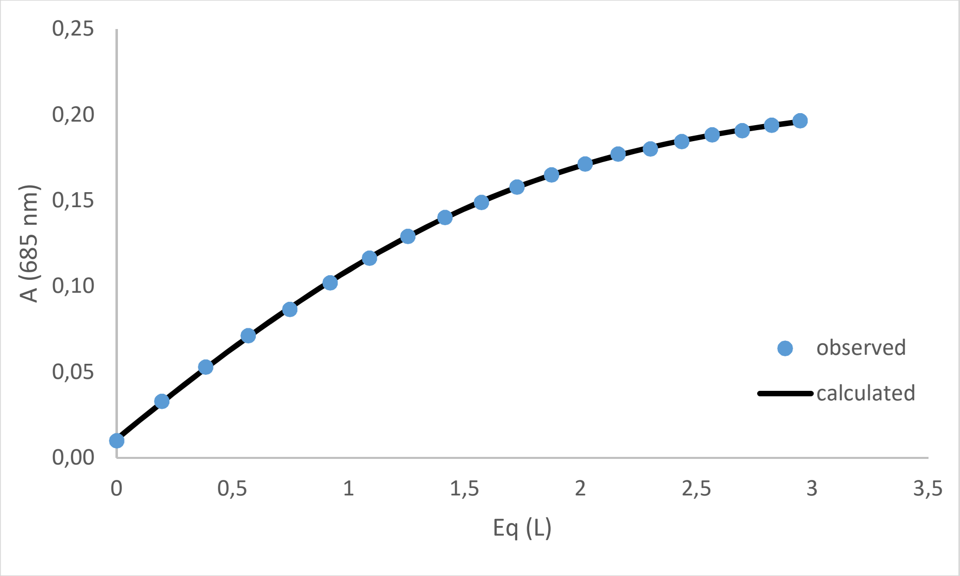

Figure S31. Curve fitting for the titration of Cu(II) with ligand **10c**.

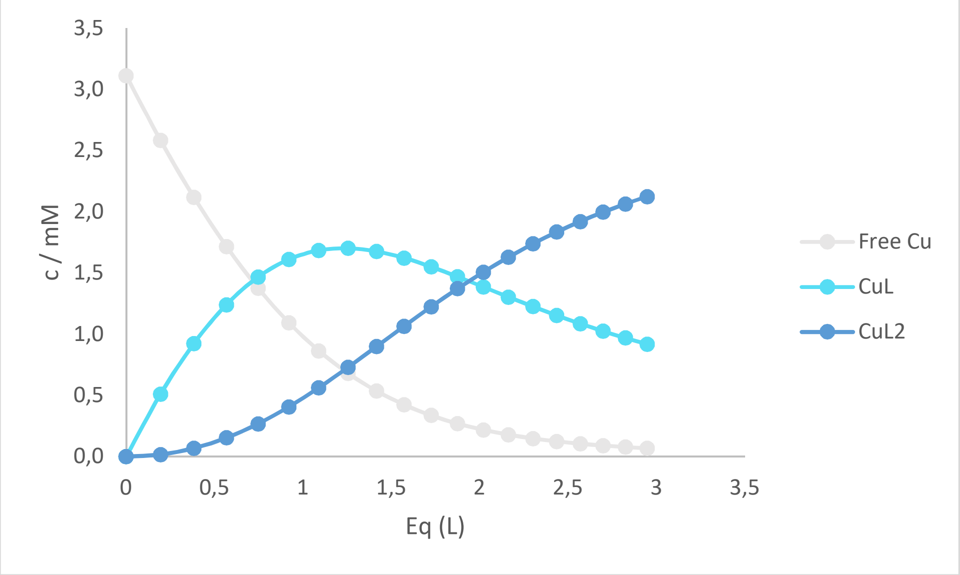

Figure S32. Species distribution for the titration of Cu(II) with ligand **10c**.

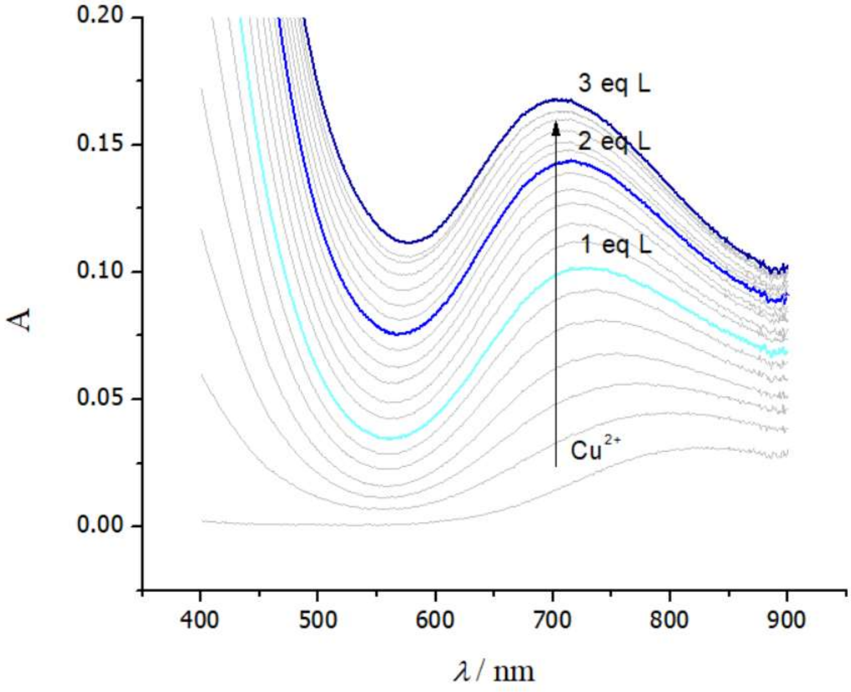

Figure S33. UV-Vis titration of Cu(II) with ligand **11a**.

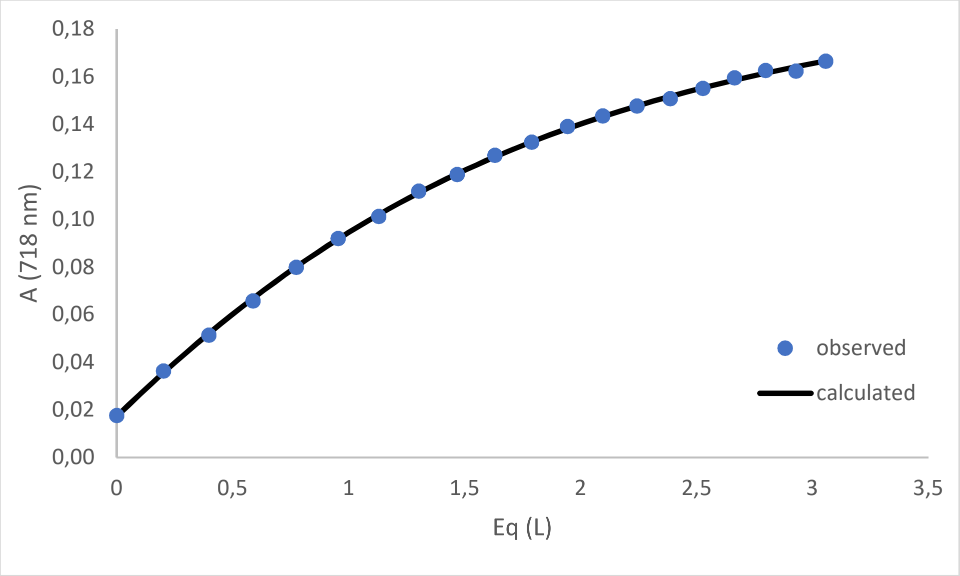

Figure S34. Curve fitting for the titration of Cu(II) with ligand **11a**.

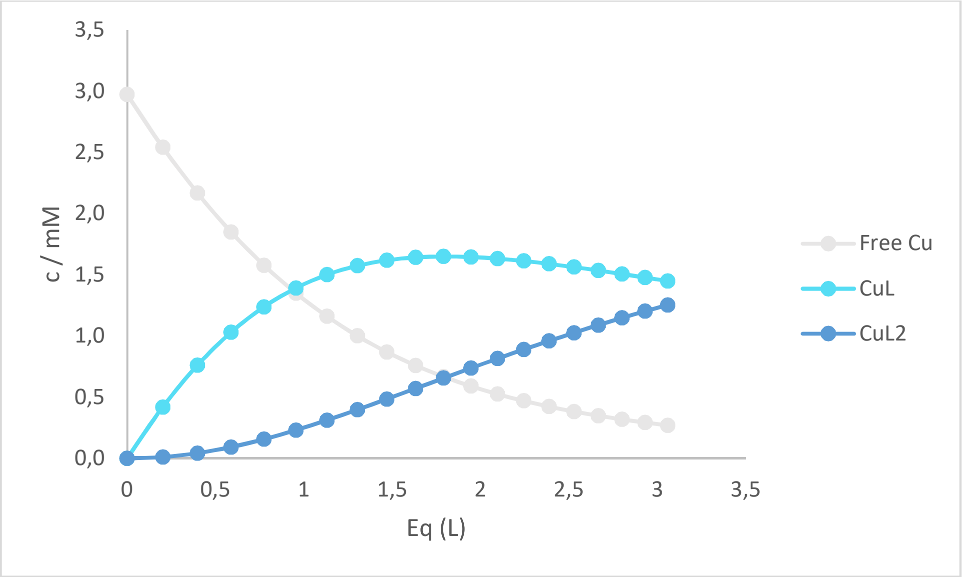

Figure S35. Species distribution for the titration of Cu(II) with ligand **11a**.

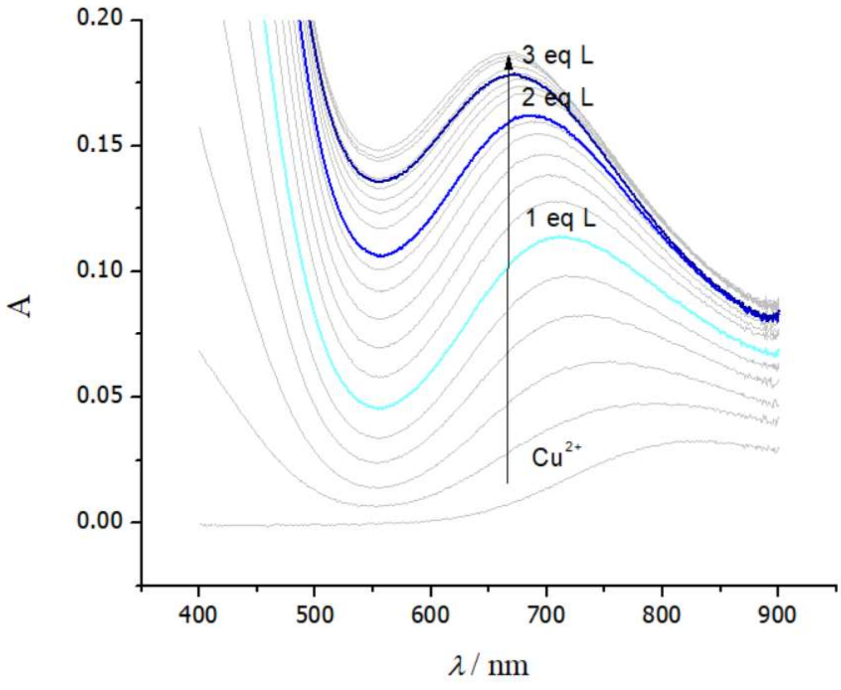

Figure S36. UV-Vis titration of Cu(II) with ligand **13a**.

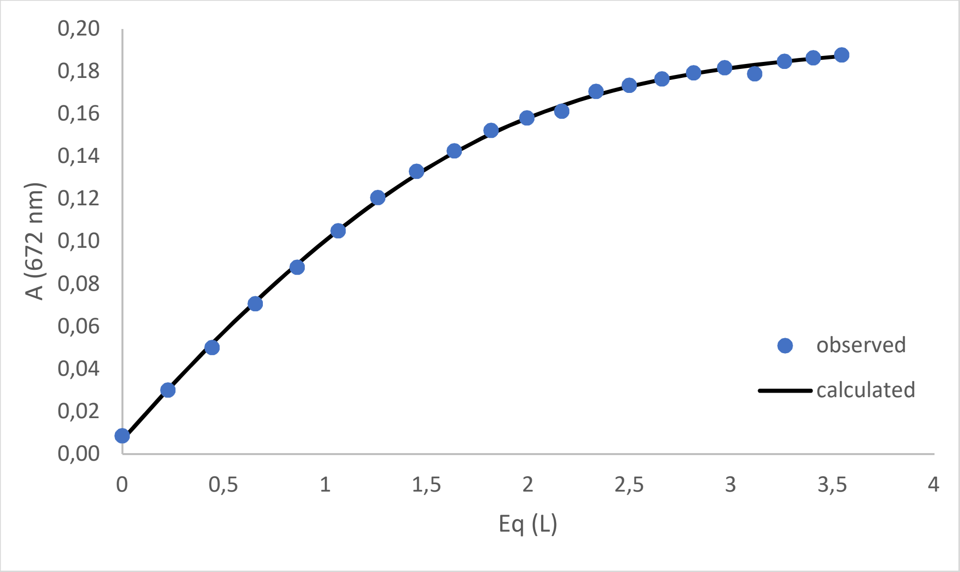

Figure S37. Curve fitting for the titration of Cu(II) with ligand **13a**.

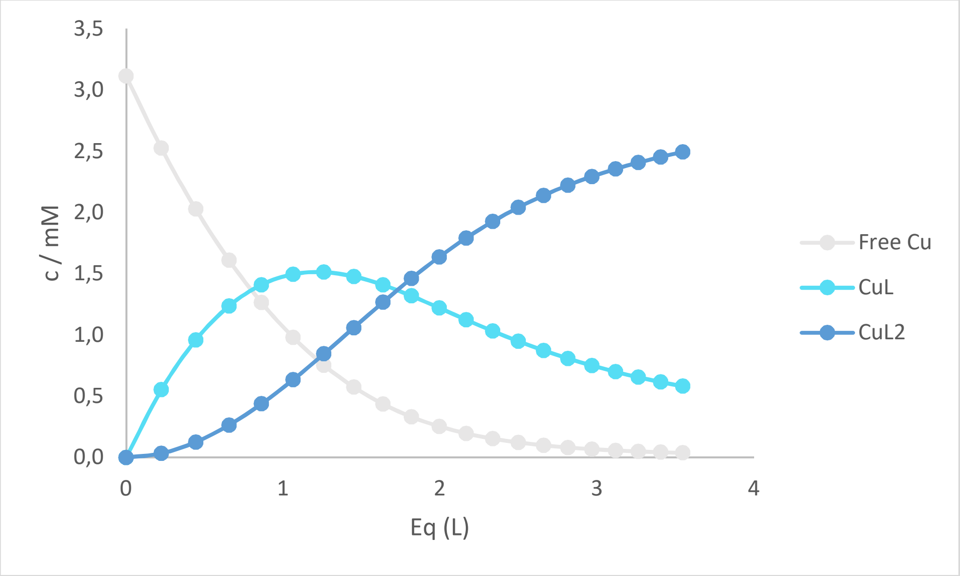

Figure S38. Species distribution for the titration of Cu(II) with ligand **13a**.

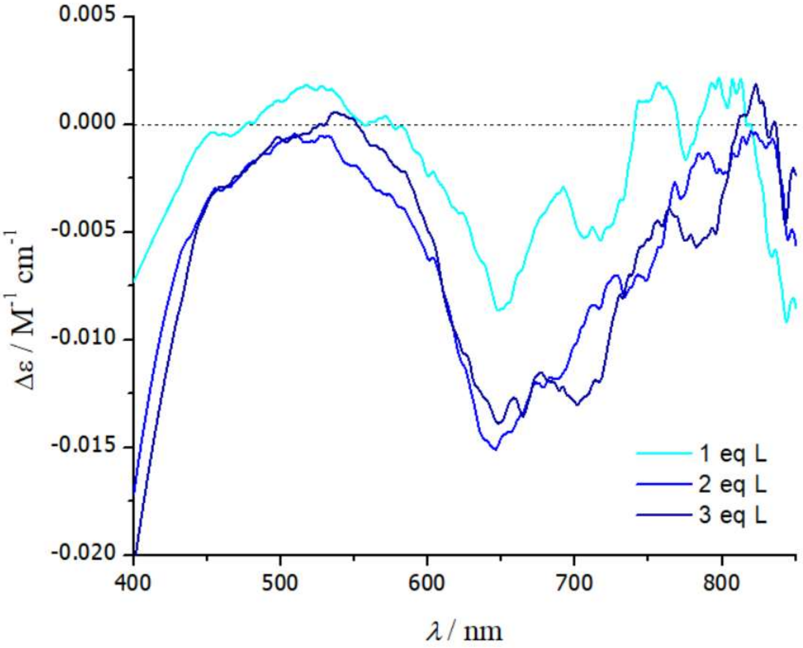

Figure S39. CD spectra of Cu(II) with 1, 2 and 3 added equivalents of ligand **13a** in a 1:1 CH_3OH:CH_2Cl_2 solvent mixture. The CD spectra were smoothed using the Savitzky-Golay method with 300 points of window and polynomial order 2. The observed CD signals are weak, however, the peak at 650 nm indicates transfer of chirality to the metal centre. Recording the spectra in higher concentrations was not possible due to limited solubility of the complex.

DFT calculations

Table S10. Selected bond lengths and angles for calculated Zn(II) complexes.

Complex	Isomer	M-N31 M-N31^i (Å)	M-N32 M-N32^i (Å)	M-N2 M-N2^i (Å)	N31-M-32 N31^i-M-N32^i (°)	N2-M-N2^i (°)	Coordination Geometry, RMSD / Å
[Zn(**14a**)$_2$]$^{2+}$	*cis-fac*	2.164 2.164	2.176 2.189	2.394 2.357	104.60 104.29	115.19	Octahedron (distorted) 0.638
	mer	2.207 2.205	2.212 2.219	2.272 2.289	150.89 150.00	165.89	Pentagonal bipyramid with a vacancy (equatorial) (distorted) 0.667
	trans-fac	2.197 2.197	2.260 2.261	2.282 2.282	96.18 96.23	165.00	Octahedron (distorted) 0.561
[Zn(**14b**)$_2$]$^{2+}$	*cis-fac*	2.147 2.159	2.168 2.208	2.603 2.441	95.89 93.76	109.98	Octahedron (distorted) 0.571
	mer	2.194 2.193	2.224 2.222	2.316 2.320	151.60 151.45	167.73	Octahedron (distorted) 0.649
	trans-fac	2.202 2.202	2.224 2.224	2.425 2.425	94.83 94.84	157.35	Pentagonal bipyramid with a vacancy (equatorial) (distorted) 0.663
[Zn(**14c**)$_2$]$^{2+}$	*cis-fac*	2.136 2.142	2.128 2.140	2.614 2.613	94.20 94.07	107.99	Octahedron (distorted) 0.555
	mer	2.140	2.155	2.679	137.51	168.99	Irregular (n/a)

		2.131	2.156	2.891	129.93		
	trans-fac	2.207 2.214	2.185 2.186	2.467 2.465	93.49 94.10	152.77	Pentagonal bipyramid with a vacancy (equatorial) (distorted) 0.671
[Zn(**14d**)$_2$]$^{2+}$	*cis-fac*	2.101 2.132	2.154 2.142	3.136 3.156	103.02 96.94	119.61	Tetrahedron (distorted) 0.586
	mer	2.158 2.158	2.140 2.140	2.876 2.876	132.42 132.43	163.29	Tetrahedron (distorted) 0.776
	trans-fac	2.141 2.165	2.187 2.181	2.877 2.570	97.85 91.00	150.60	Irregular (n/a)

[i] symmetry related atom

* For FindGeo analysis of calculated complexes, one donor N was changed to O in the input file, due to a bug in the program

Threshold coordination distance was set to 2.8 Å (default).

Table S11. Selected bond lengths and angles for calculated Cu(II) complexes.

Complex	Isomer	M-N31 M-N31^{i} (Å)	M-N32 M-N32^{i} (Å)	M-N2 M-N2^{i} (Å)	N31-M-32 N31^{i}-M-N32^{i} (°)	N2-M-N2^{i} (°)	Coordination Geometry, RMSD / Å
[Cu(**14a**)$_2$]$^{2+}$	*cis-fac*	2.064 2.041	2.067 2.299	2.494 2.164	96.44 104.59	113.36	Octahedron (distorted) 0.544
	mer	2.351 2.084	2.325 2.096	2.116 2.097	155.40 160.08	170.87	Octahedron (distorted) 0.508
	trans-fac	2.070 2.070	2.093 2.092	2.405 2.406	93.85 93.79	168.15	Octahedron (distorted) 0.526
[Cu(**14b**)$_2$]$^{2+}$	*cis-fac*	2.239 2.050	2.050 2.053	2.207 2.760	96.06 90.39	111.22	Octahedron (distorted) 0.526
	mer	2.092 2.092	2.070 2.070	2.436 2.437	151.00 151.00	170.82	Octahedron (distorted) 0.648
	trans-fac	2.075 2.076	2.056 2.056	2.621 2.624	92.82 92.83	157.07	Pentagonal bipyramid with a vacancy (equatorial) (distorted) 0.676
[Cu(**14c**)$_2$]$^{2+}$	*cis-fac*	2.029 2.022	2.047 2.204	2.724 2.278	89.90 97.77	105.57	Octahedron (distorted) 0.500
	mer	2.060 2.060	2.034 2.034	2.523 2.522	149.65 149.70	168.90	Octahedron (distorted) 0.679

	trans-fac	2.058 2.071	2.051 2.042	2.670 2.561	91.60 92.10	156.90	Pentagonal bipyramid with a vacancy (equatorial) (distorted) 0.638
$[Cu(\mathbf{14d})_2]^{2+}$	*cis-fac*	2.123 2.121	2.145 2.187	3.059 3.188	99.71 95.82	121.27	Tetrahedron (distorted) 0.568
	mer	2.141 2.121	2.147 2.122	3.289 3.200	123.30 125.81	167.15	Tetrahedron (regular) 0.399
	trans-fac	2.043 2.037	2.063 2.083	3.066 3.206	91.85 90.48	173.68	Square plane (regular) 0.115

[i] symmetry related atom

* For FindGeo analysis of calculated complexes, one donor N was changed to O in the input file, due to a bug in the program

If not noted otherwise, the threshold coordination distance was set to 2.8 Å

Table S12. Selected bond lengths and angles for calculated Cu(II) complexes.

Complex	denticity	Cu-N1_1 (Å)	Cu-N1_2 (Å)	Cu-X[a] (Å)	N1_1-Cu-N1_2 (°)	X-Cu-X[a] (°)	Coordination Geometry, RMSD / Å
$[Cu(\mathbf{8a})_2]^{2+}$	3	2.056 2.056	2.059 2.059	2.404 2.404	85.89 85.89	180.00	Octahedron (regular) 0.088
$[Cu(\mathbf{8a})_2]^{2+}$	2	2.058 2.058	2.062 2.062	2.316 2.316	84.92 84.93	180.00	Octahedron (regular) 0.159
$[Cu(\mathbf{8d})_2]^{2+}$	3	2.057 2.057	2.058 2.058	2.399 2.401	85.76 85.91	179.38	Octahedron (regular) 0.091
$[Cu(\mathbf{8d})_2]^{2+}$	2	2.056 2.056	2.067 2.067	2.339 2.339	85.38 85.38	180.00	Octahedron (regular) 0.165

[a] X = N3 in tridentate ligands and X = O1 in bidentate ligands.

Calculated UV-Vis spectra

UV-Vis spectra were calculated for all three isomers of complex **[Cu(14d)$_2$]$^{2+}$**. The results show that the spectra are similar for *mer* and *cis-fac* complexes, showing two peaks, while the *trans-fac* isomer showed a significantly different spectrum, showing one peak due to the higher symmetry of the *trans-fac* isomer.[3]

The calculated spectra could not be directly compared to the experimental spectra (UV-Vis titration of Cu(II) with **10c**, FigureS30), as the experimental spectra show a mixture of complexes of **ML** and **ML$_2$** stoichiometry (Figure S32). However, at 3 equiv of added ligand, where the composition of the solution was found to be 2% free Cu, 30% **ML** and 68% **ML$_2$**, the absorption maximum at 647 nm was closest to the value calculated for the *trans-fac* isomer (645 nm).

Table S13. Calculated UV-Vis spectra for different isomers of complex **[Cu(14d)$_2$]$^{2+}$**.

Isomer	λ_{max} / nm	Calculated spectrum
cis-fac	283, 485	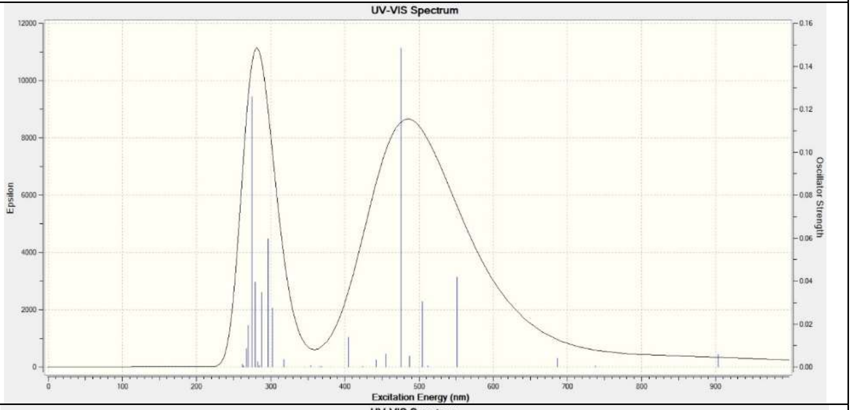
mer	280, 496	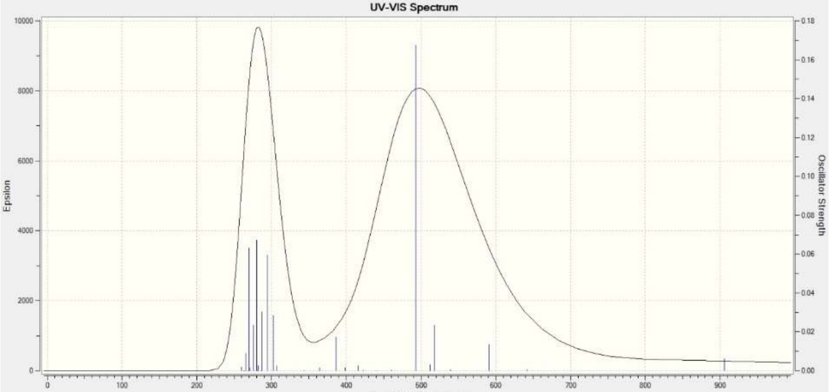
trans-fac	317, 645	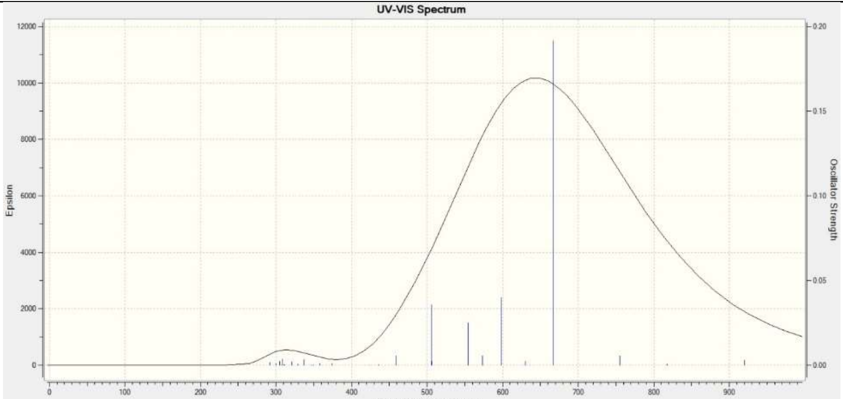

NMR spectra of compounds **1** and **7**

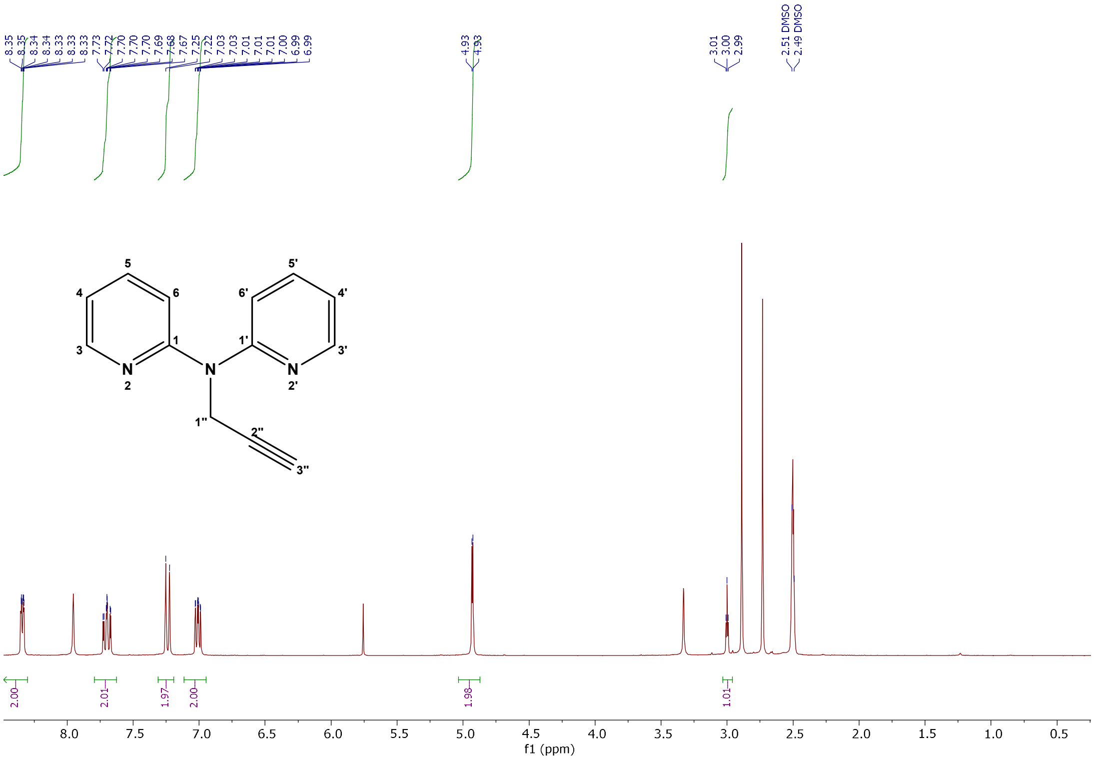

Figure S40. ^{1}H NMR (DMSO) spectrum of **1**.

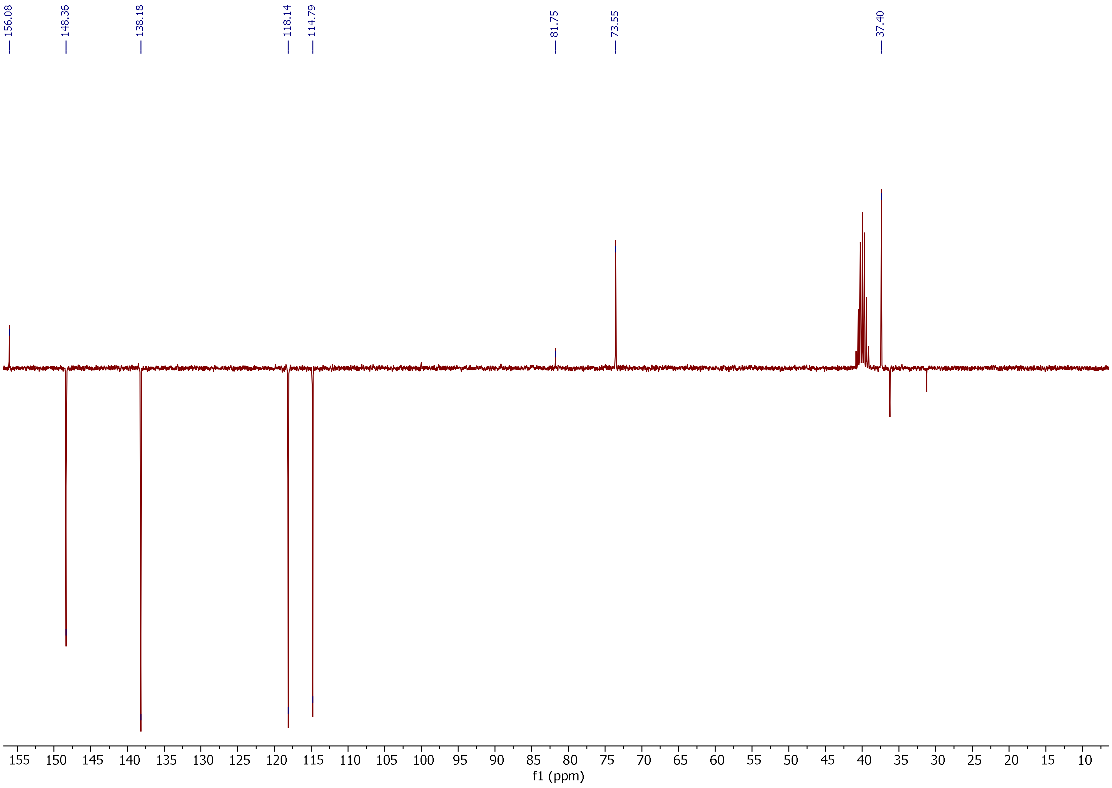

Figure S41. ^{13}C NMR (DMSO) spectrum of **1**.

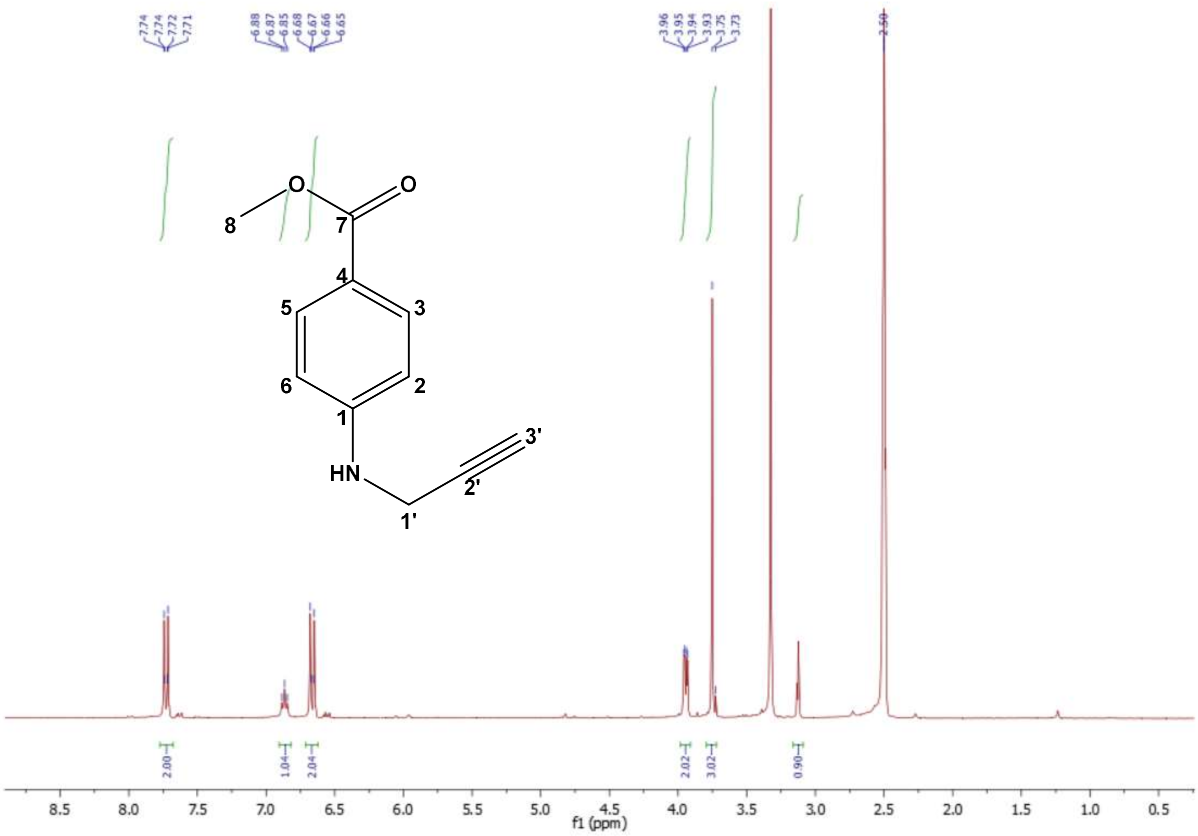

Figure S42. ^{1}H NMR (DMSO) spectrum of **6**.

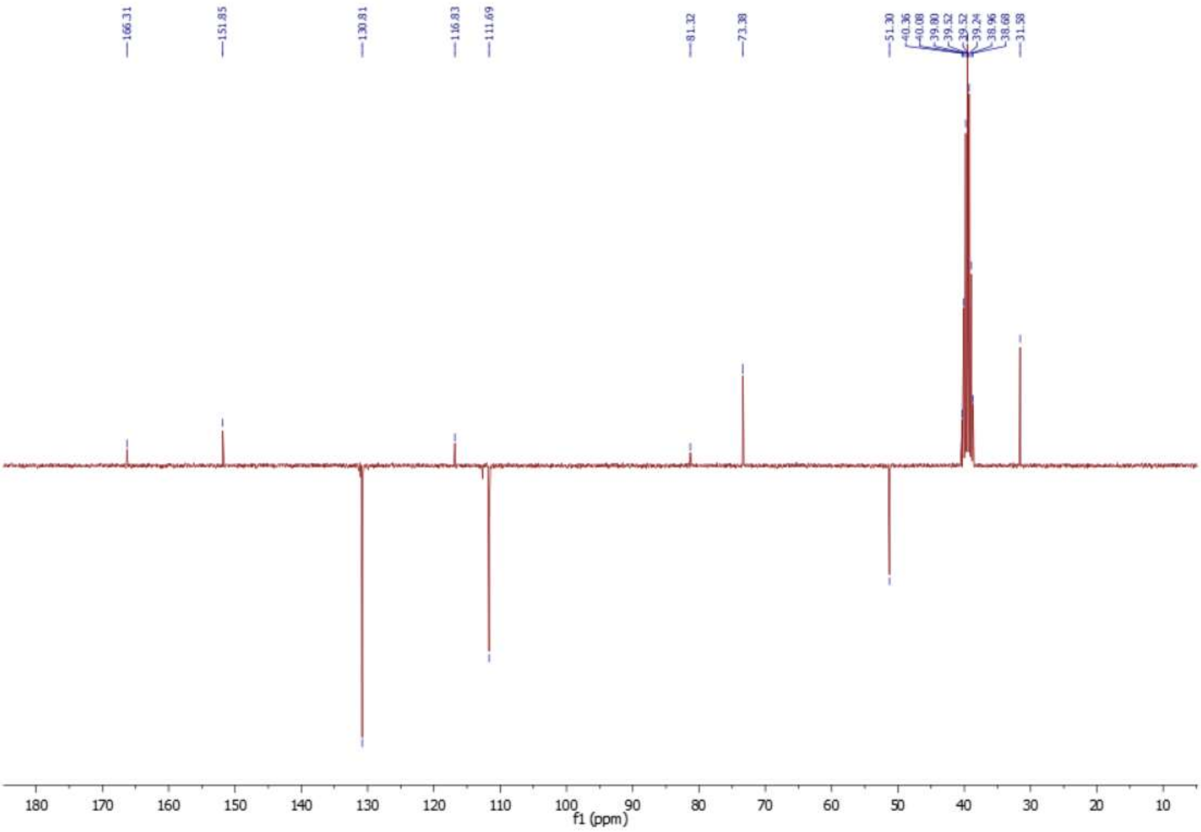

Figure S43. ^{13}C NMR (DMSO) spectrum of **6**.

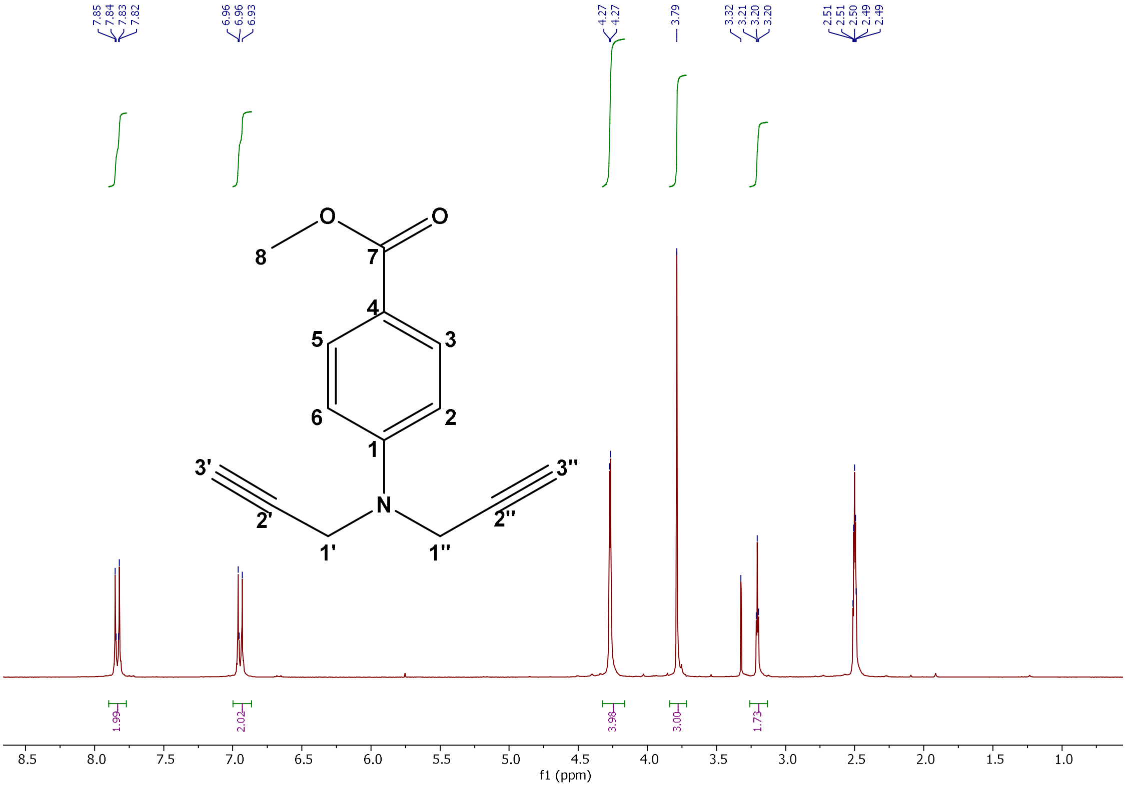

Figure S44. ^{1}H NMR (DMSO) spectrum of **7**.

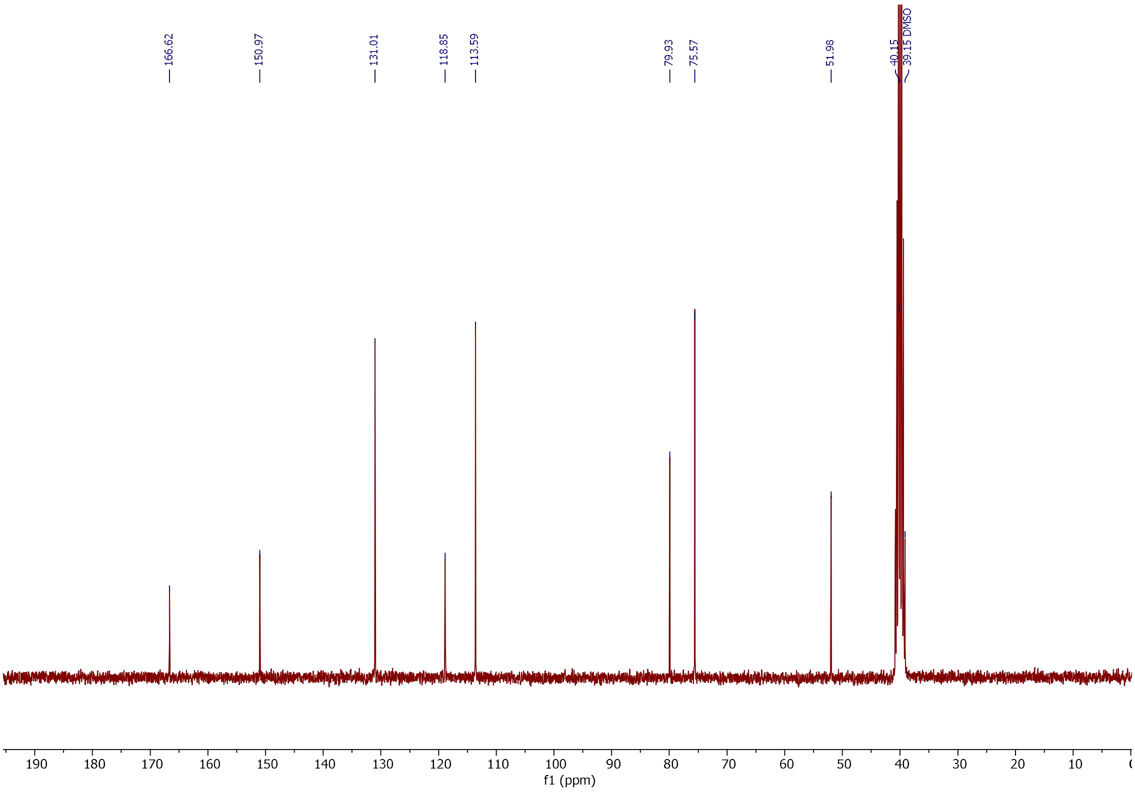

Figure S45. ^{13}C NMR (DMSO) spectrum of **7**.

NMR spectra of ligands **8a**-**13a**

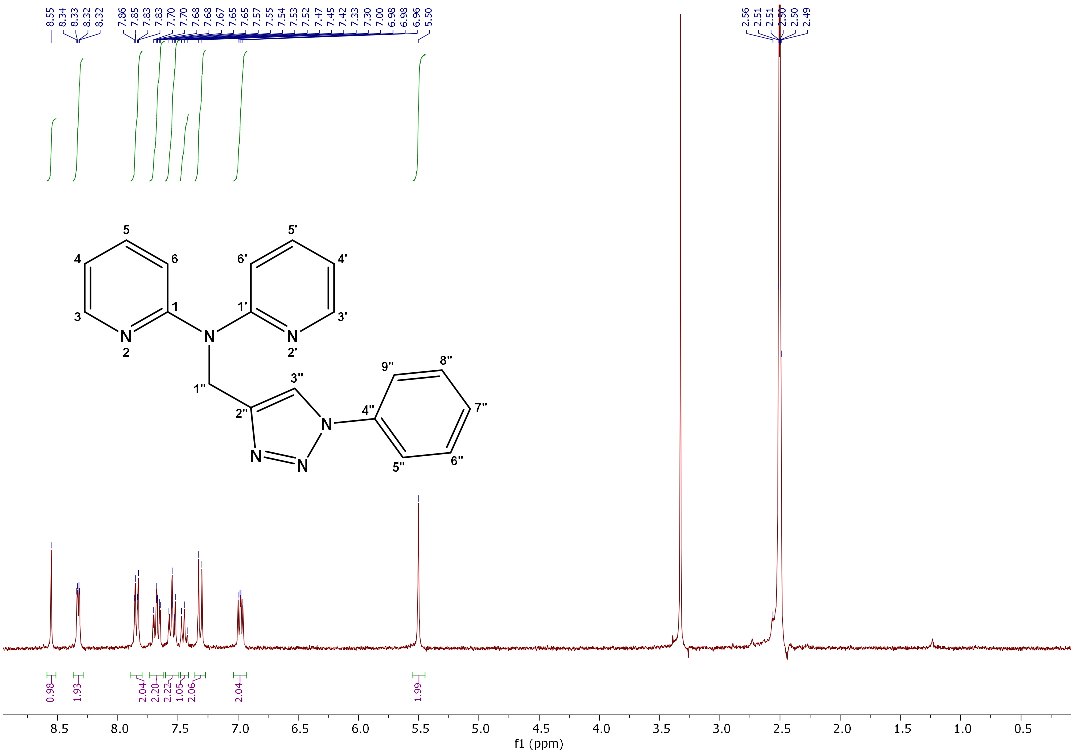

Figure S46. ^{1}H NMR (DMSO) spectrum of **8a**.

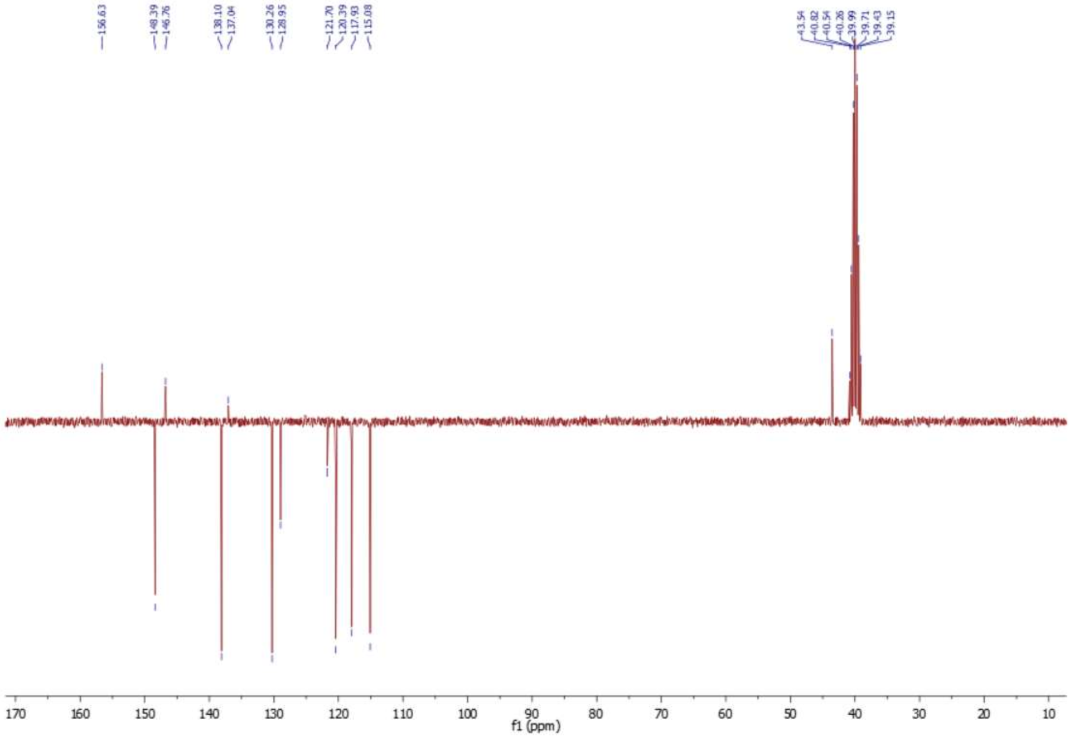

Figure S47. ^{13}C NMR (DMSO) spectrum of **8a**.

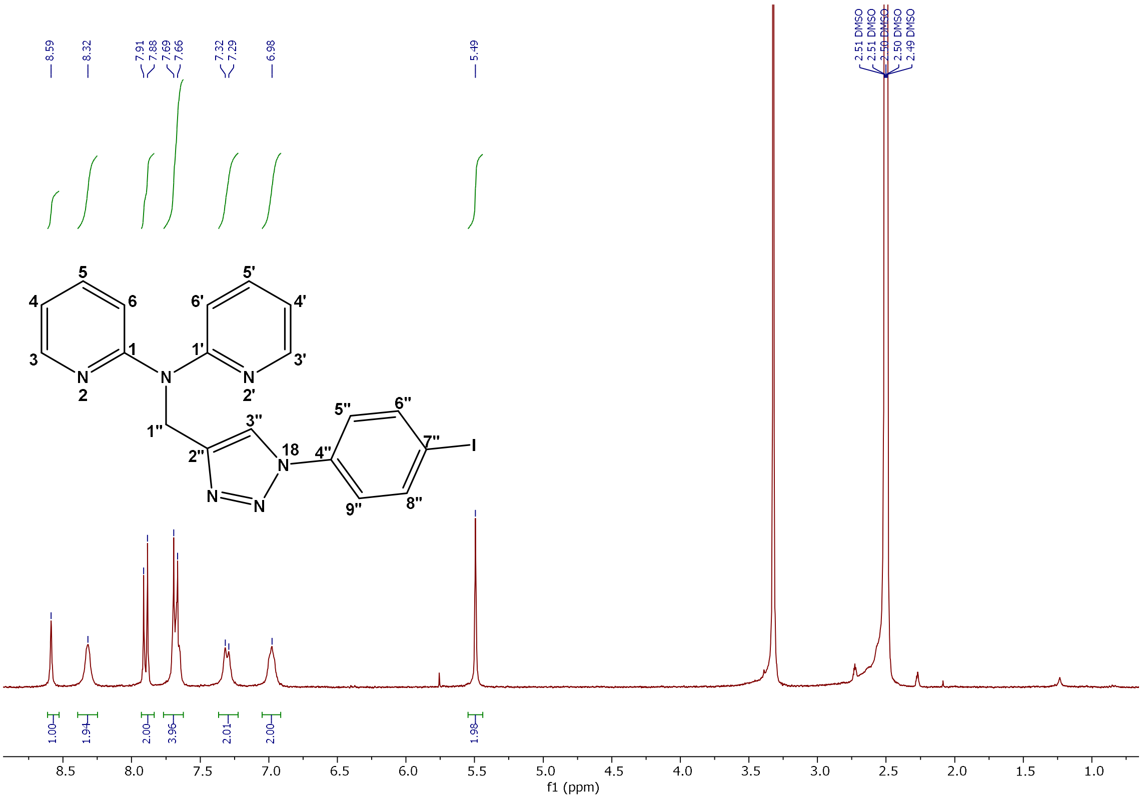

Figure S48. ^{1}H NMR (DMSO) spectrum of **8b**.

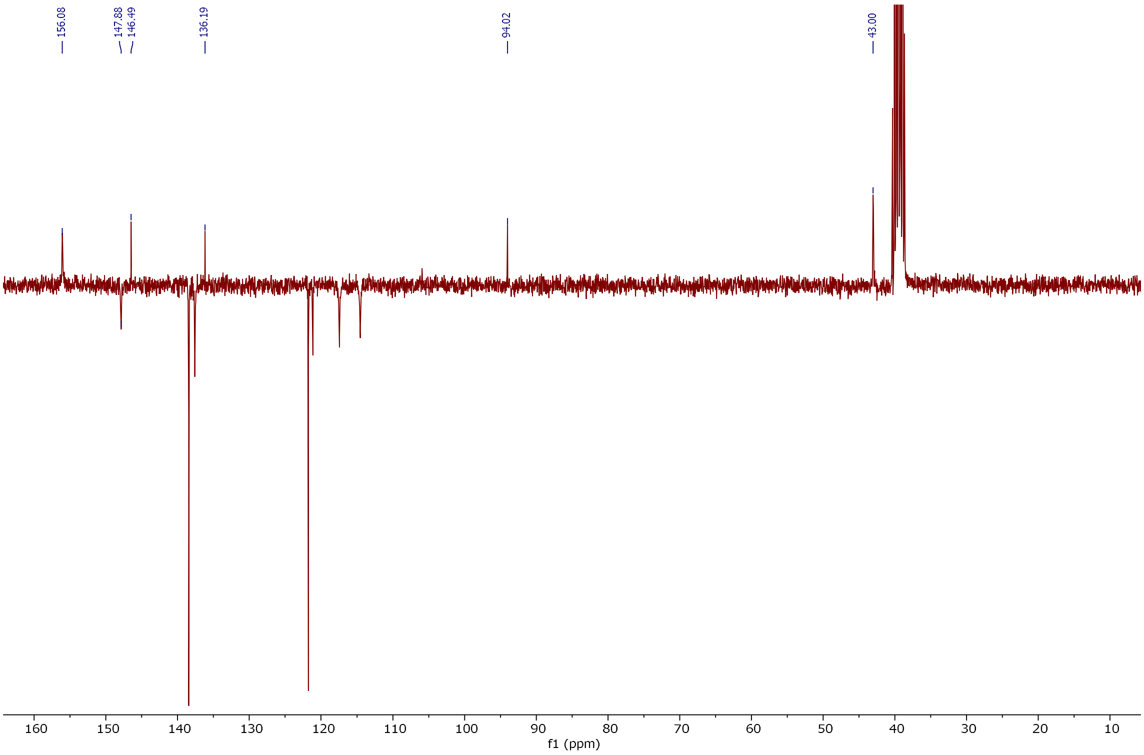

Figure S49. ^{13}C NMR (DMSO) spectrum of **8b**.

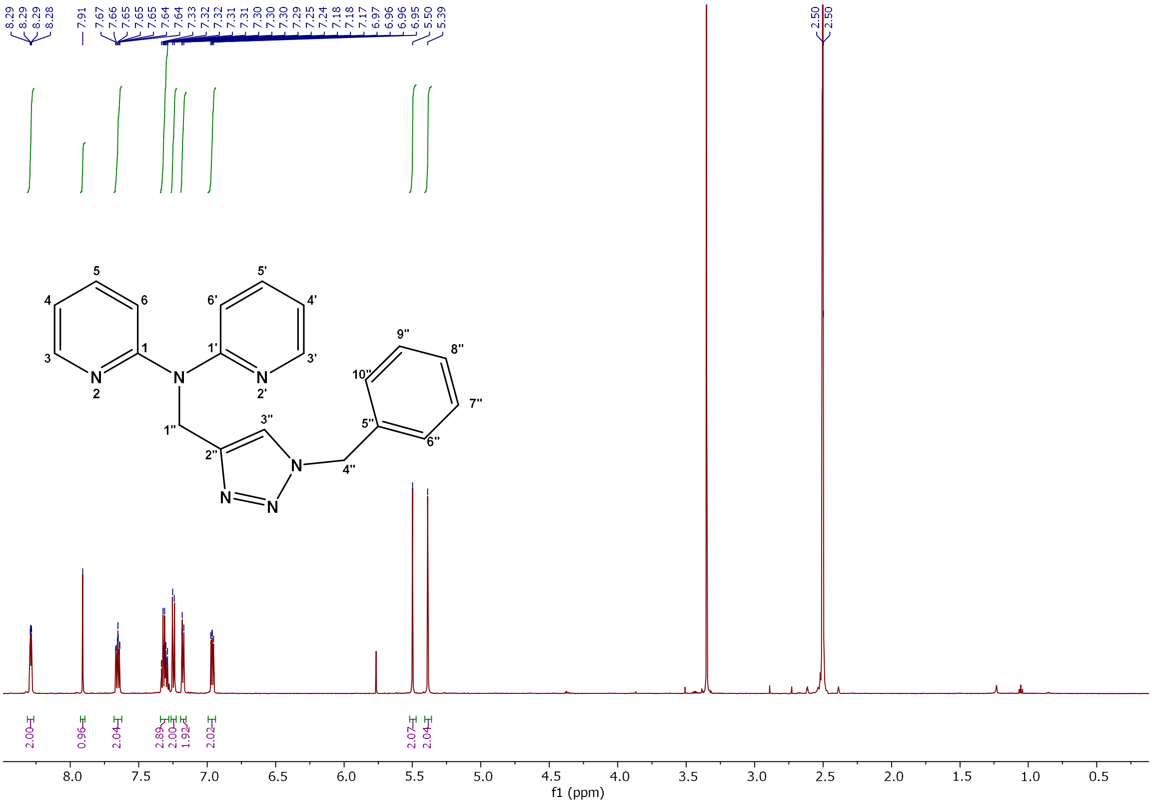

Figure S50. ^{1}H NMR (DMSO) spectrum of **8c**.

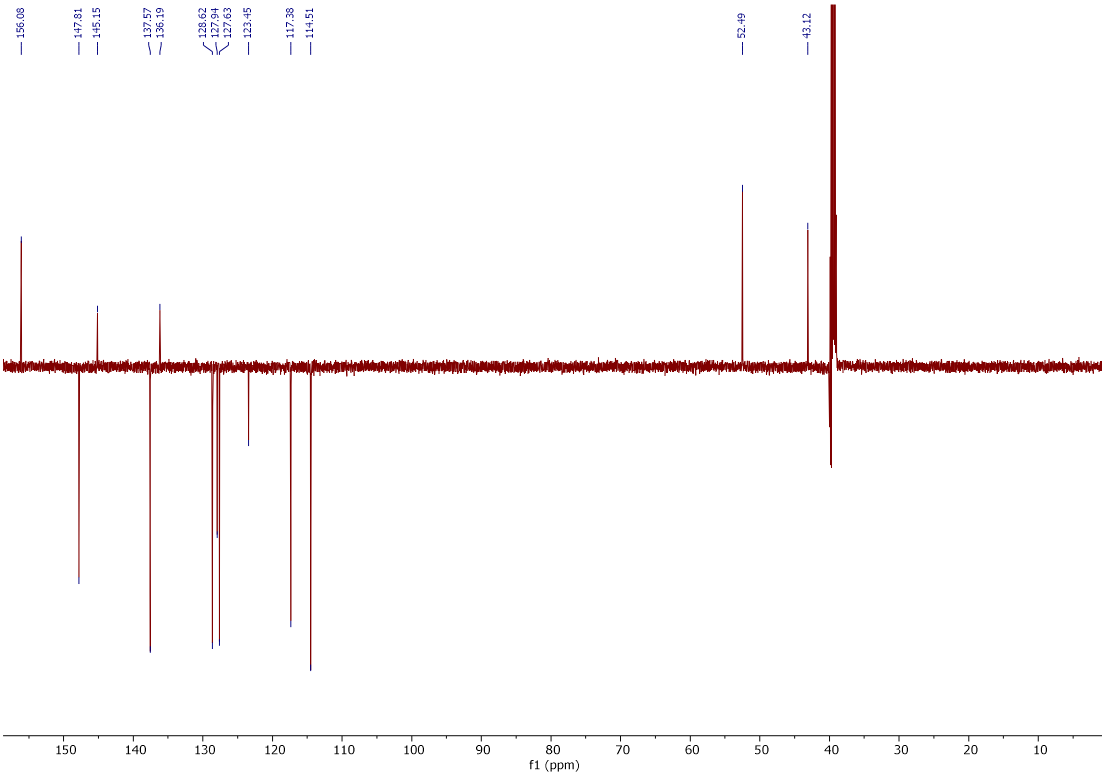

Figure S51. ^{13}C NMR (DMSO) spectrum of **8c**.

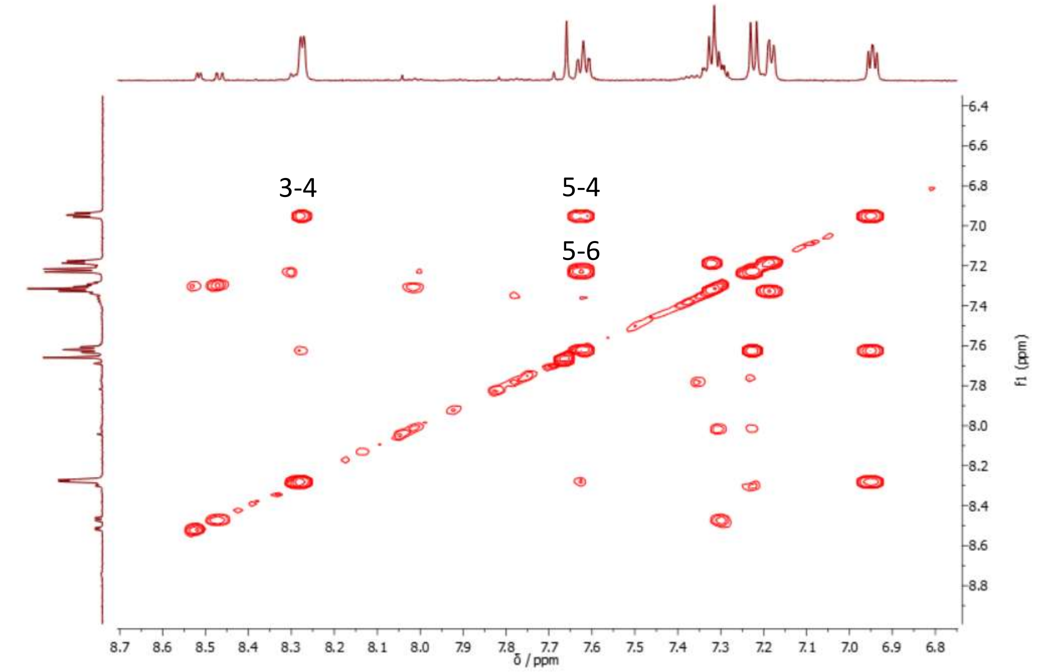

Figure S52. ^{1}H-^{1}H COSY (CD$_3$CN) spectrum of **8c.**

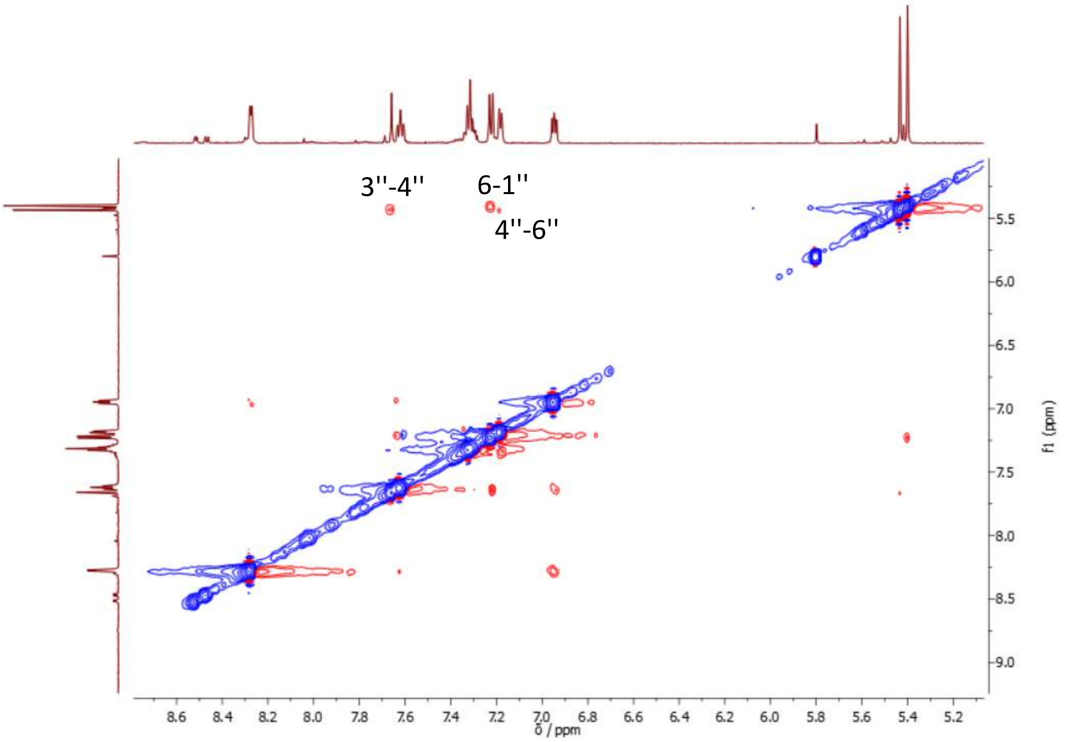

Figure S53. ^{1}H-^{1}H NOESY (CD$_3$CN) spectrum of **8c.**

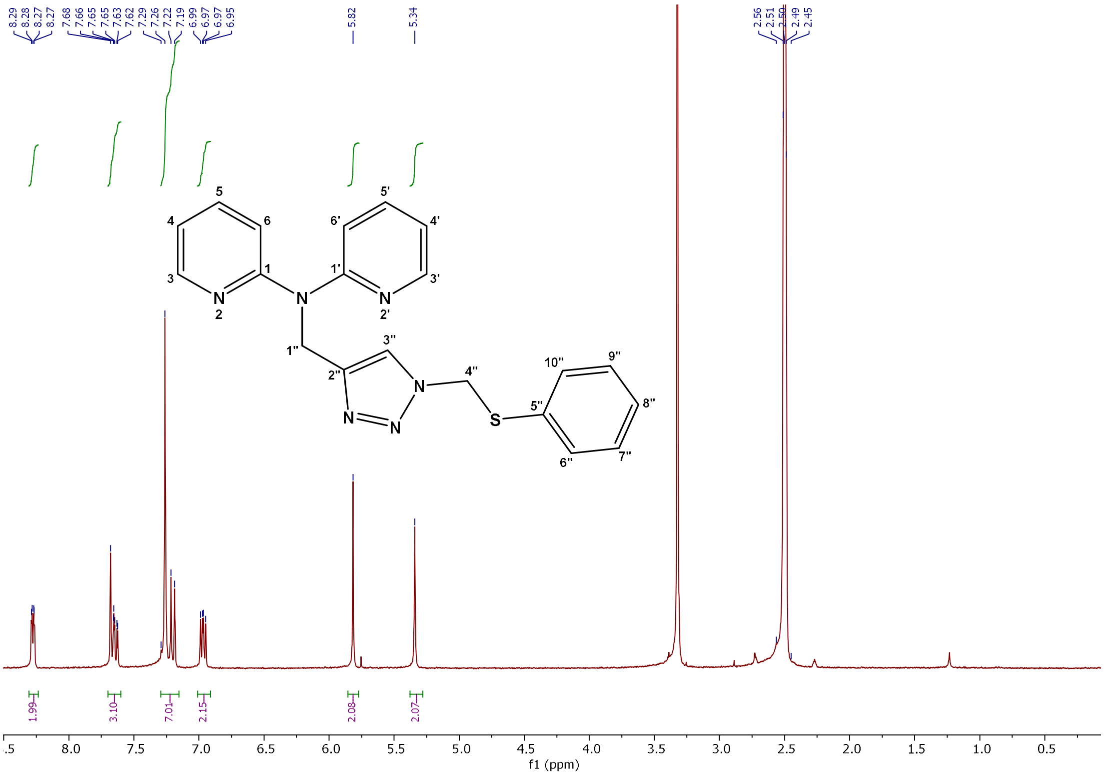

Figure S54. ^{1}H NMR (DMSO) spectrum of **8d**.

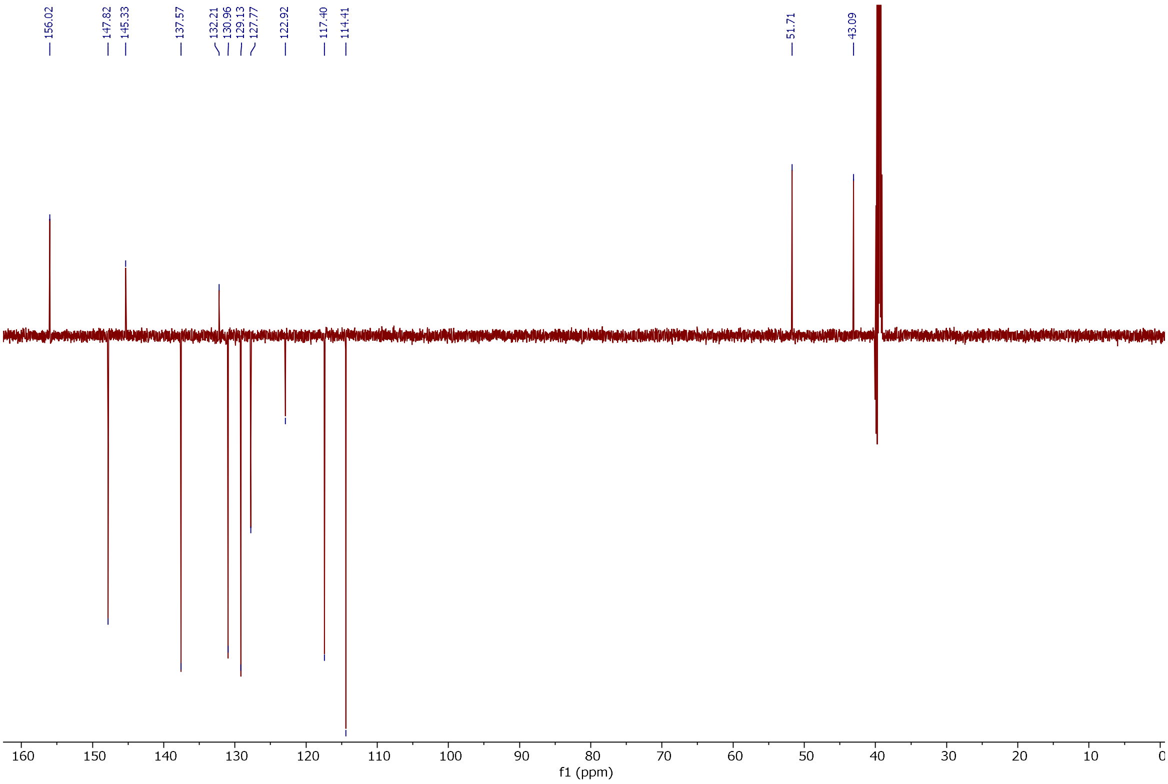

Figure S55. ^{13}C NMR (DMSO) spectrum of **8d**.

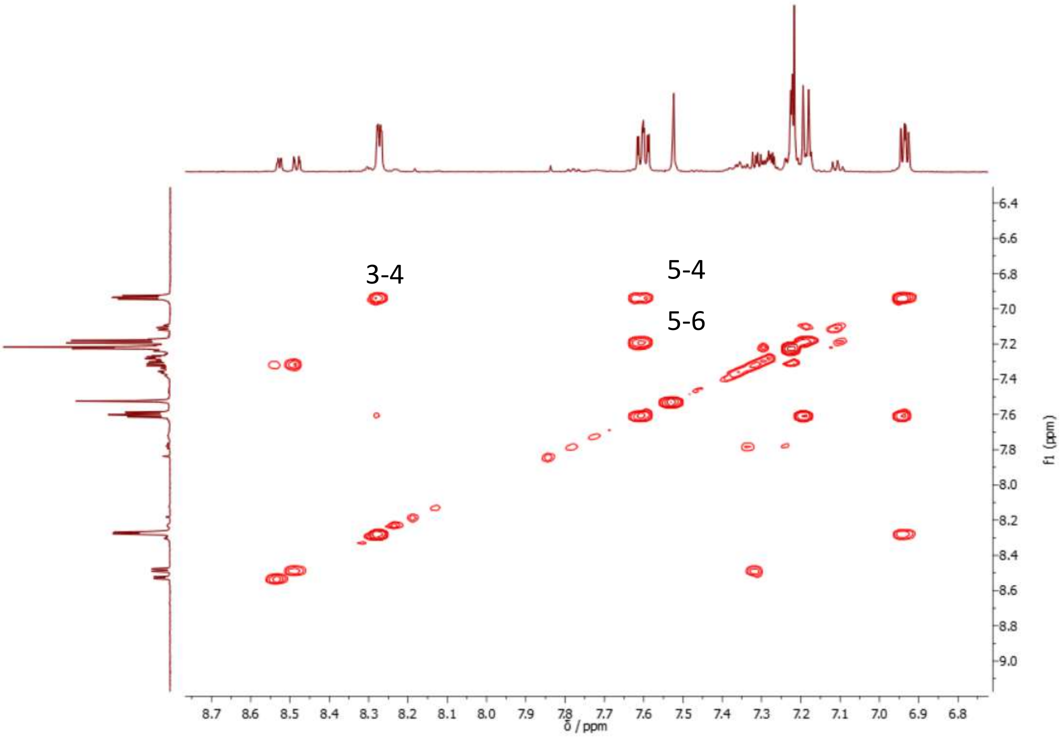

Figure S56. ^{1}H-^{1}H COSY (CD$_3$CN) spectrum of **8d.**

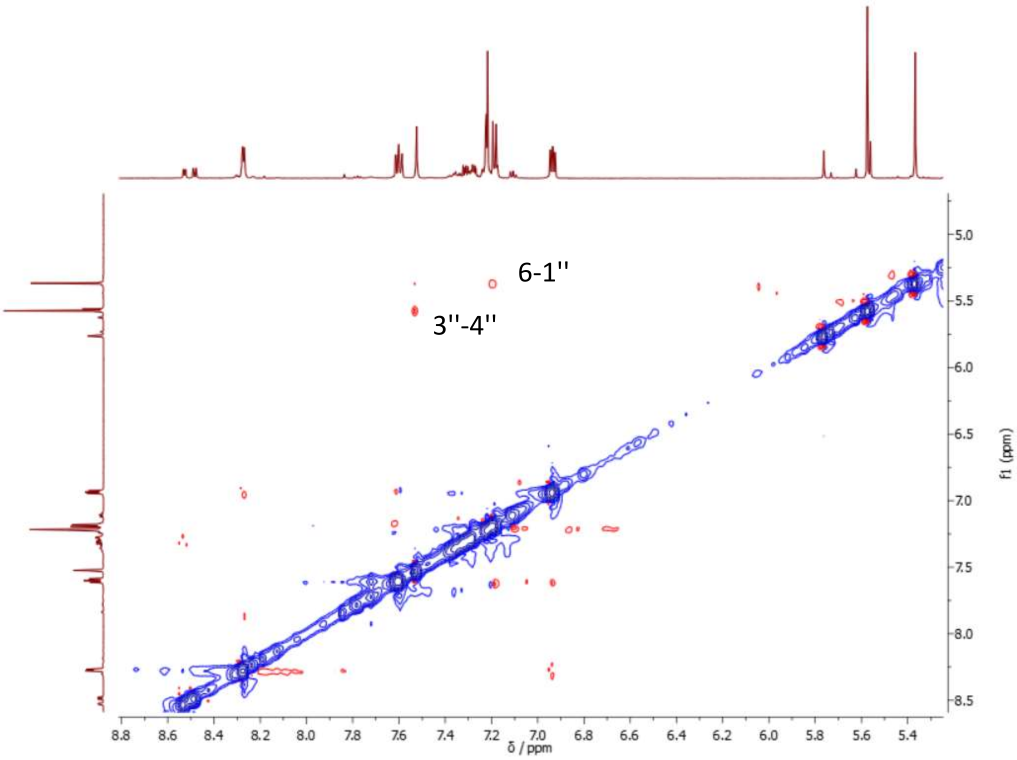

Figure S57. ^{1}H-^{1}H NOESY (CD$_3$CN) spectrum of **8d.**

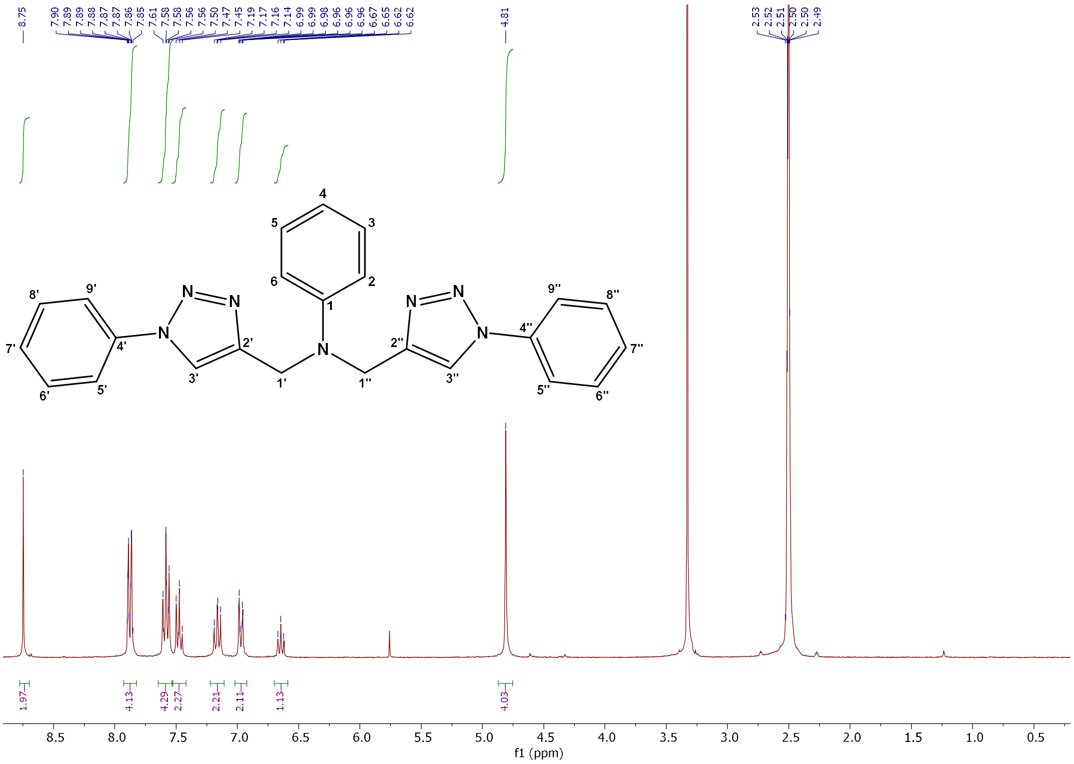

Figure S58. ^{1}H NMR (DMSO) spectrum of **9a**.

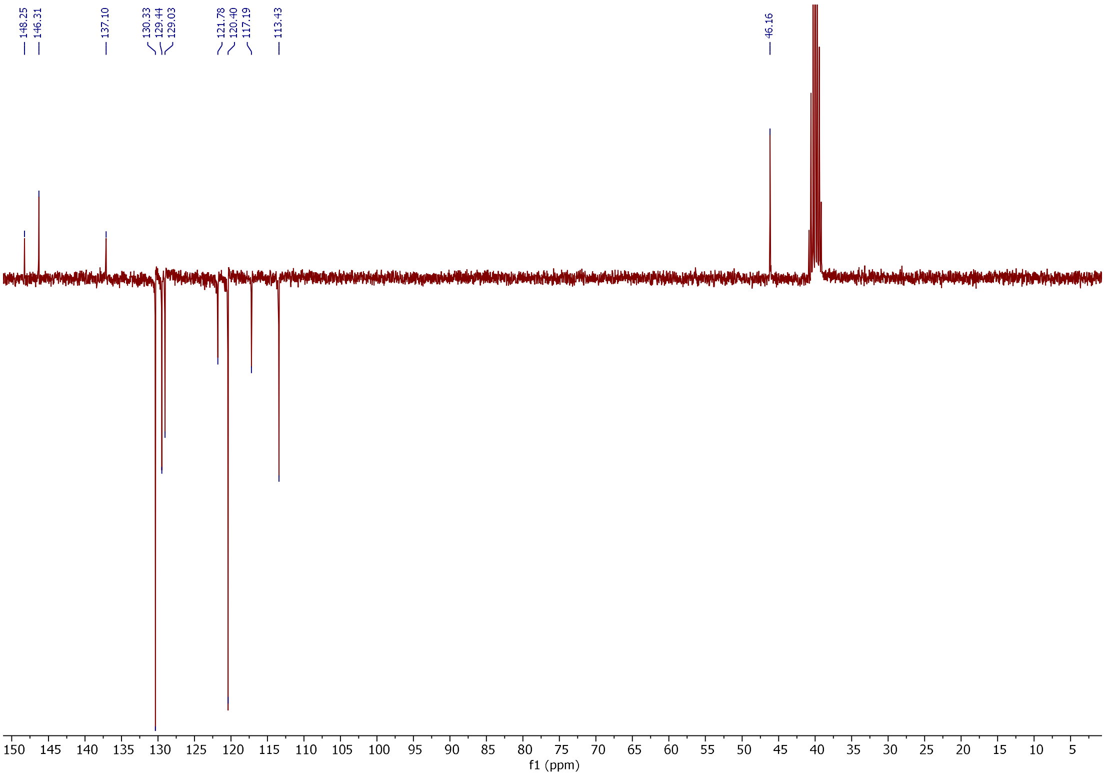

Figure S59. ^{13}C NMR (DMSO) spectrum of **9a**.

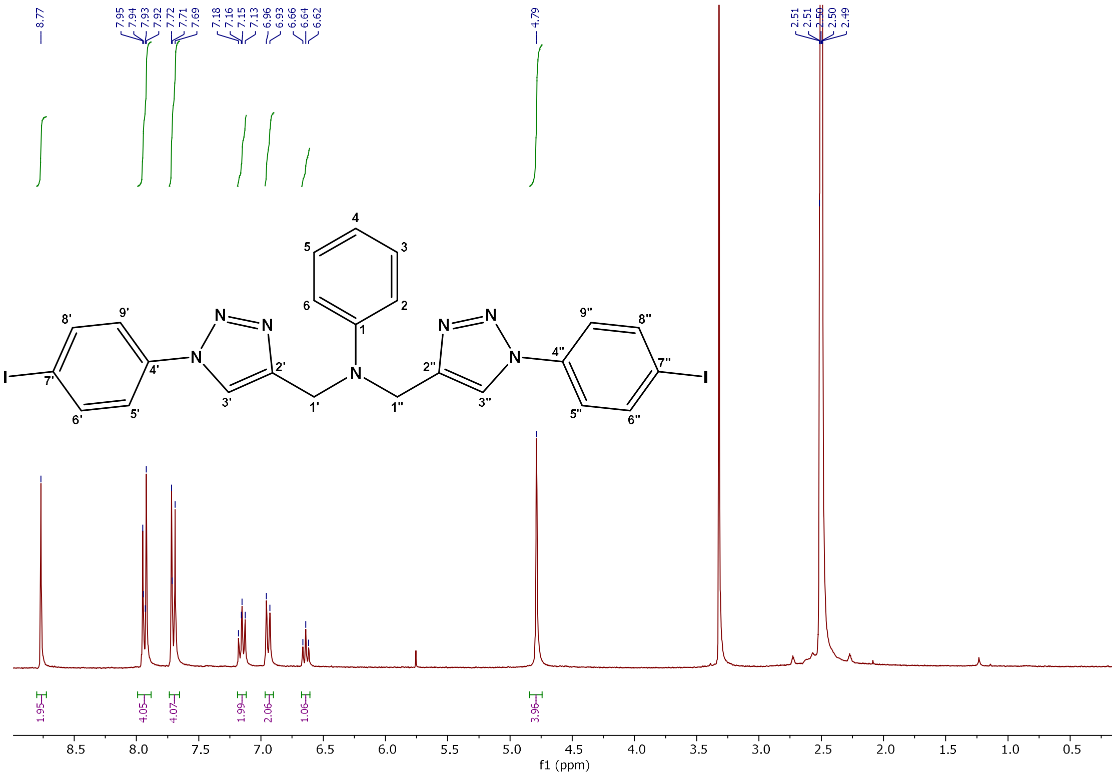

Figure S60. ^{1}H NMR (DMSO) spectrum of **9b**.

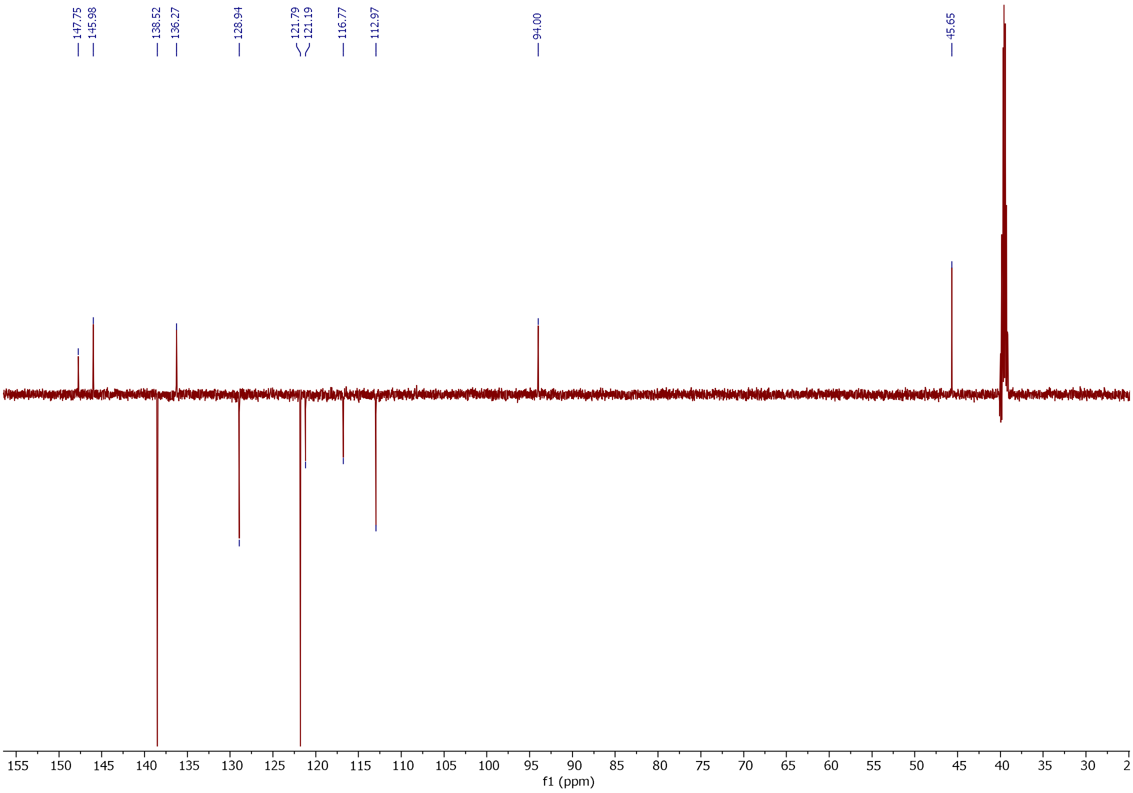

Figure S61. ^{13}C NMR (DMSO) spectrum of **9b**.

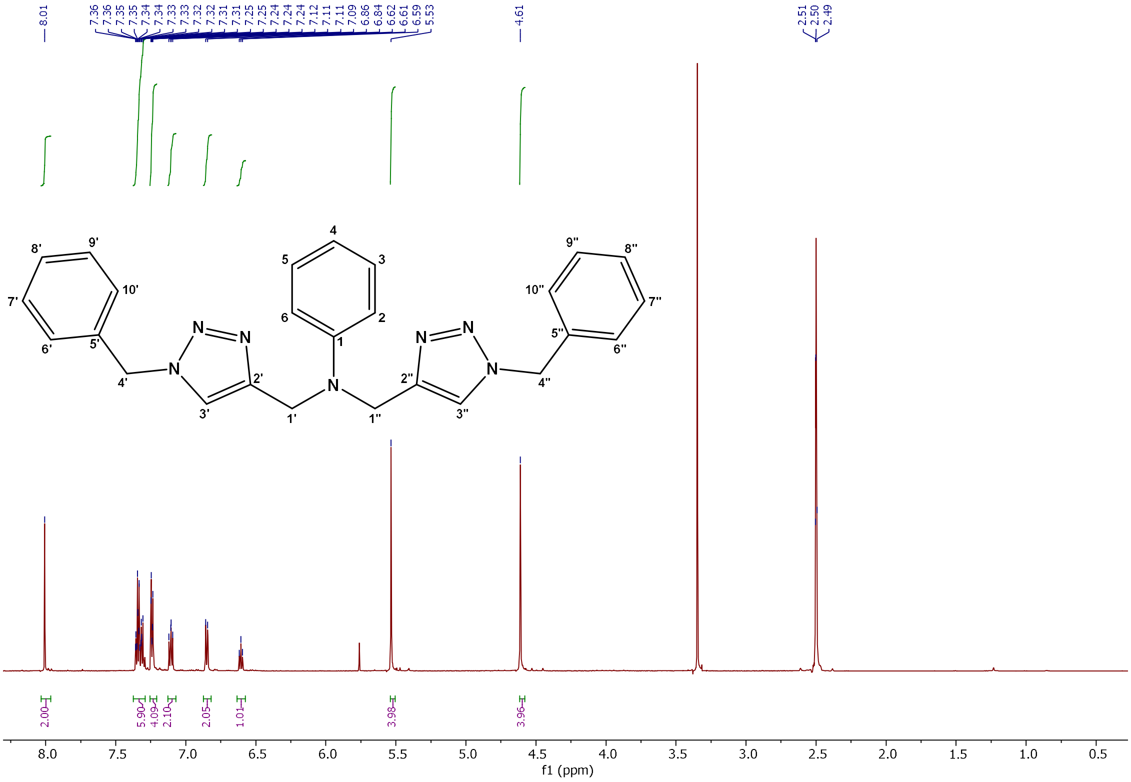

Figure S62. ^{1}H NMR (DMSO) spectrum of **9c**.

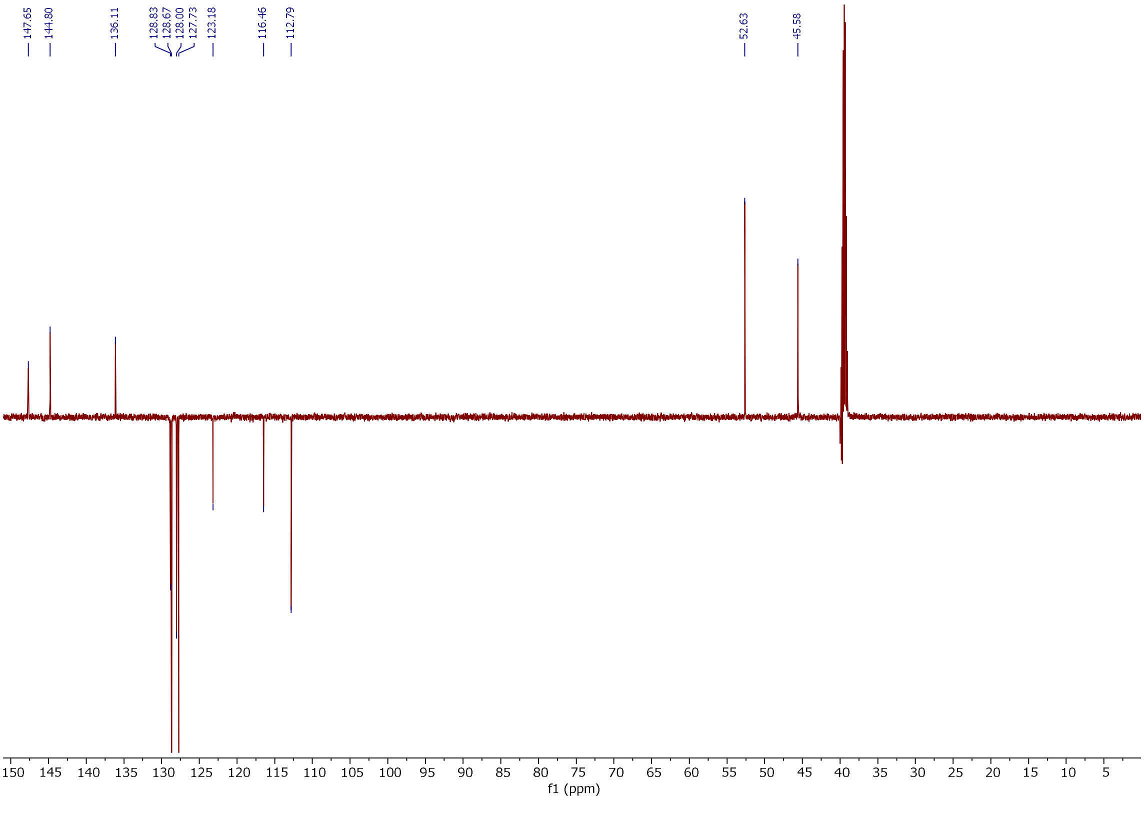

Figure S63. ^{13}C NMR (DMSO) spectrum of **9c**.

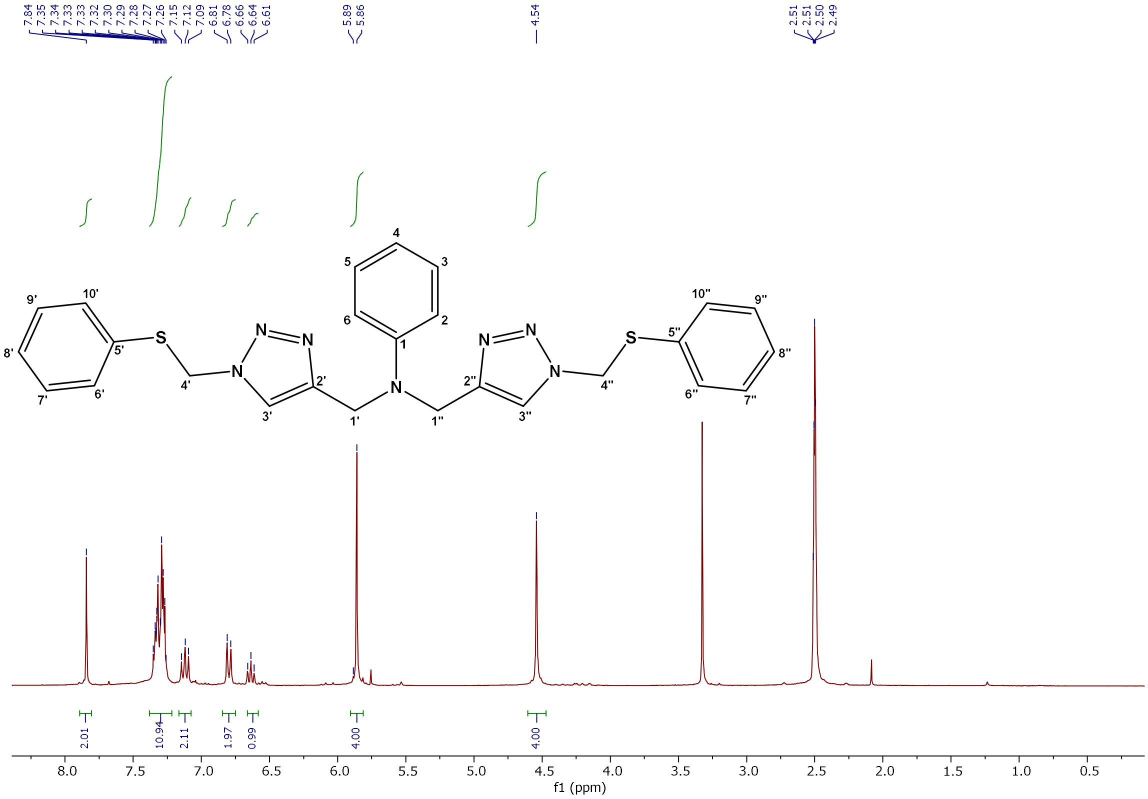

Figure S64. ^{1}H NMR (DMSO) spectrum of **9d**.

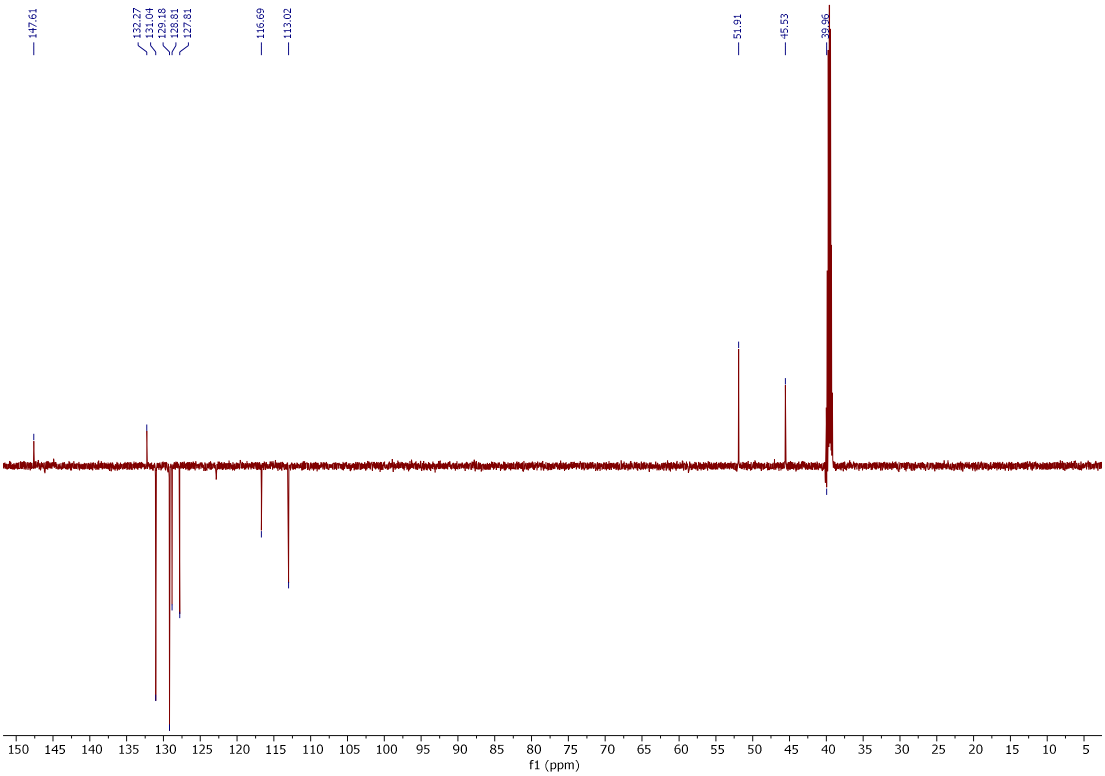

Figure S65. ^{13}C NMR (DMSO) spectrum of **9d**.

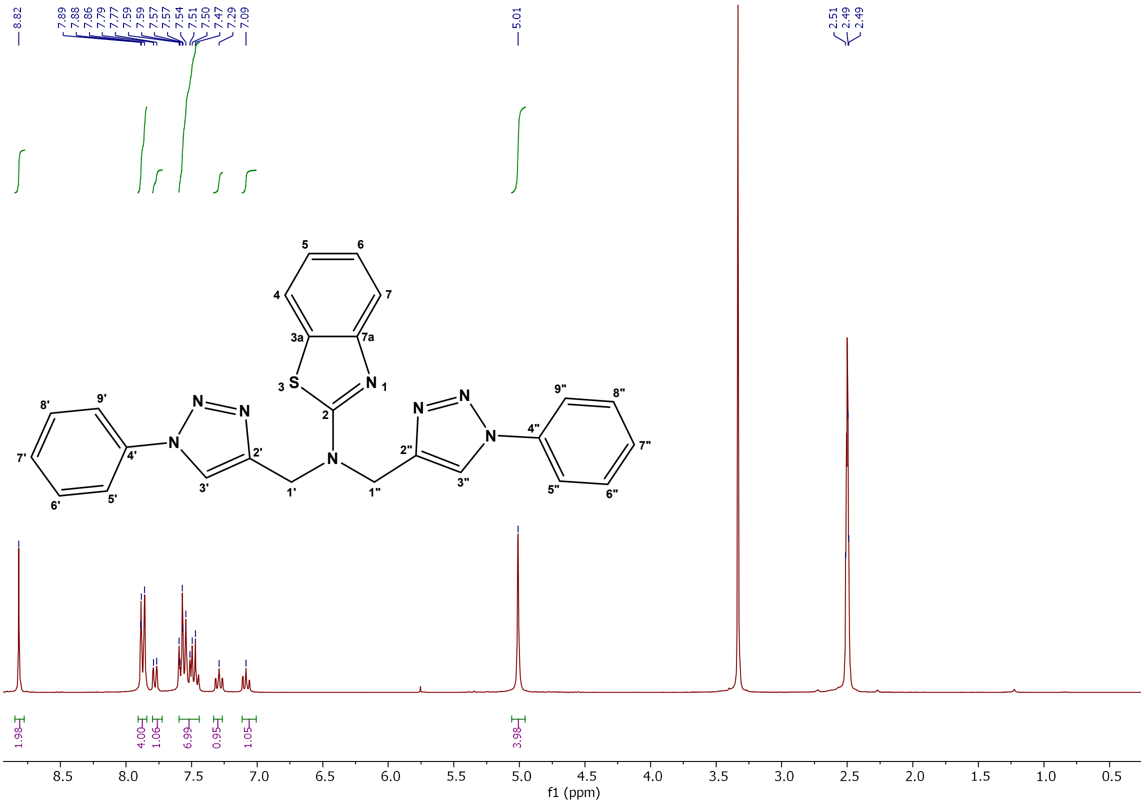

Figure S66. ^{1}H NMR (DMSO) spectrum of **10a**.

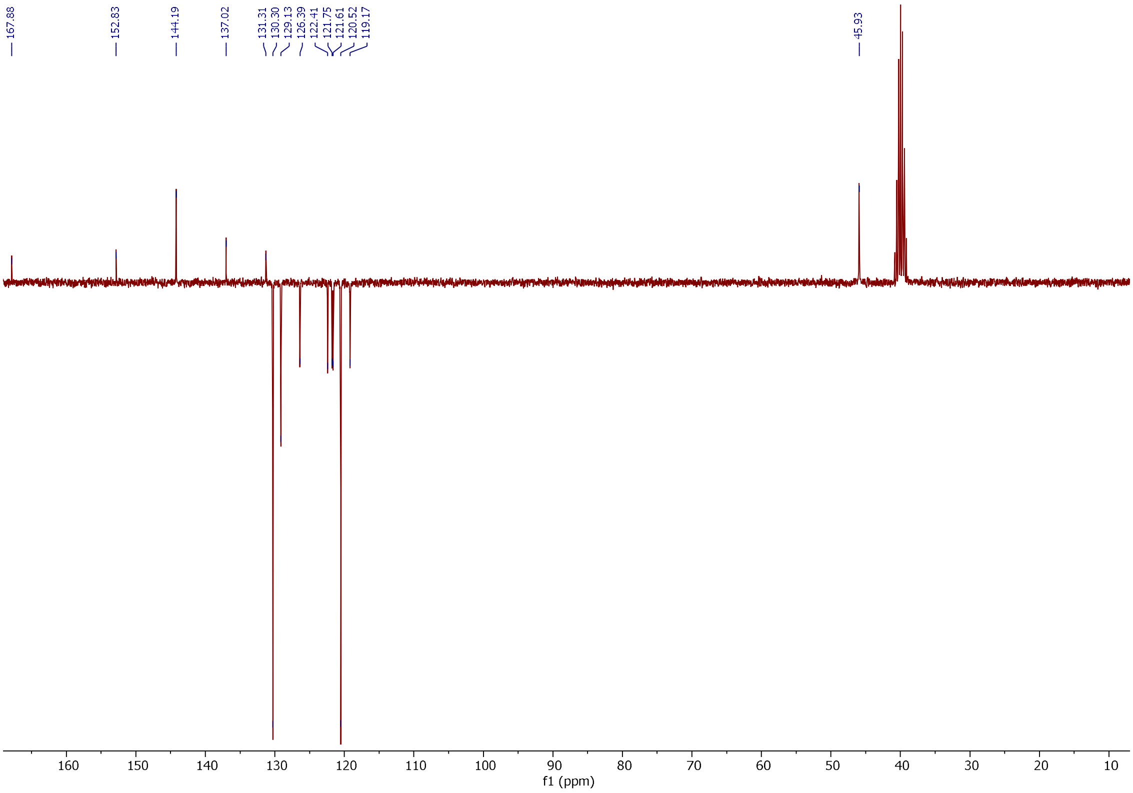

Figure S67. ^{13}C NMR (DMSO) spectrum of **10a**.

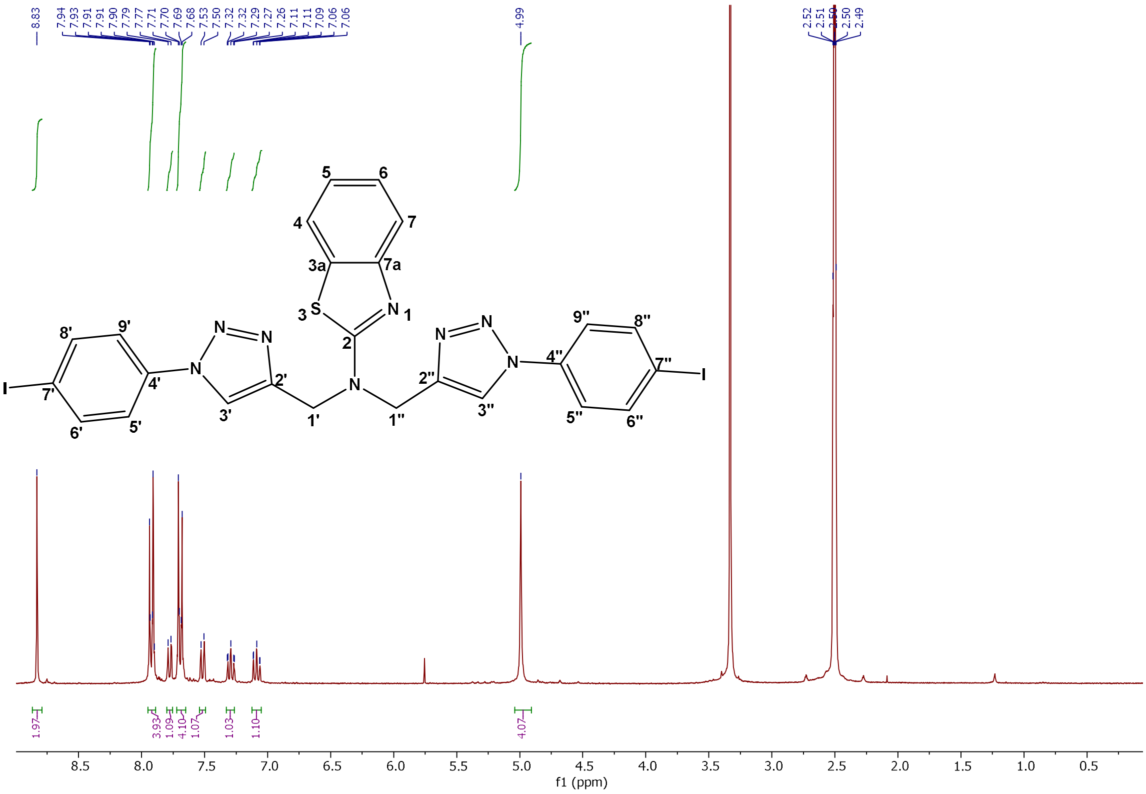

Figure S68. ^{1}H NMR (DMSO) spectrum of **10b**.

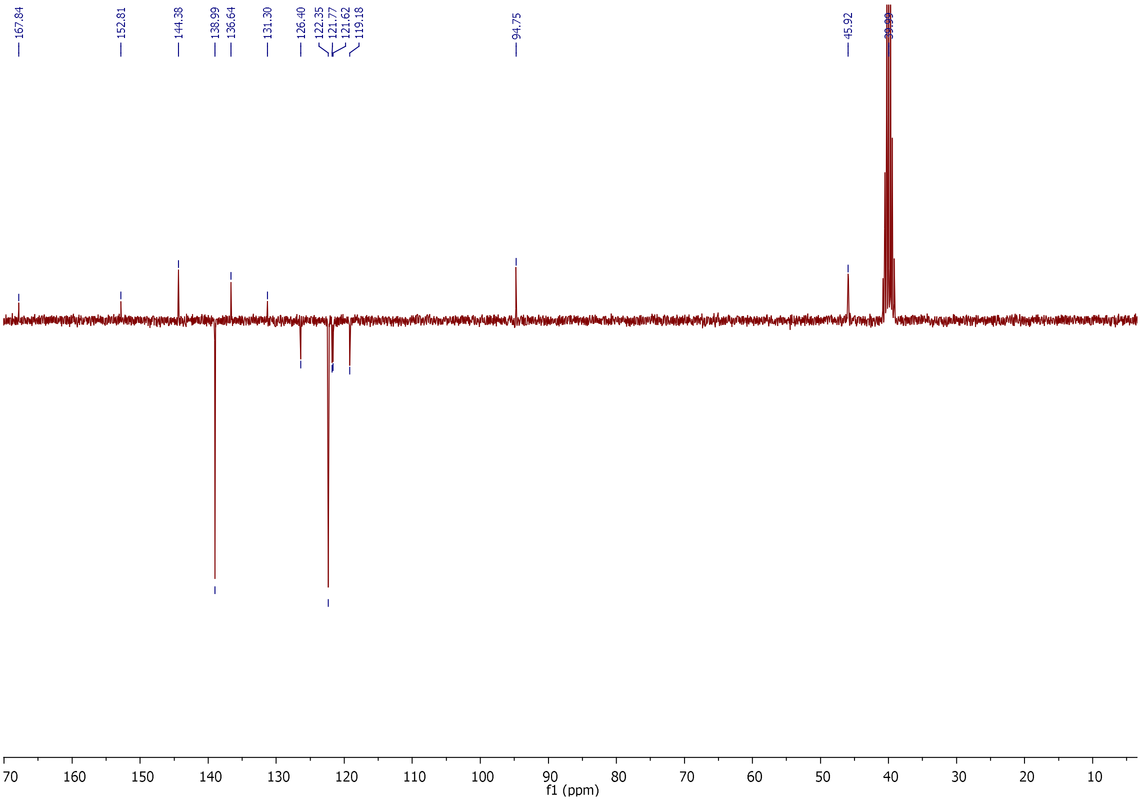

Figure S69. ^{13}C NMR (DMSO) spectrum of **10b**.

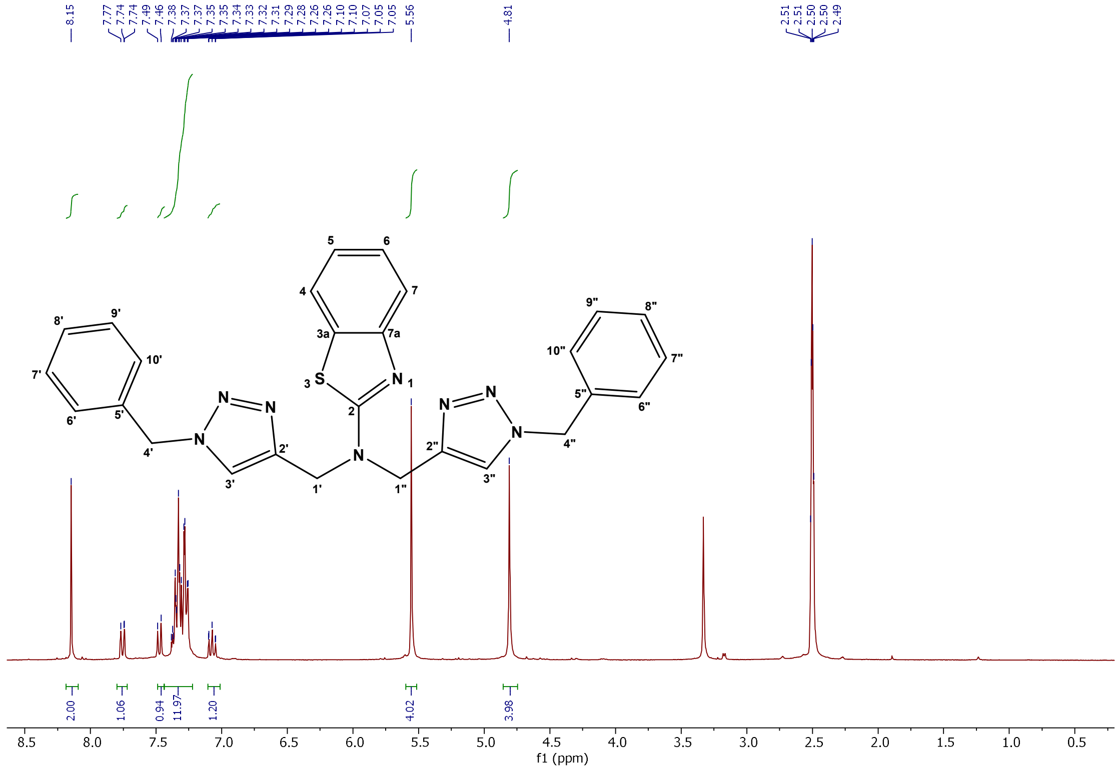

Figure S70. ^{1}H NMR (DMSO) spectrum of **10c**.

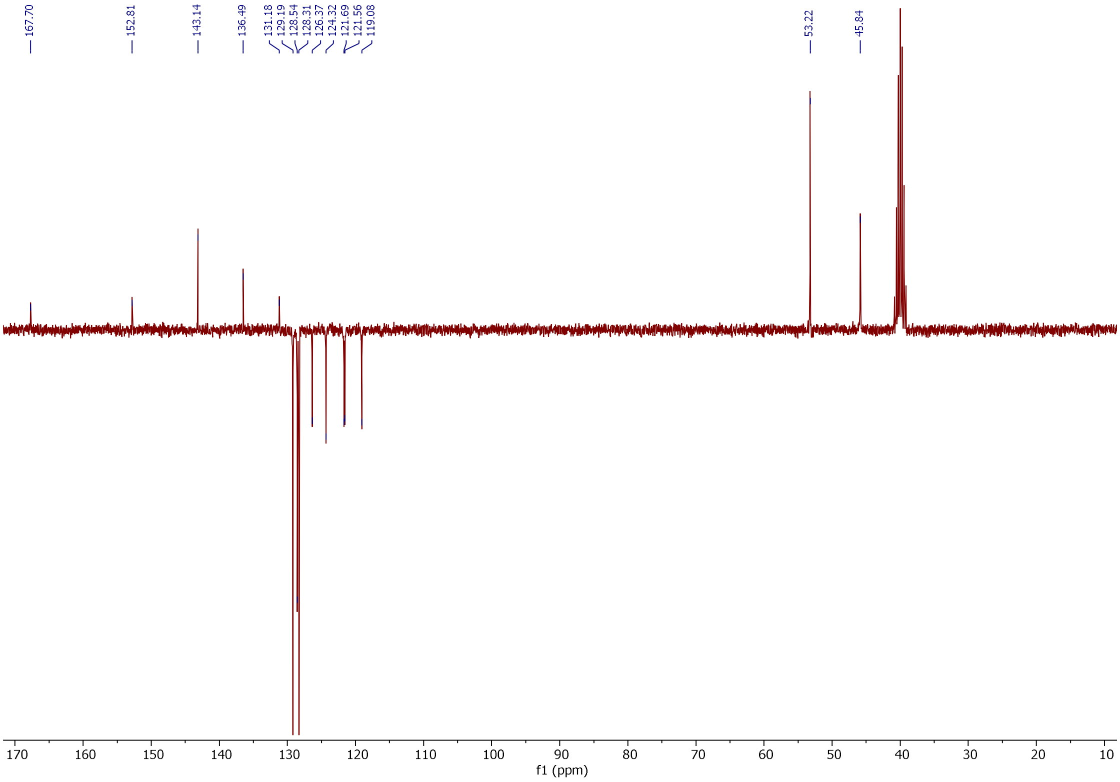

Figure S71. ^{13}C NMR (DMSO) spectrum of **10c**.

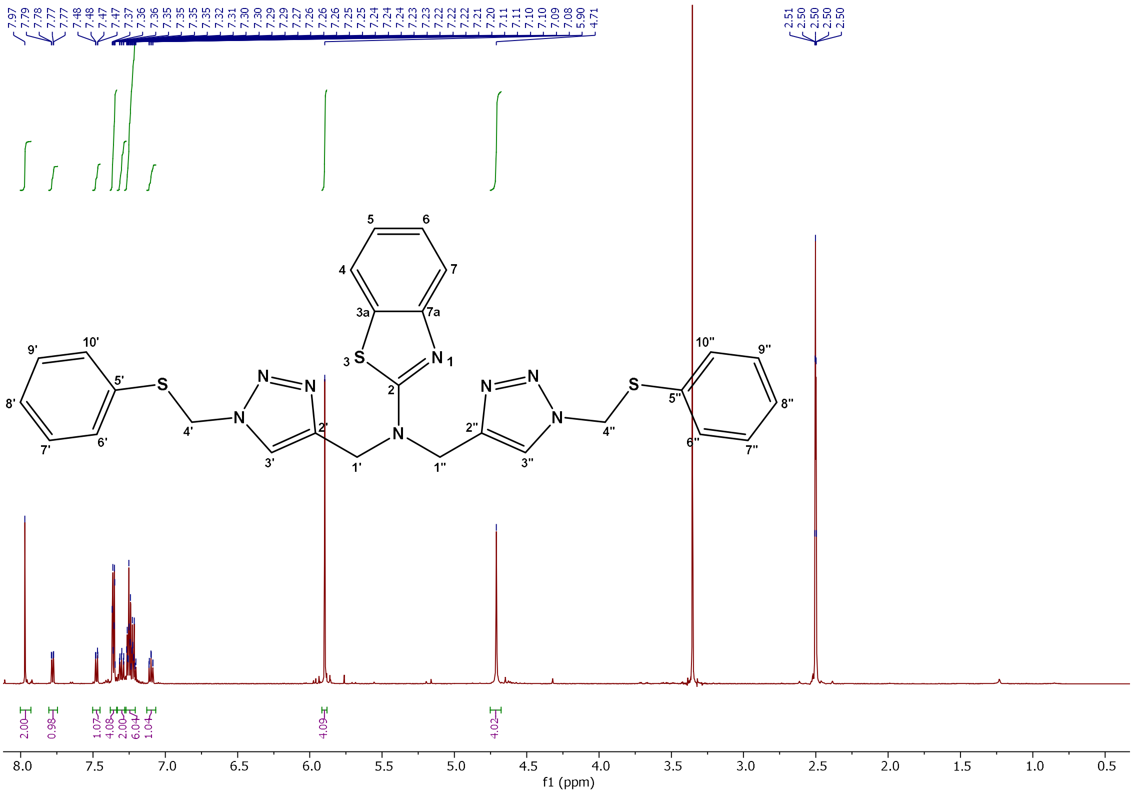

Figure S72. ^{1}H NMR (DMSO) spectrum of **10d**.

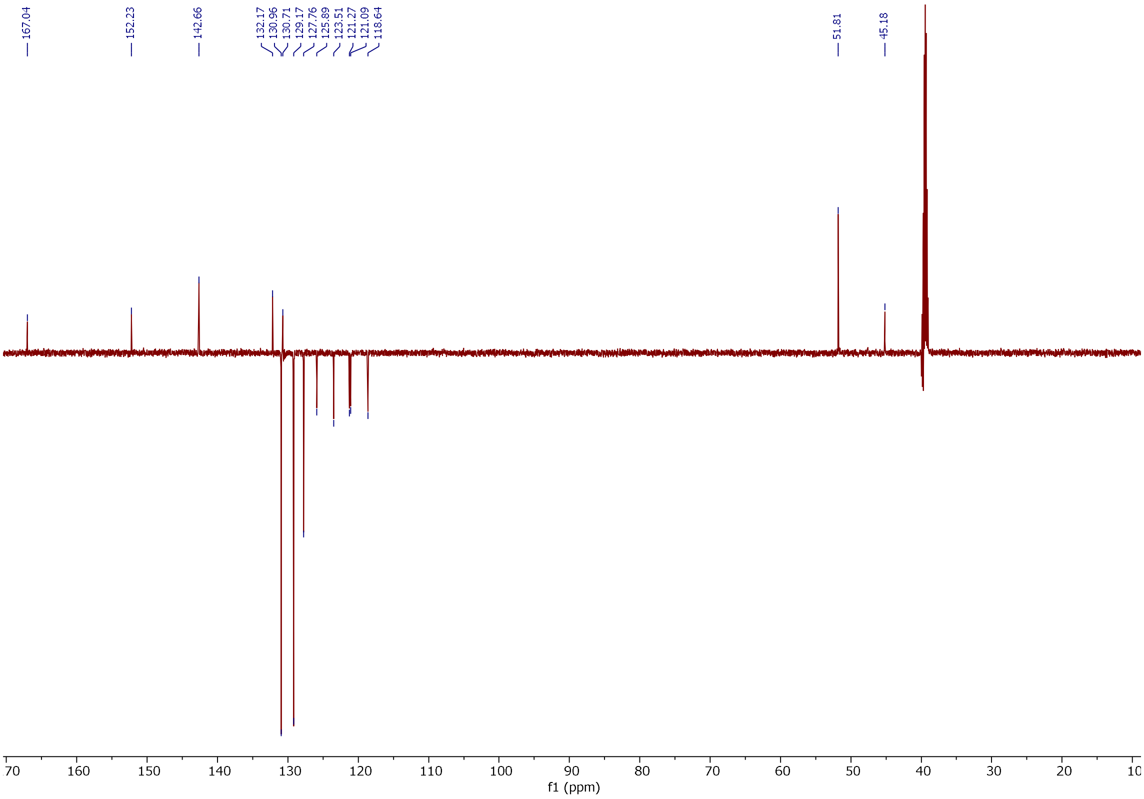

Figure S73. ^{13}C NMR (DMSO) spectrum of **10d**.

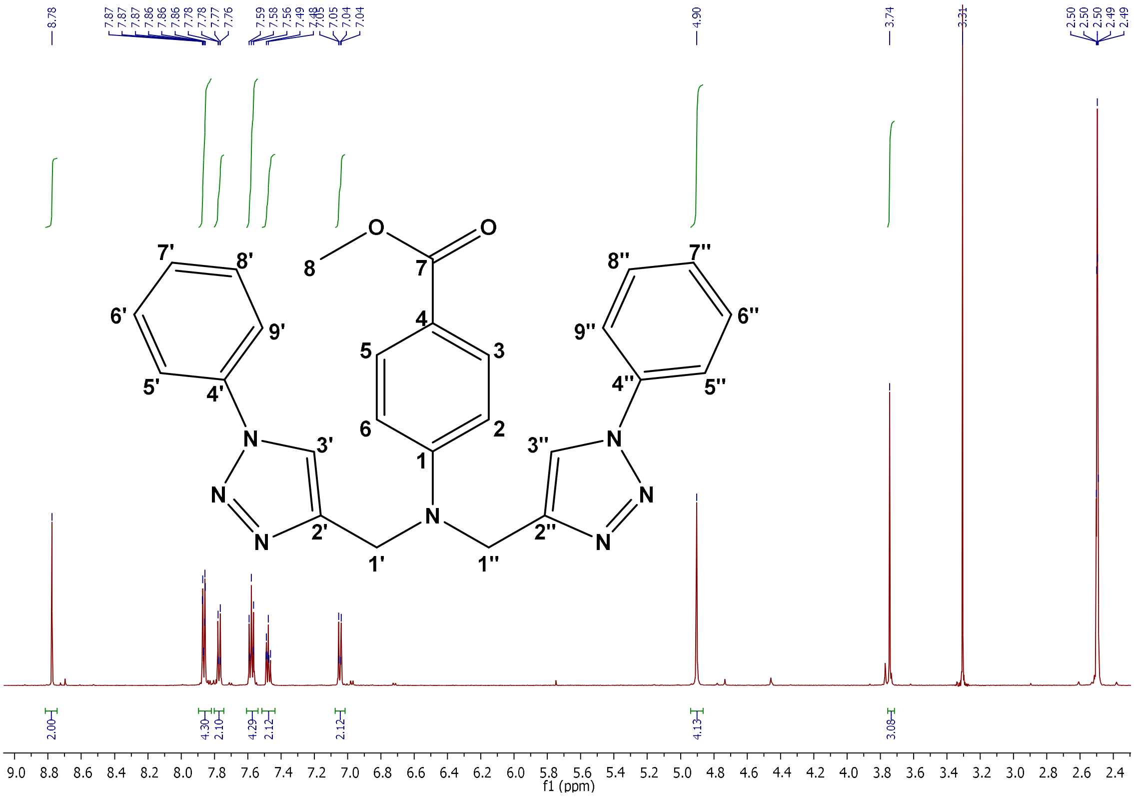

Figure S74. ^{1}H NMR (DMSO) spectrum of **11a**.

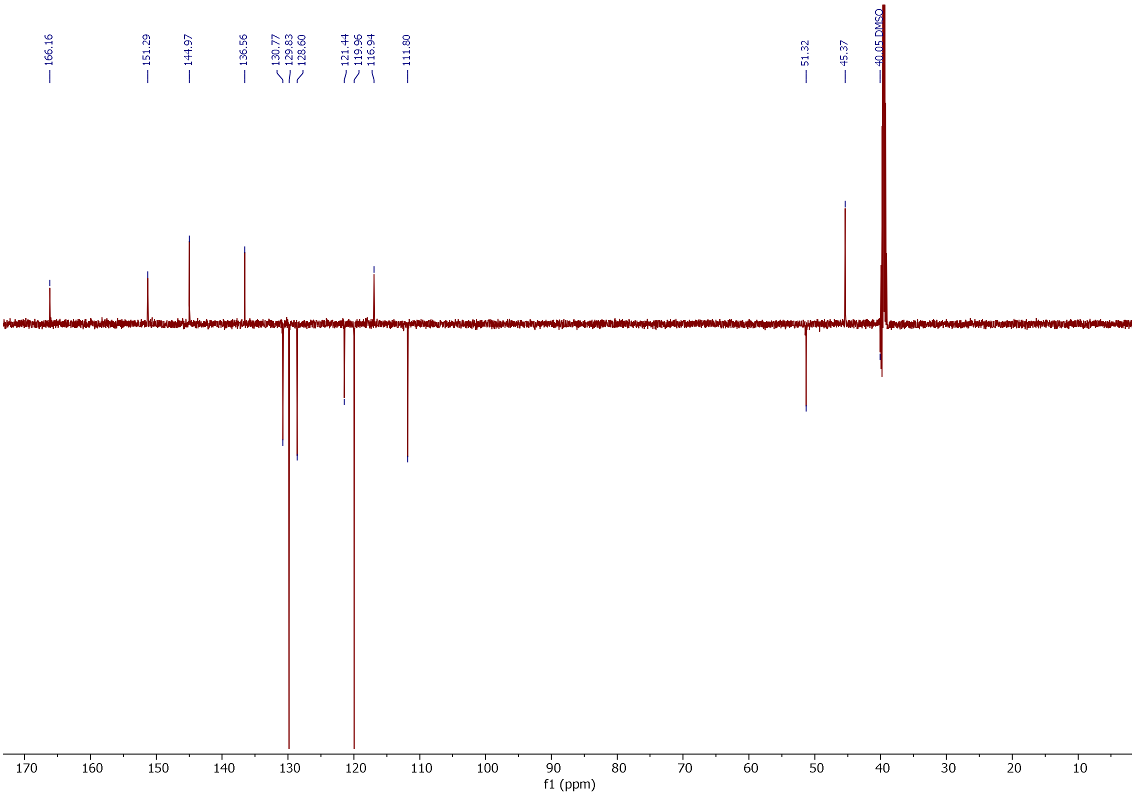

Figure S75. ^{13}C NMR (DMSO) spectrum of **11a**.

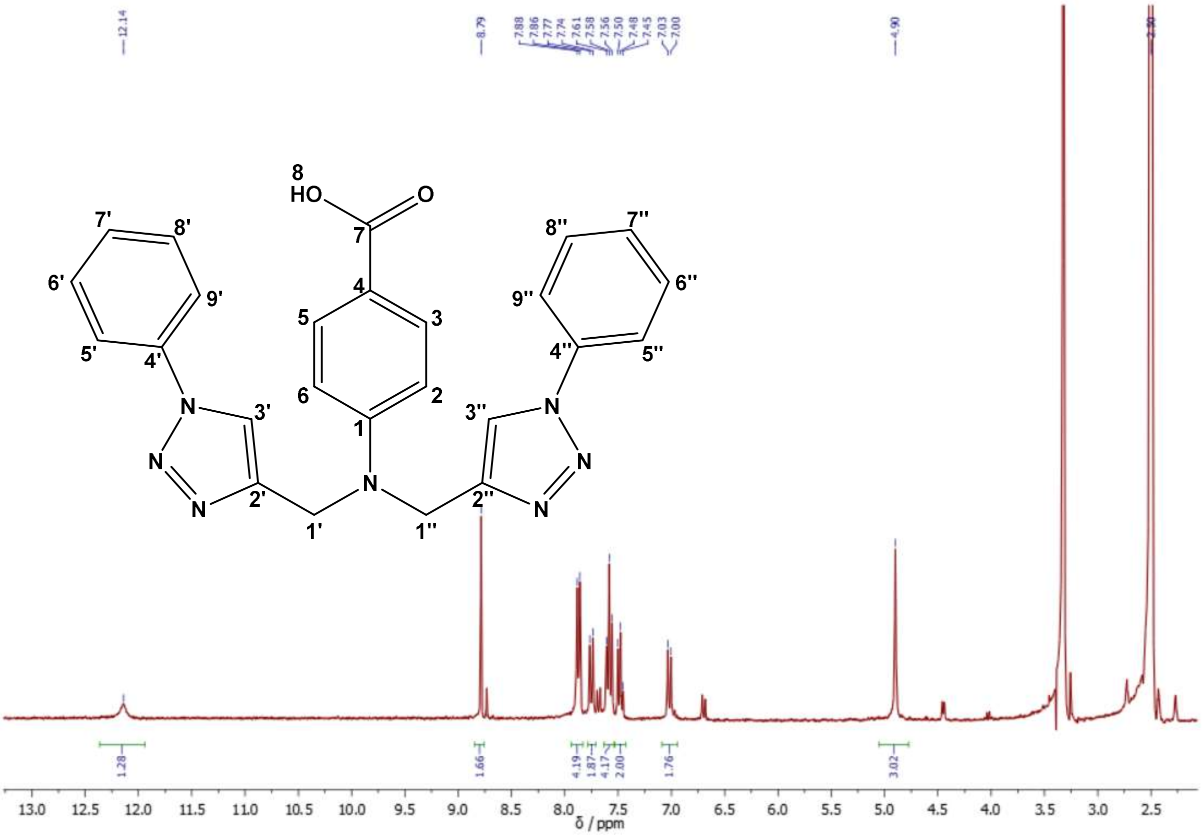

Figure S76. ^{1}H NMR (DMSO) spectrum of **12a**.

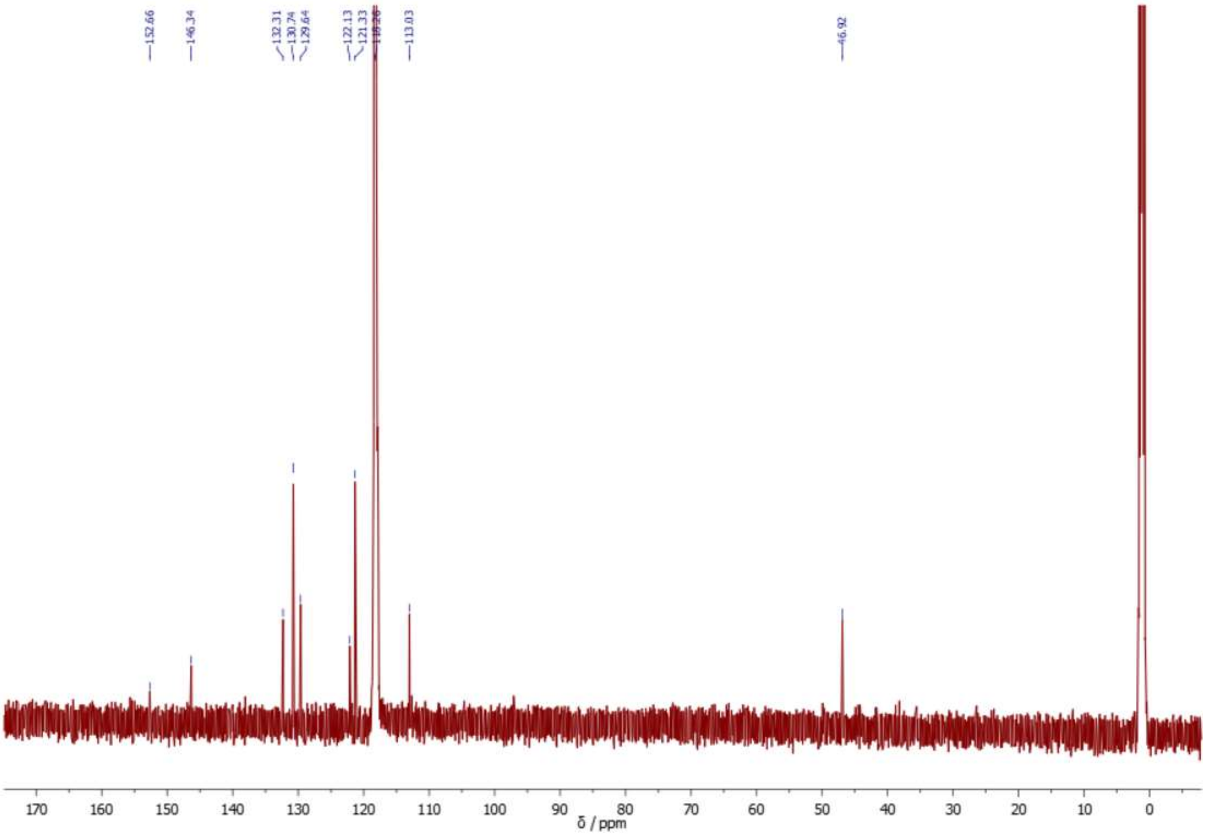

Figure S77. ^{13}C NMR (CD_3CN) spectrum of **12a**.

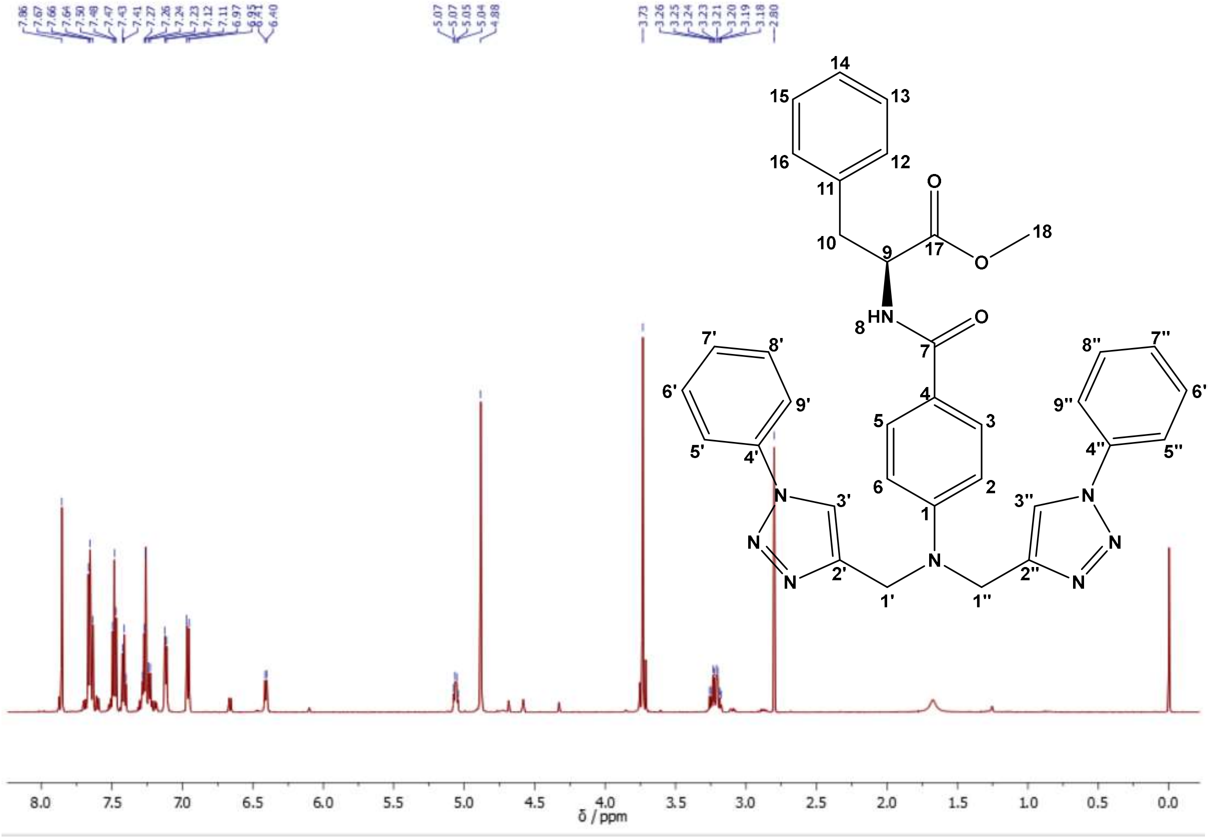

Figure S78. ^{1}H NMR ($CDCl_3$) spectrum of **13a**.

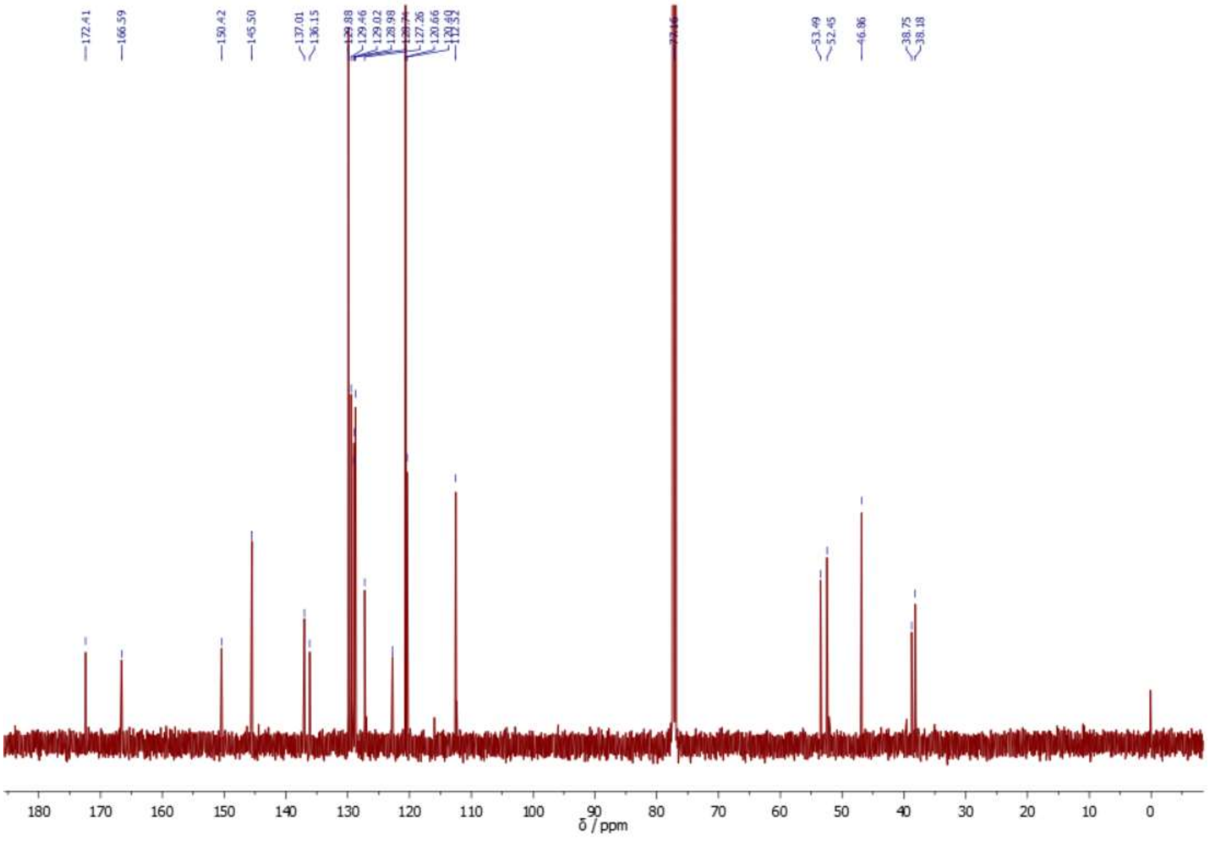

Figure S79. ^{13}C NMR ($CDCl_3$) spectrum of **13a**.

^{1}H, ^{13}C and 2D NMR spectra of in situ prepared complex of **9c** and Zn(BF$_4$)$_2$ in a 2:1 ratio.

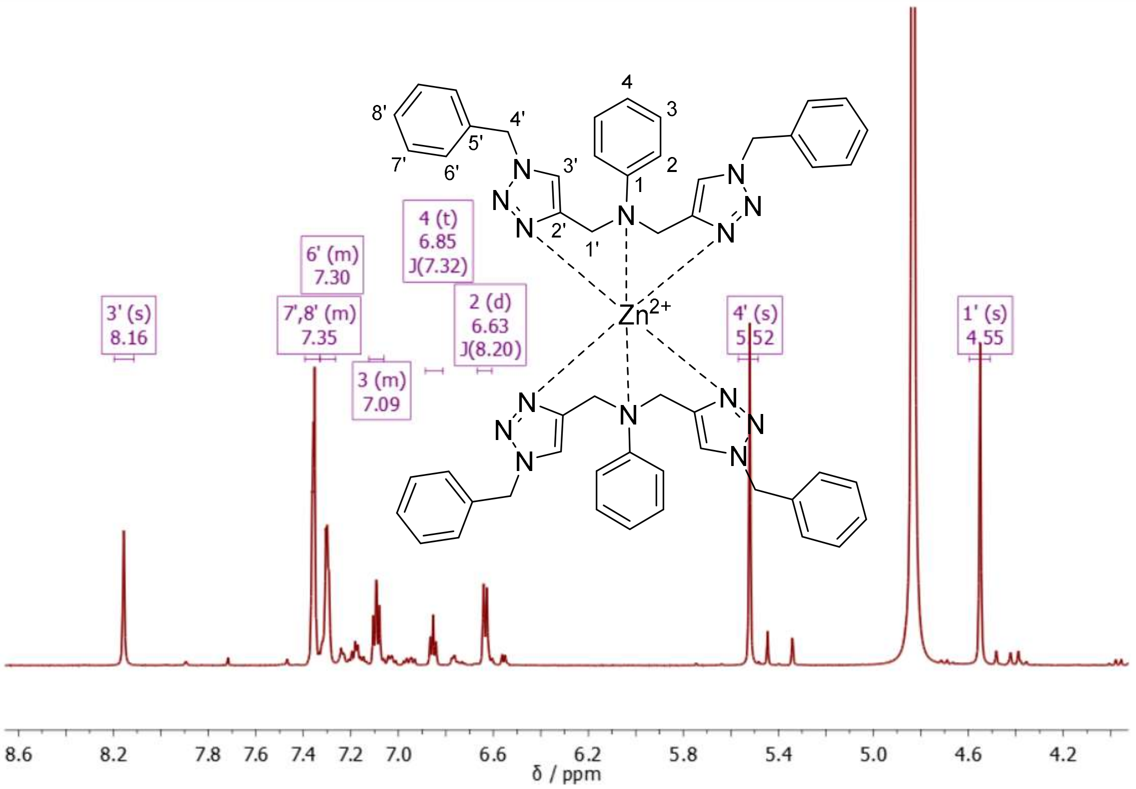

Figure S80. ^{1}H NMR (CD$_3$OD) spectrum of in situ prepared complex of **9c** and Zn(BF$_4$)$_2$ in a 2:1 ratio.

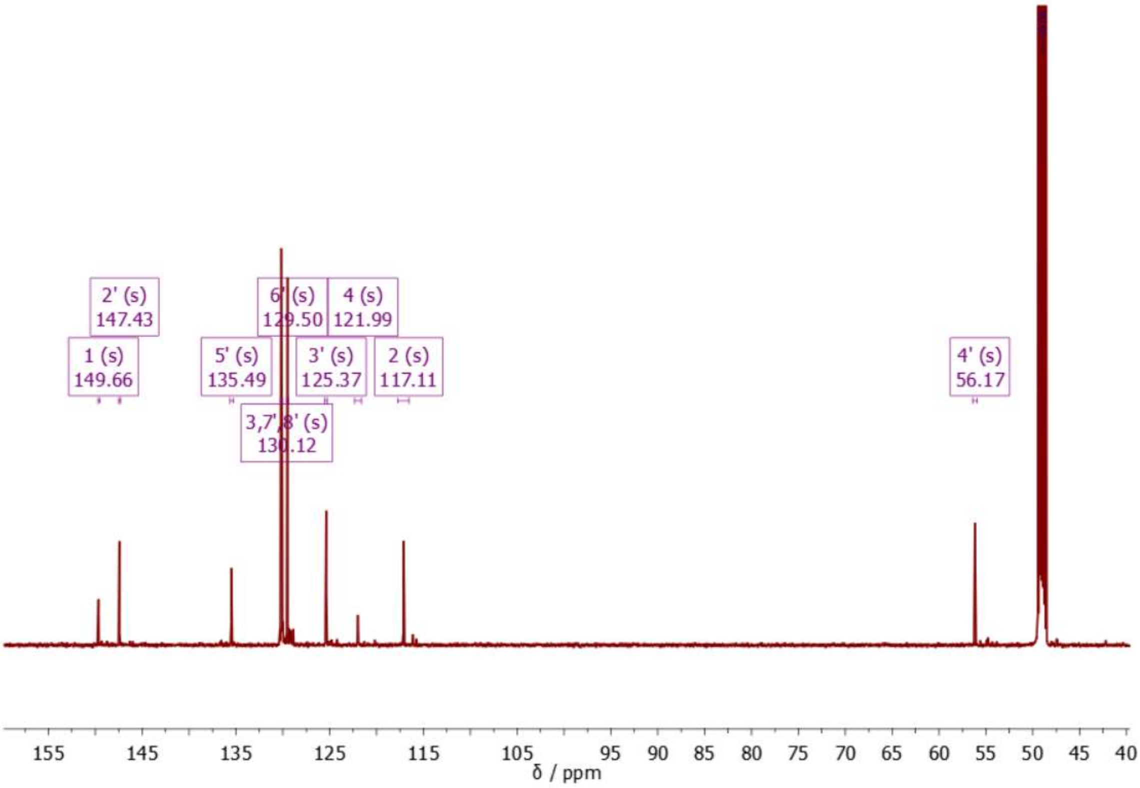

Figure S81. ^{13}C NMR (CD$_3$OD) spectrum of in situ prepared complex of **9c** and Zn(BF$_4$)$_2$ in a 2:1 ratio.

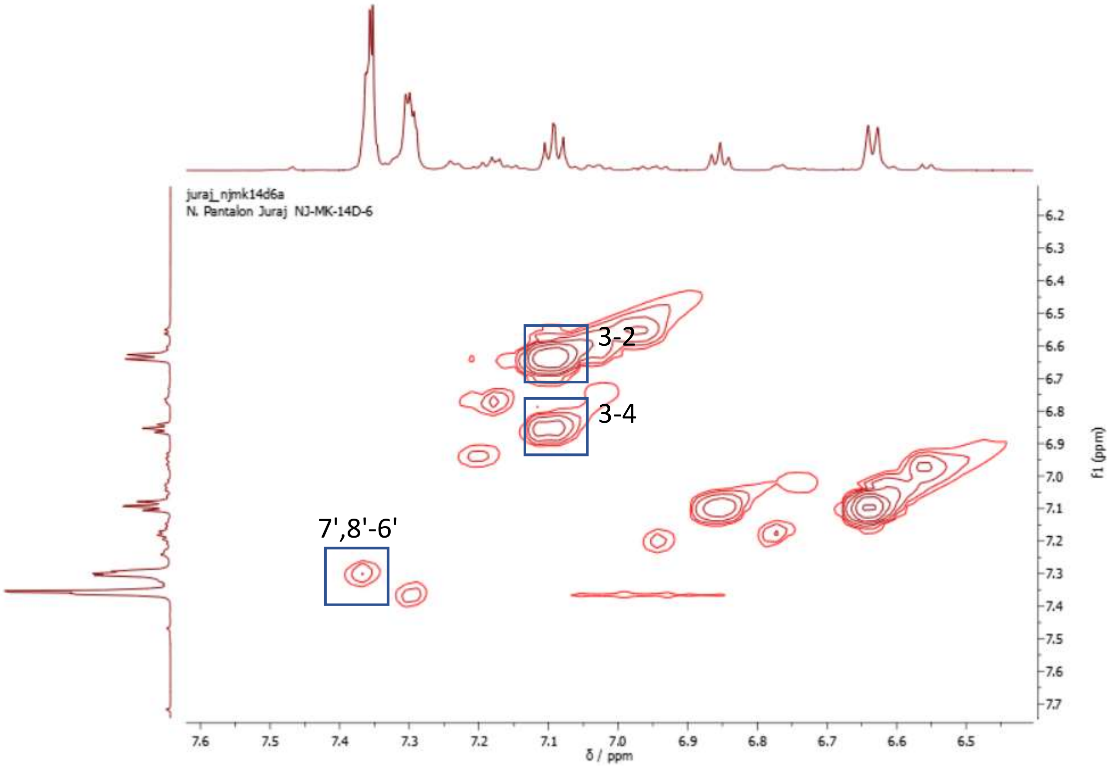

Figure S82. ^{1}H-^{1}H COSY (CD$_3$OD) spectrum of in situ prepared complex of **9c** and Zn(BF$_4$)$_2$ in a 2:1 ratio.

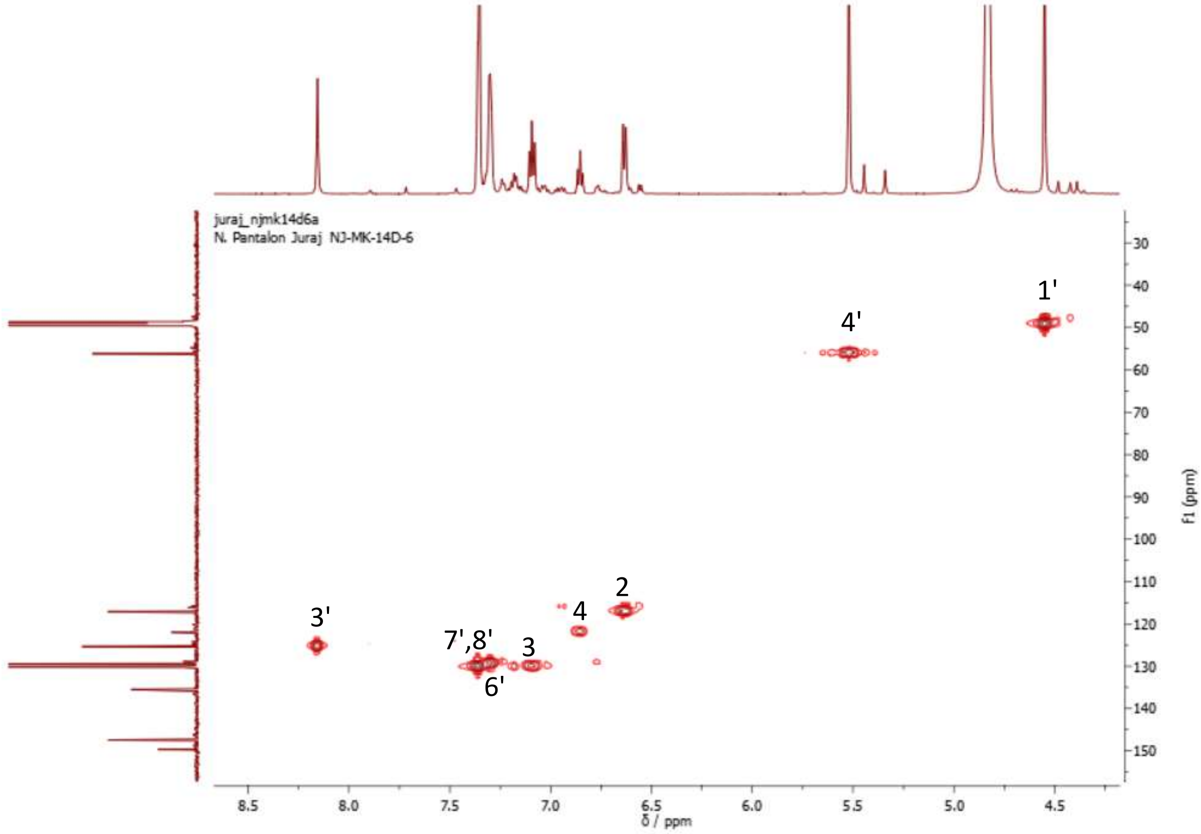

Figure S83. ^{1}H-^{13}C HSQC (CD$_3$OD) spectrum of in situ prepared complex of **9c** and Zn(BF$_4$)$_2$ in a 2:1 ratio.

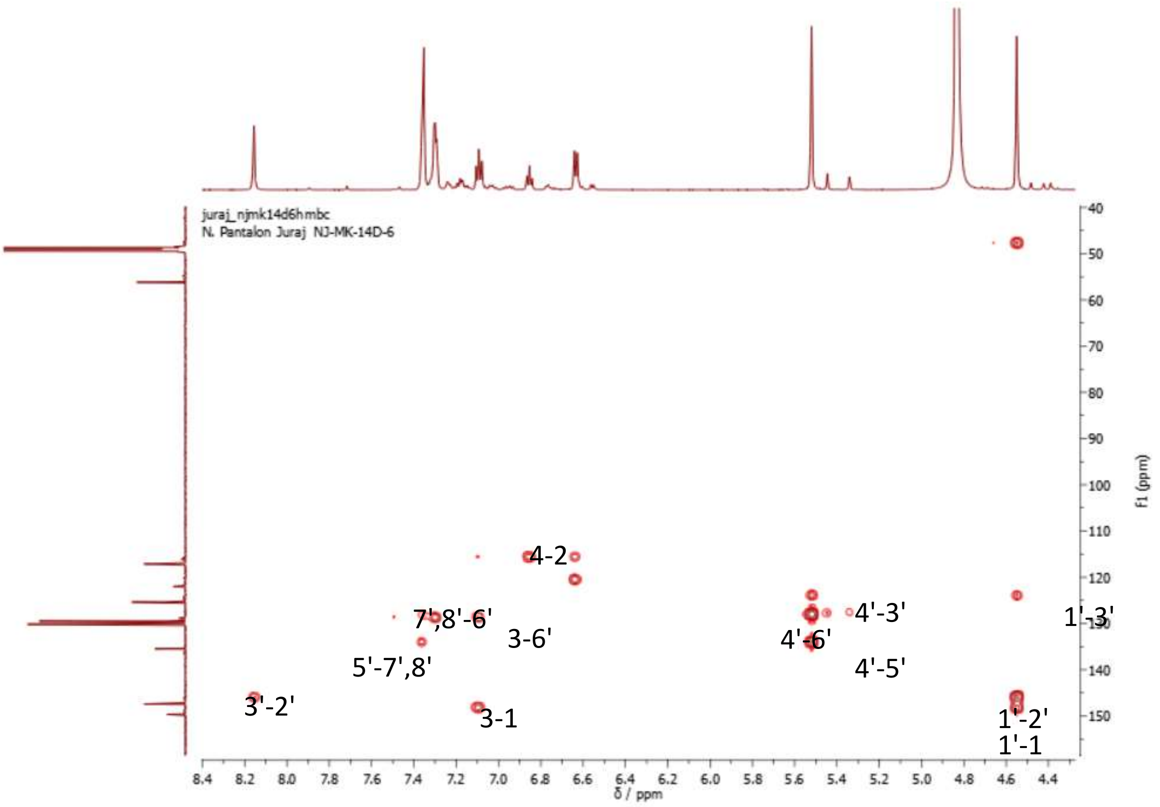

Figure S84. ^{1}H-^{13}C HMBC (CD$_3$OD) spectrum of in situ prepared complex of **9c** and Zn(BF$_4$)$_2$ in a 2:1 ratio.

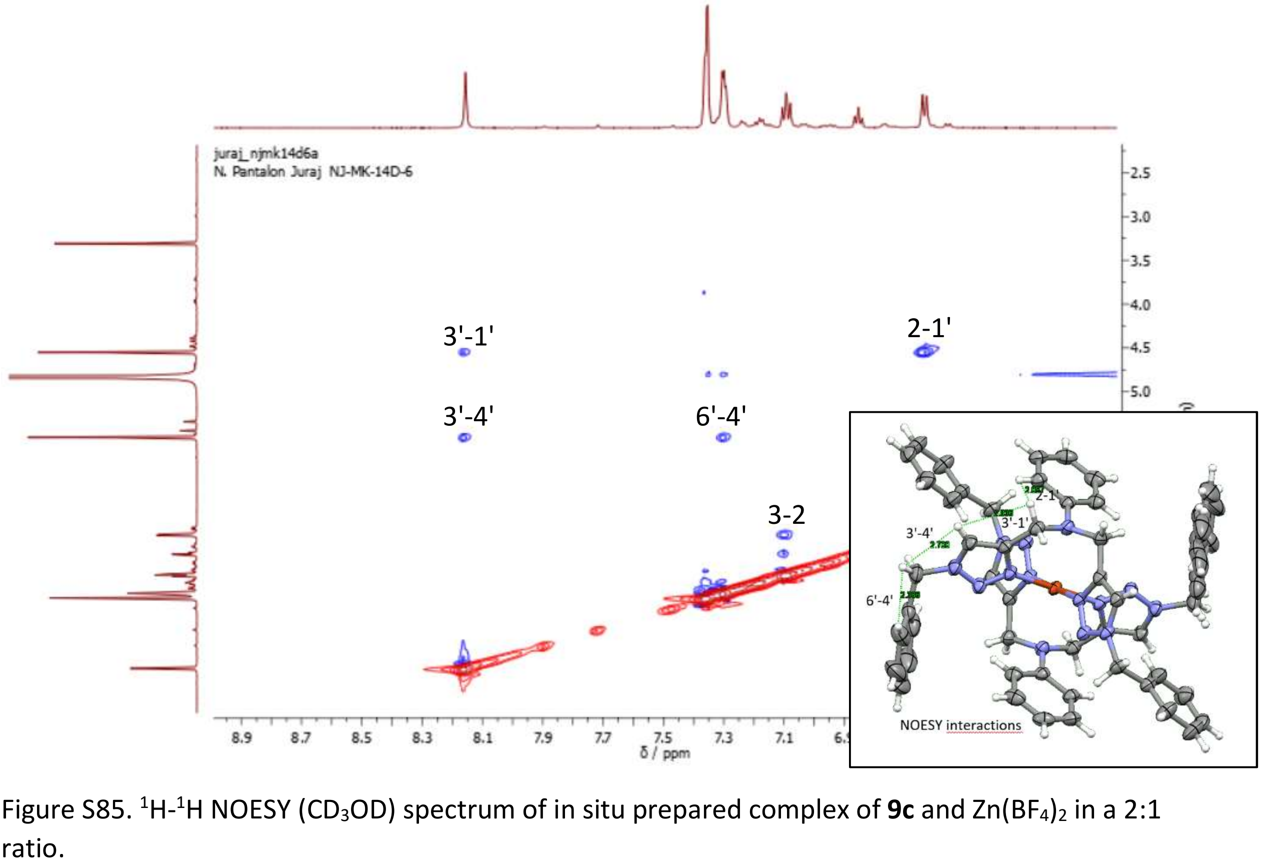

Figure S85. ^{1}H-^{1}H NOESY (CD$_3$OD) spectrum of in situ prepared complex of **9c** and Zn(BF$_4$)$_2$ in a 2:1 ratio.

IR spectra of ligands **8a**-**13a**.

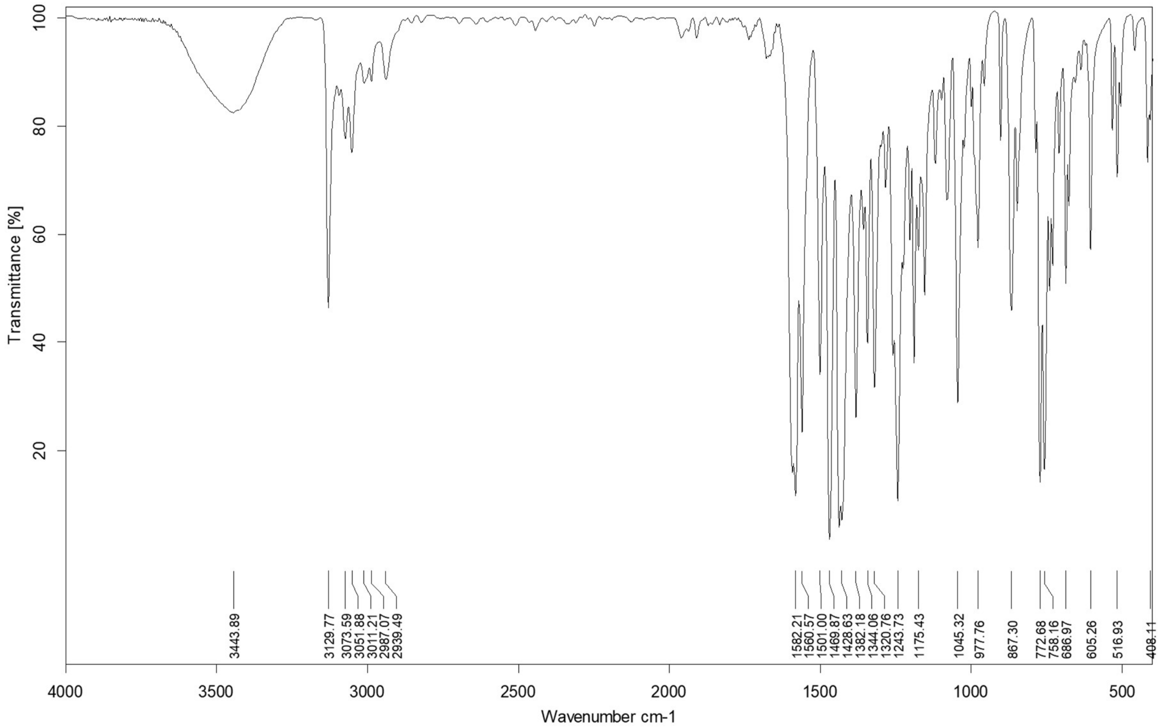

Figure S86. IR(KBr) spectrum of **8a**.

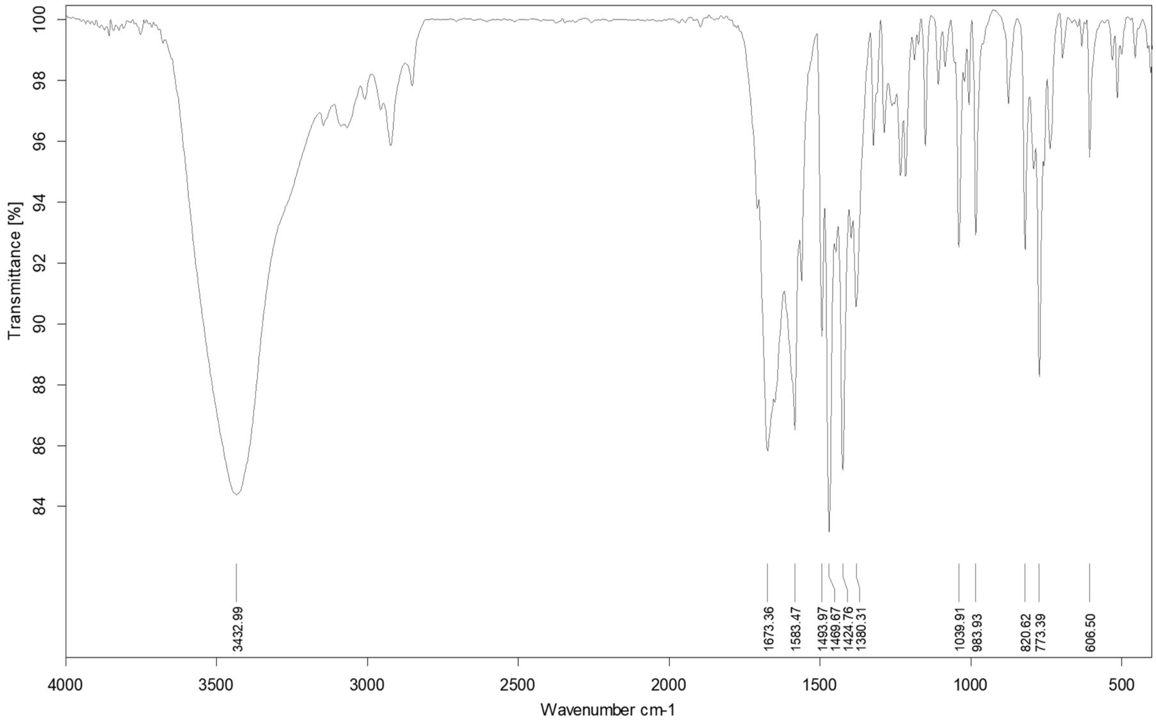

Figure S87. IR(KBr) spectrum of **8b**.

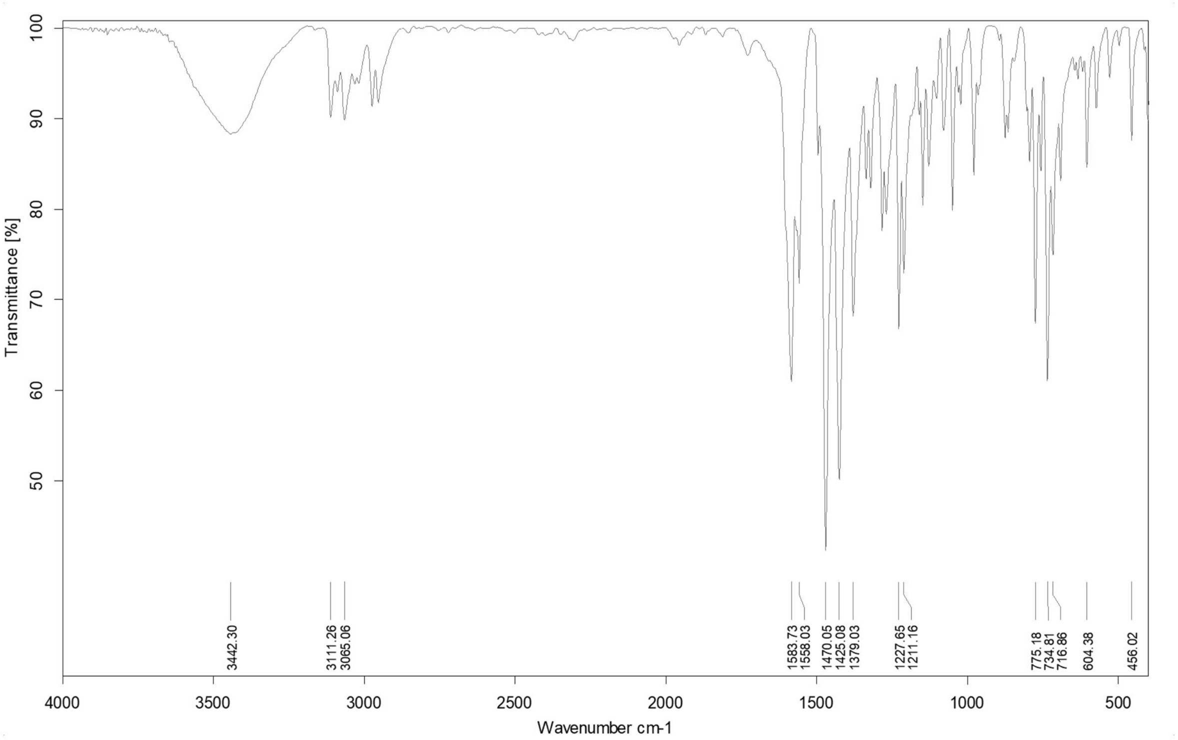

Figure S88. IR(KBr) spectrum of **8c**.

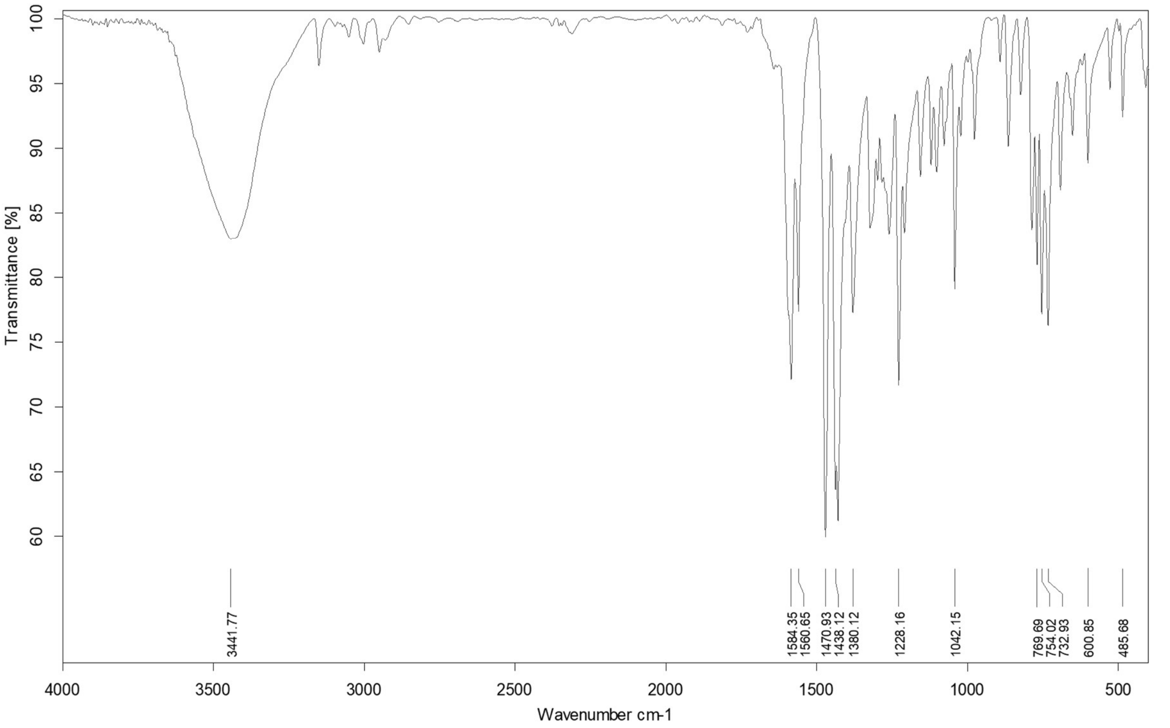

Figure S89. IR(KBr) spectrum of **8d**.

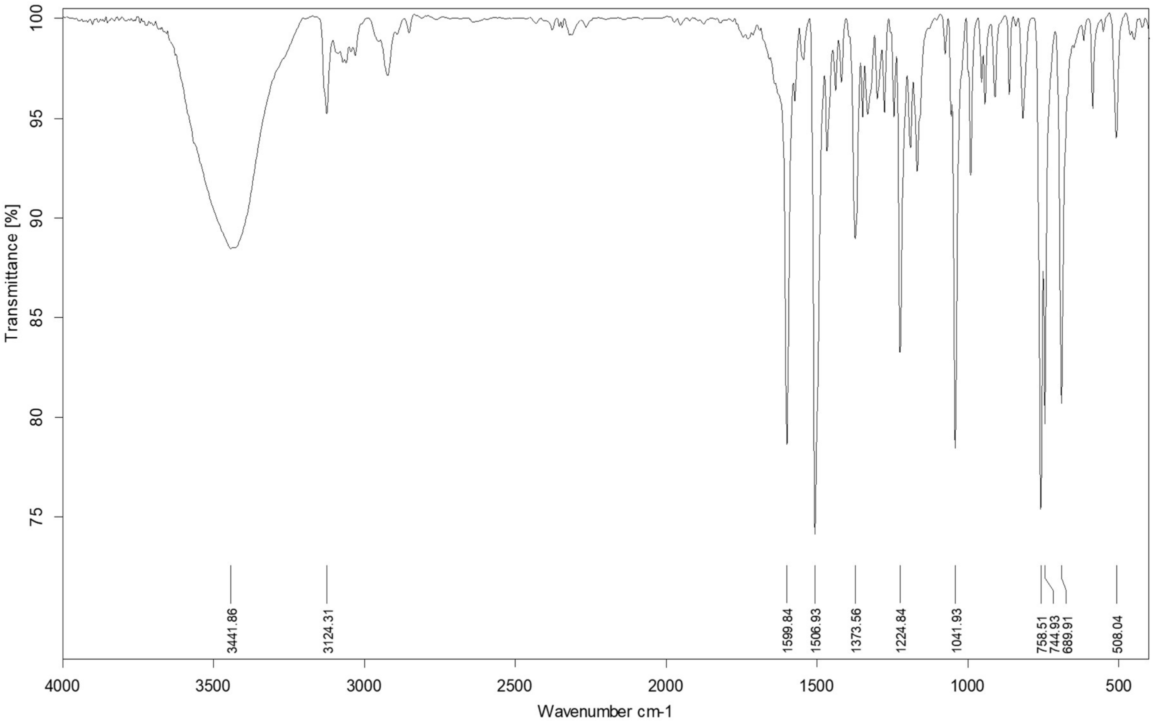

Figure S90. IR(KBr) spectrum of **9a**.

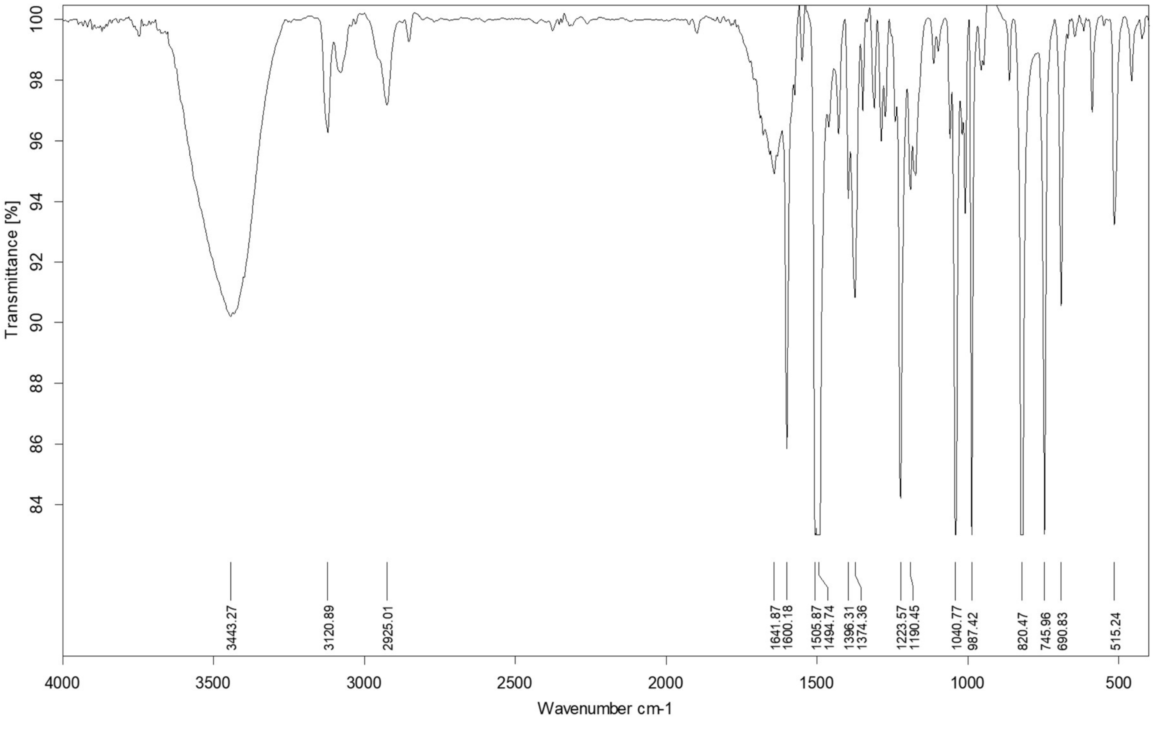

Figure S91. IR(KBr) spectrum of **9b**.

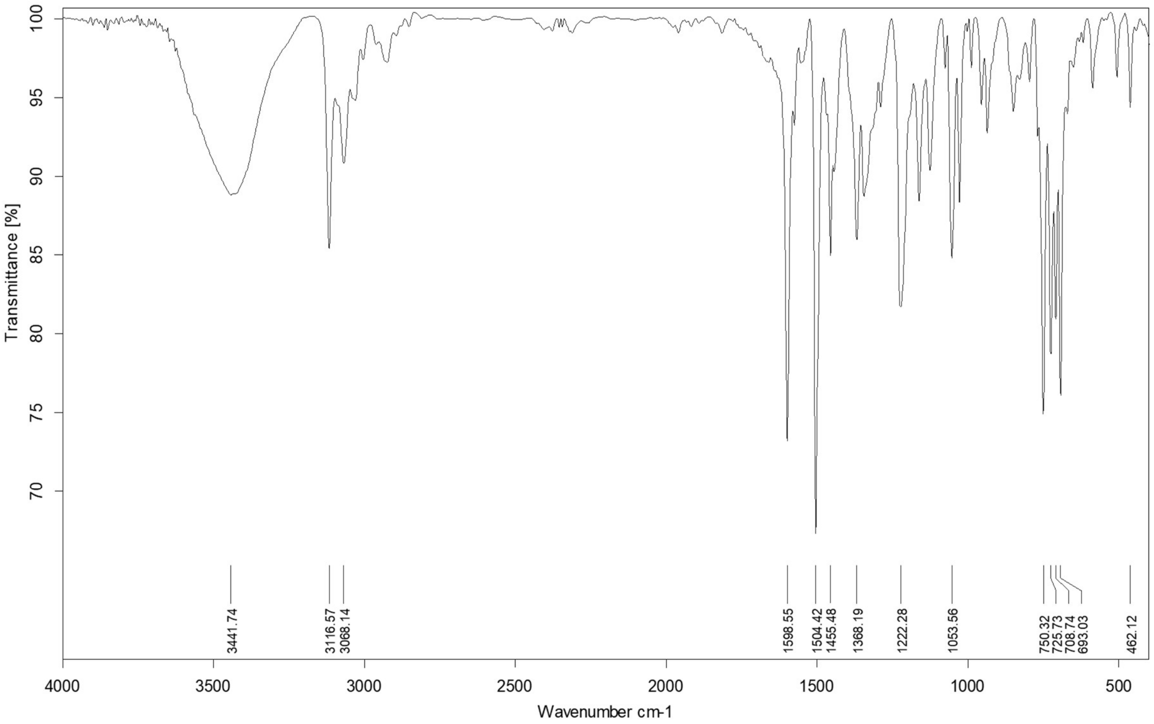

Figure S92. IR(KBr) spectrum of **9c**.

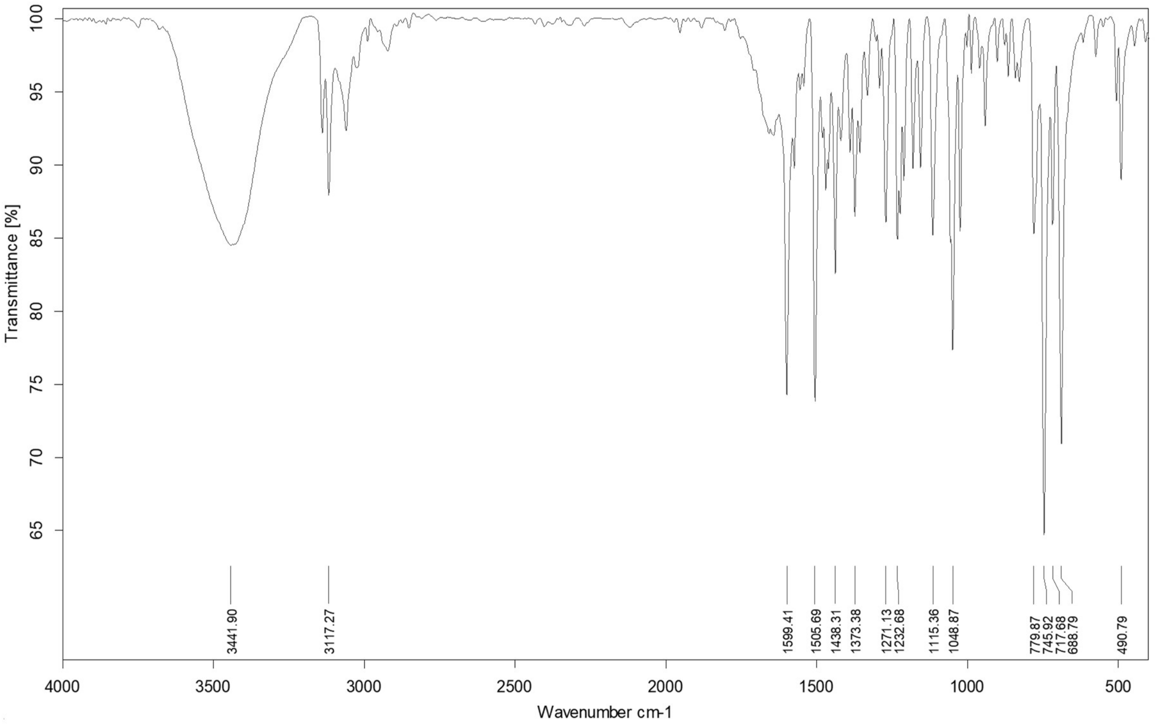

Figure S93. IR(KBr) spectrum of **9d**.

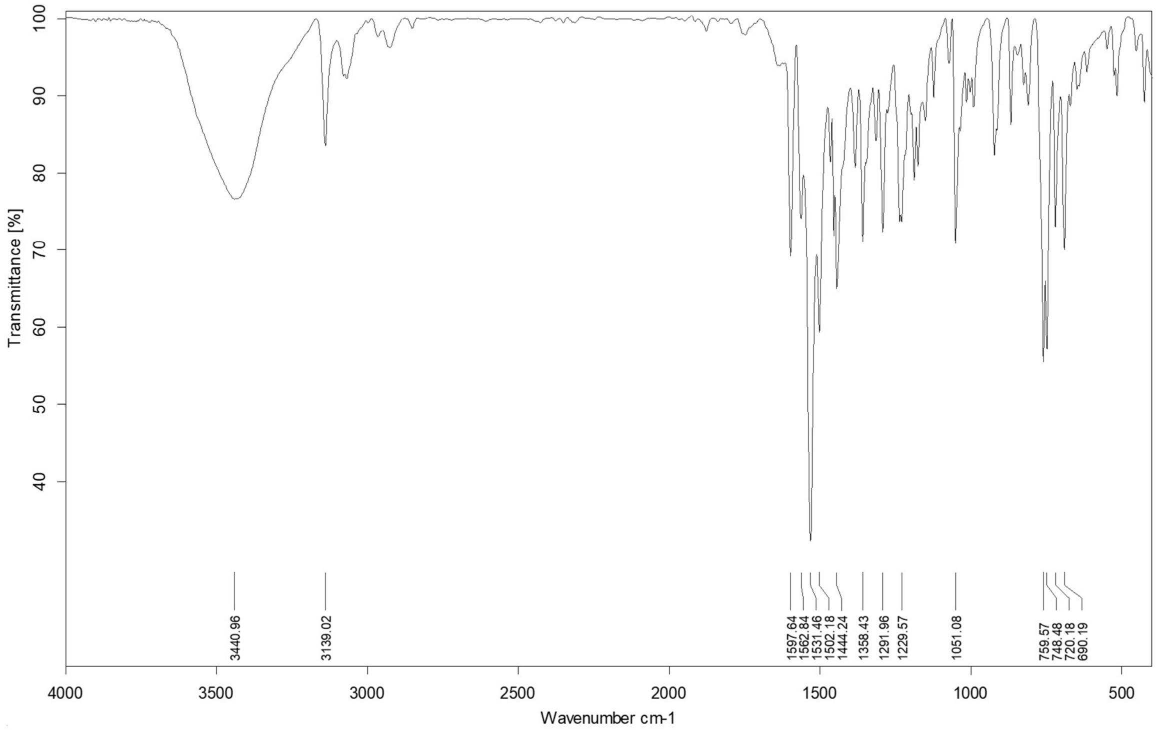

Figure S94. IR(KBr) spectrum of **10a**.

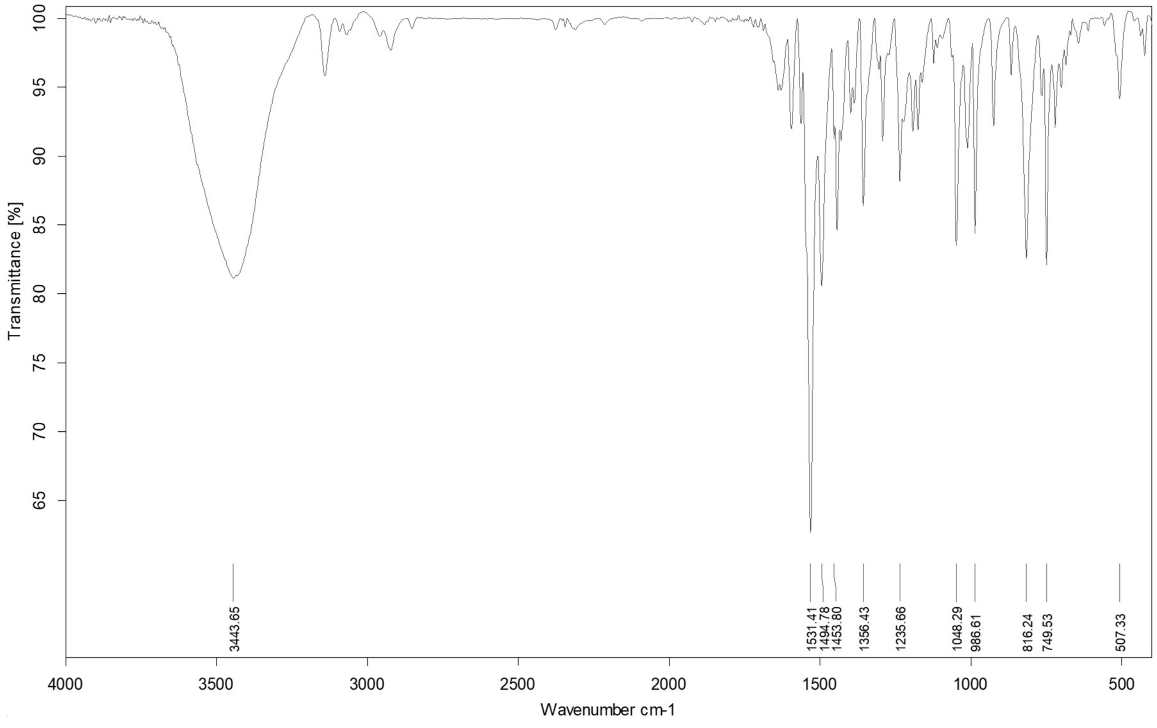

Figure S95. IR(KBr) spectrum of **10b**.

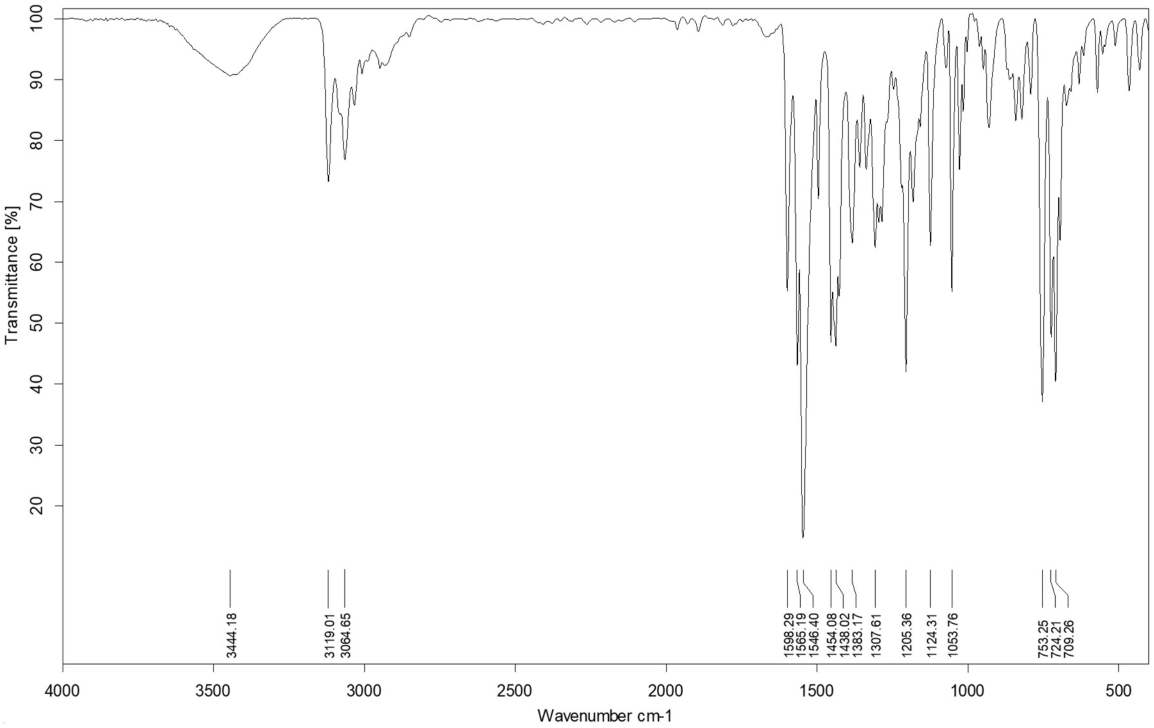

Figure S96. IR(KBr) spectrum of **10c**.

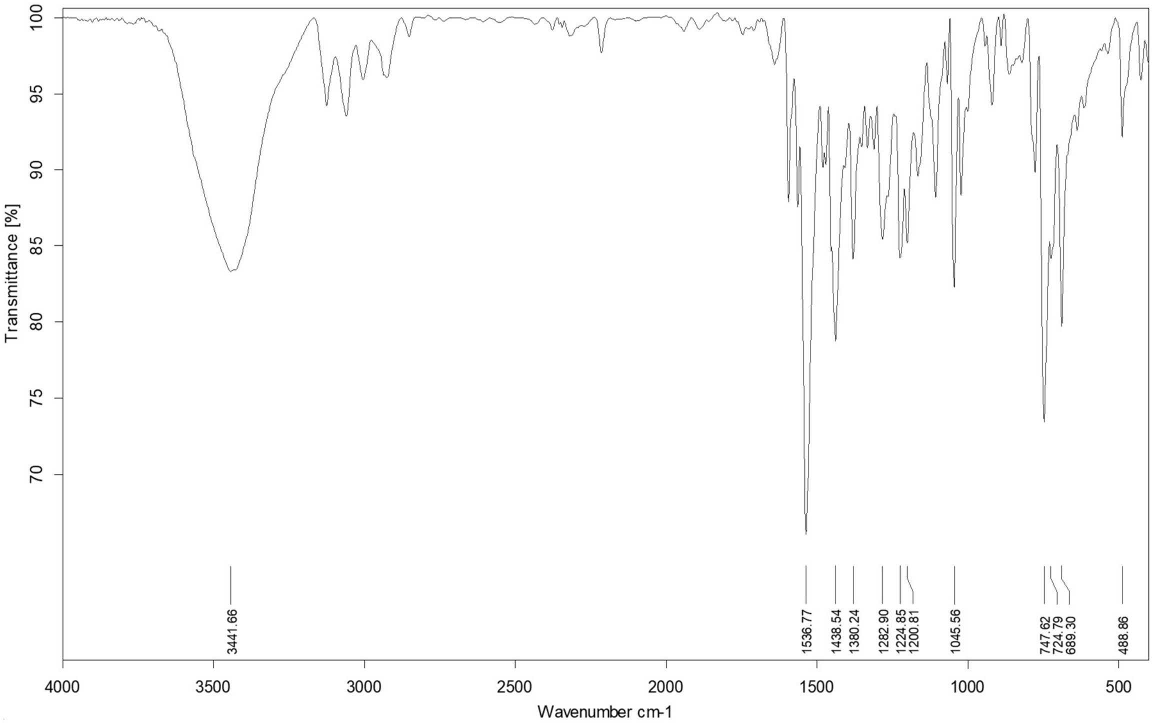

Figure S97. IR(KBr) spectrum of **10d**.

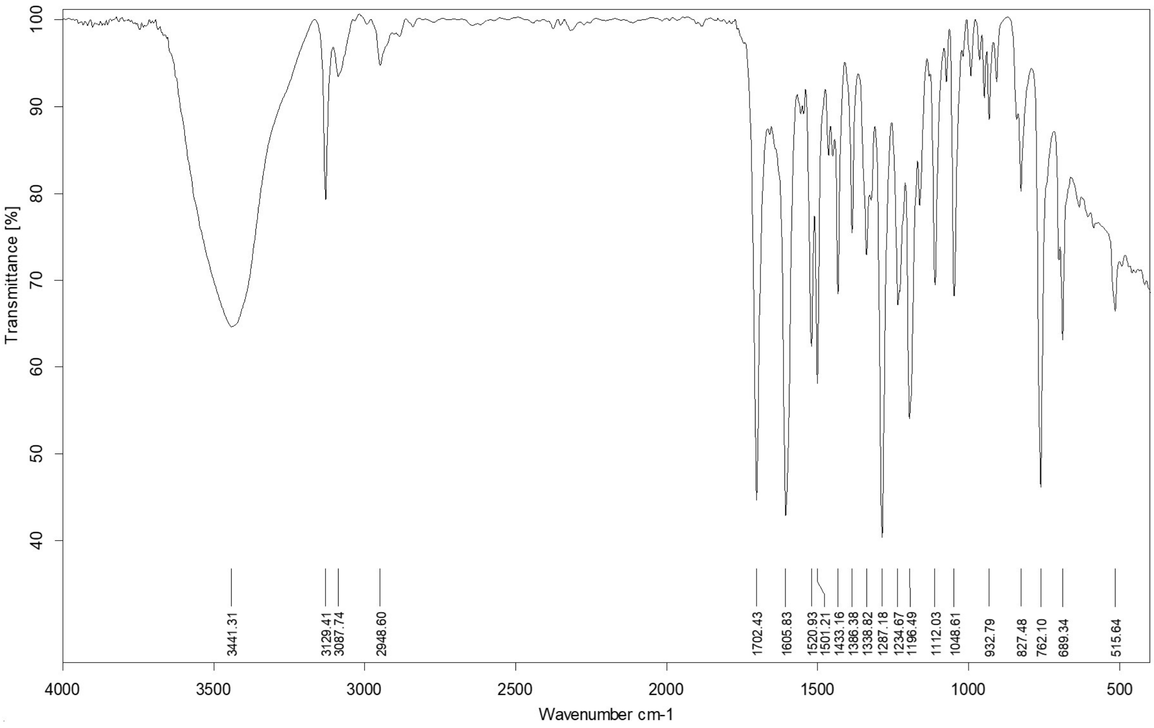

Figure S98. IR(KBr) spectrum of **11a**.

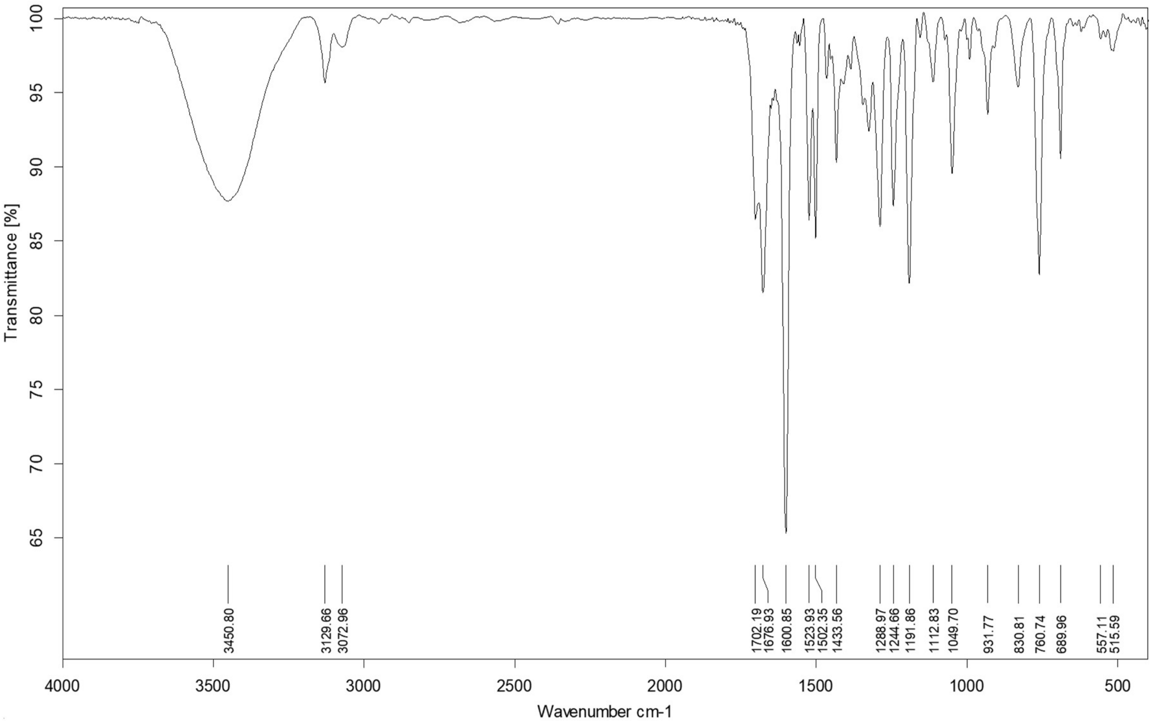

Figure S99. IR(KBr) spectrum of **12a**.

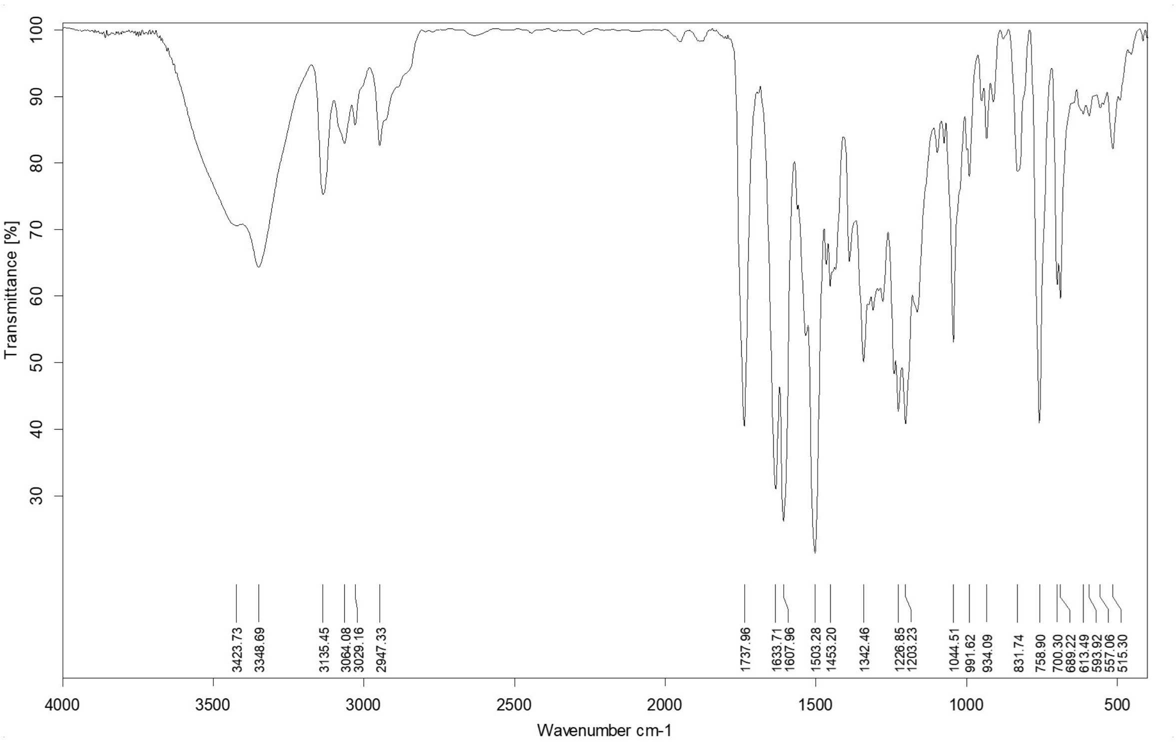

Figure S100. IR(KBr) spectrum of **13a**.

IR spectra of metal complexes

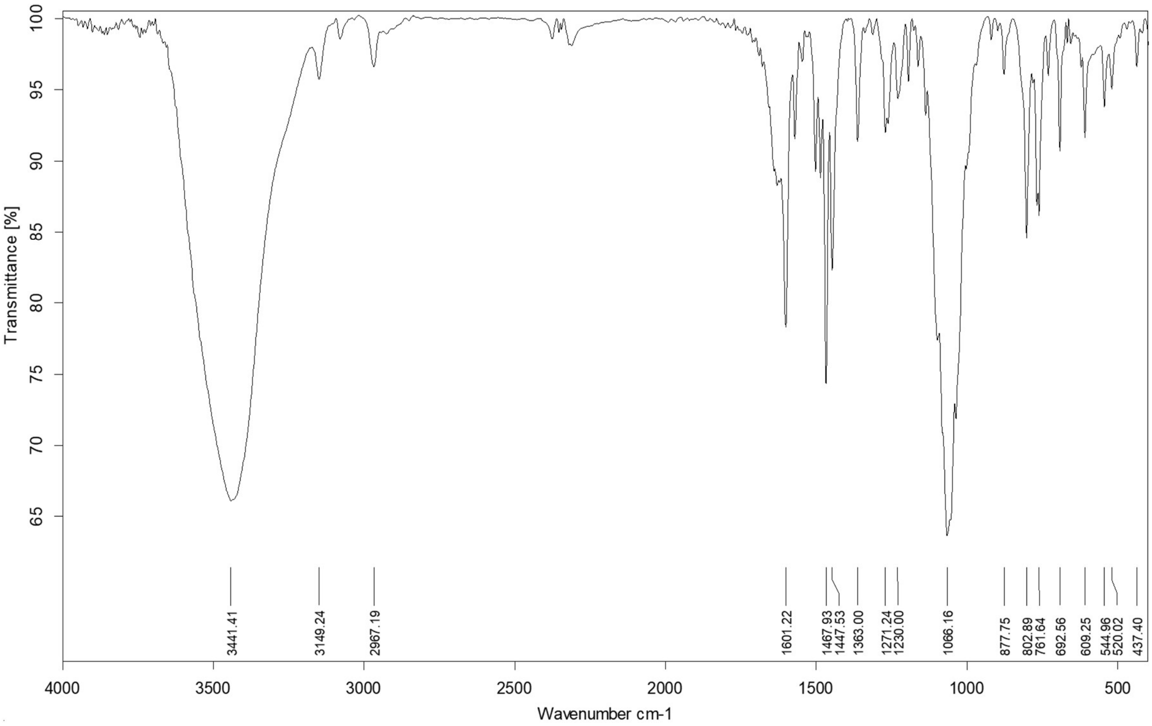

Figure S101. IR(KBr) spectrum of **8a$_{Cu}$**.

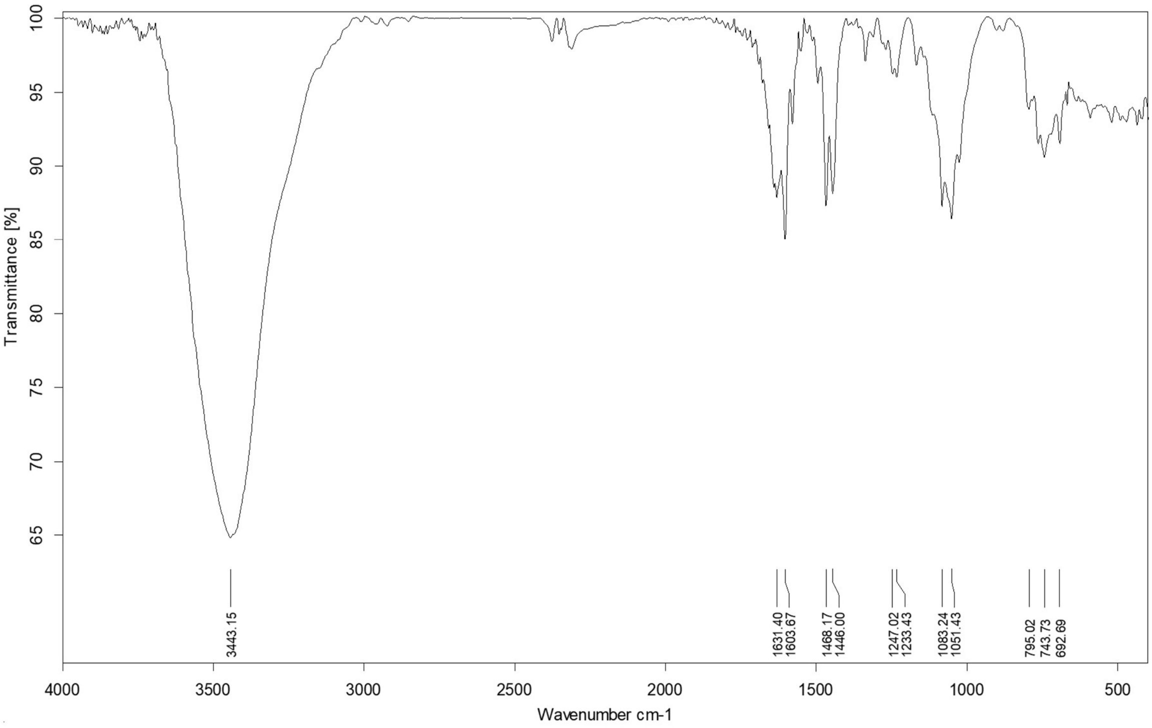

Figure S102. IR(KBr) spectrum of **8d$_{Cu}$**.

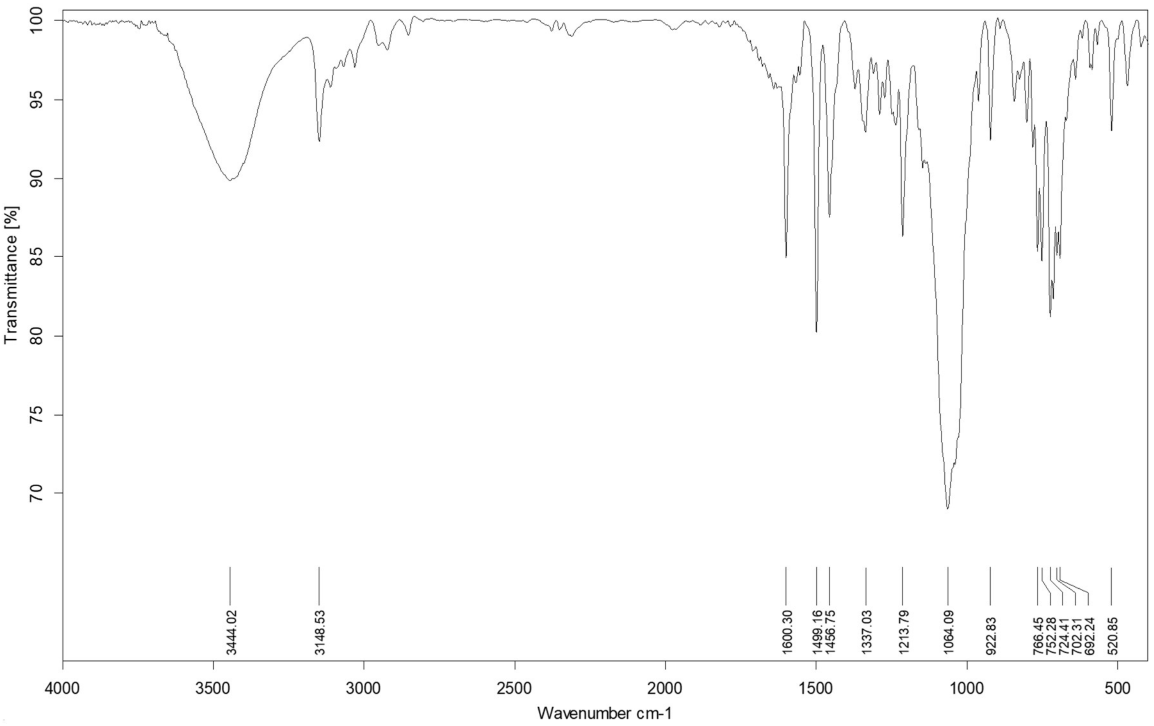

Figure S103. IR(KBr) spectrum of **9c**$_{\mathrm{Cu}}$.

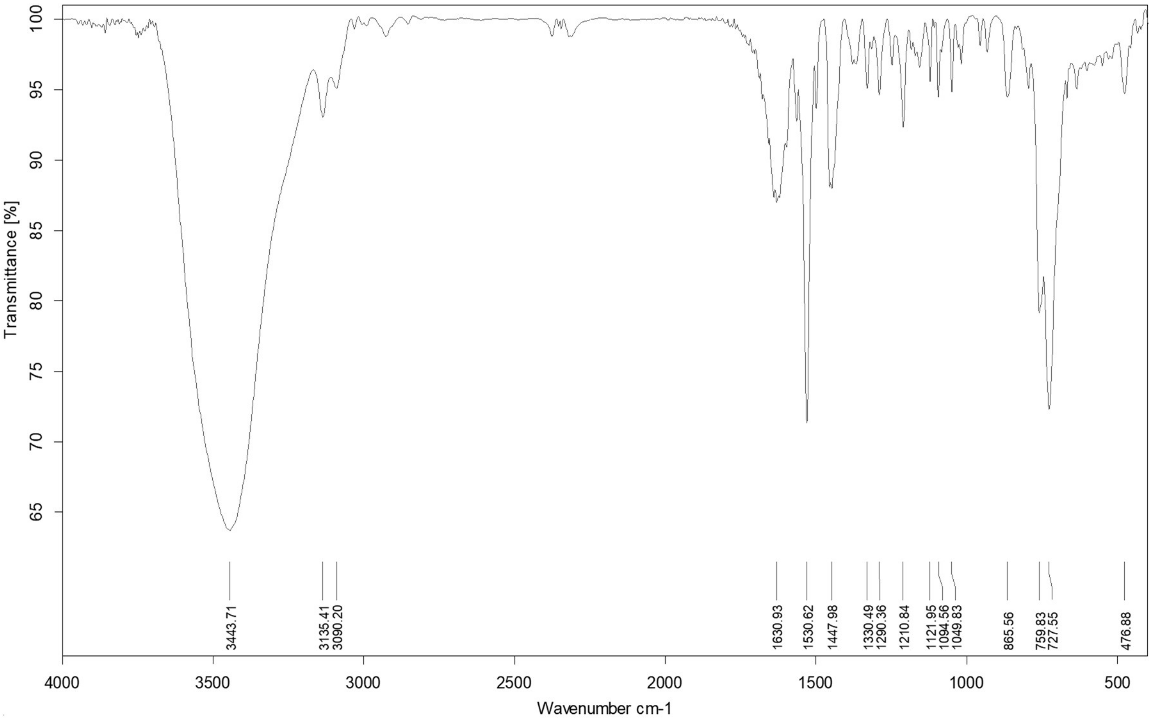

Figure S104. IR(KBr) spectrum of **10c**$_{\mathrm{Cu}}$.

IR (KBr) spectra of the complexes were compared to the IR spectra of the ligands, and shifts of several peaks were observed upon complexation. The alkene C-H stretching (3100-3000 cm^{-1}) peaks were shifted to higher wavenumbers in the complexes, and the larger O-H water peak in **8a$_{Cu}$** and **8d$_{Cu}$** possibly overlapped the C-H peaks in the complexes. Peaks between 1400 and 1700 cm^{-1} were assigned to the C=C and C=N bonds; some of them belonging to the triazole groups.[4] Significant shifts in these peaks were observed for all complexes except **9c$_{Cu}$**, where a broad band appeared at 1063 cm^{-1}. This band (but in somewhat lower intensity) was also observed for **8a$_{Cu}$** and **8d$_{Cu}$** but not for **10c$_{Cu}$**.

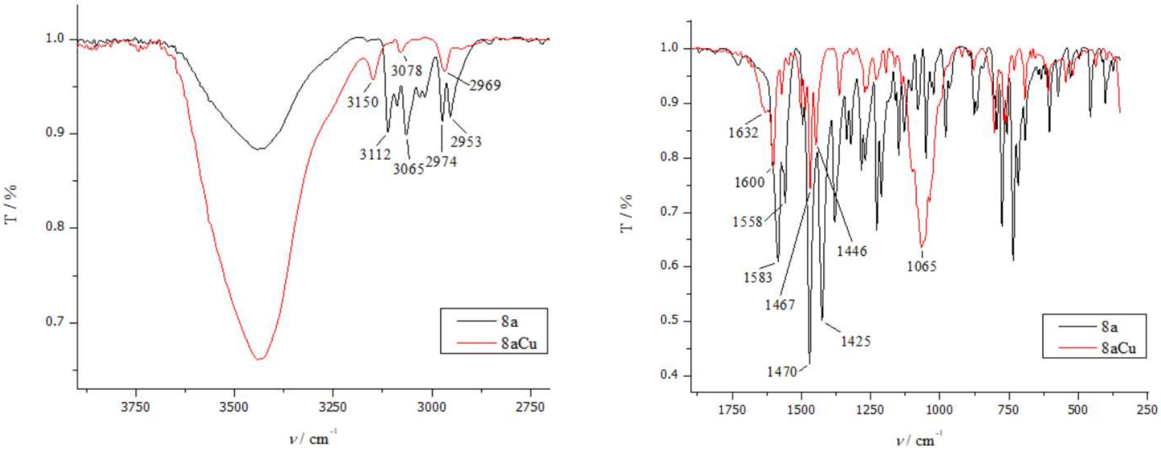

Figure S105. IR spectra of ligand **8a** and complex **8a$_{Cu}$**.

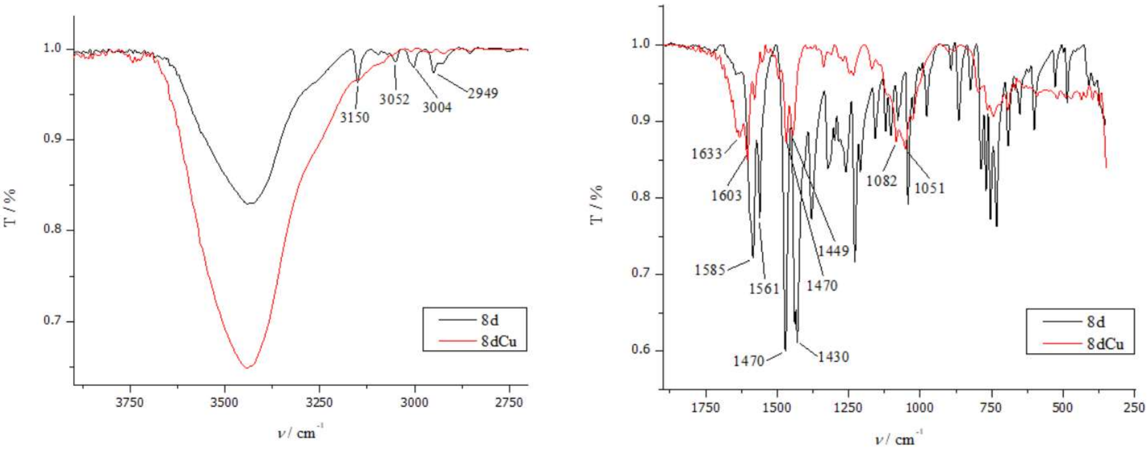

Figure S106. IR spectra of ligand **8d** and complex **8d$_{Cu}$**.

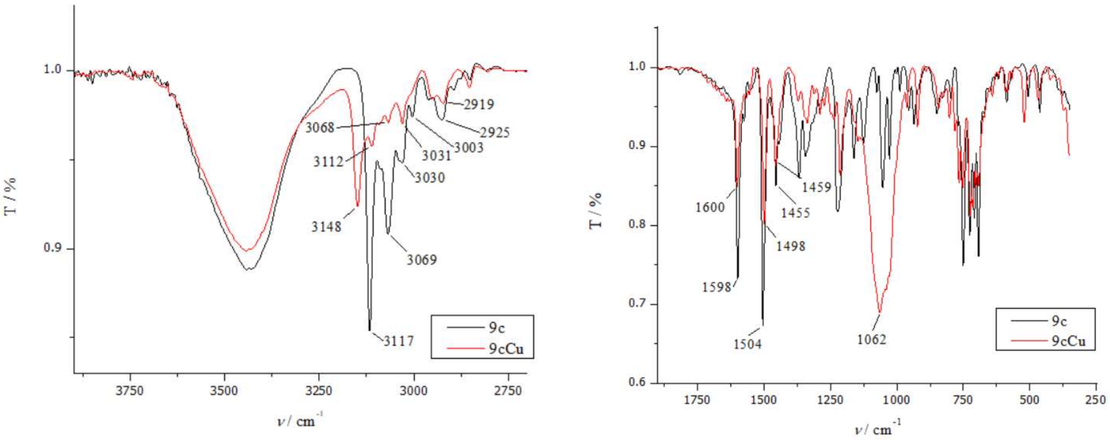

Figure S107. IR spectra of ligand **9c** and complex **9c$_{Cu}$**.

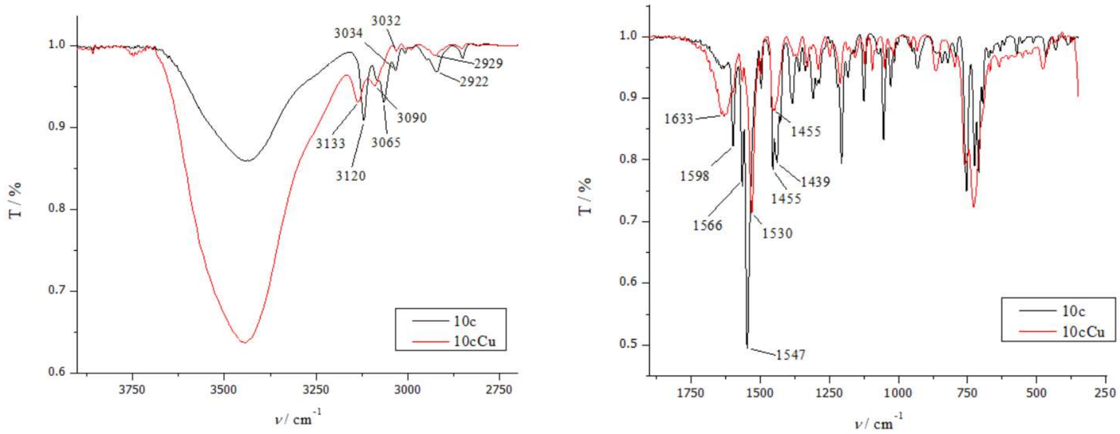

Figure S108. IR spectra of ligand **10c** and complex **10c$_{Cu}$**.

References

1 L. Farrugia, *J. Appl. Crystallogr.*, 2012, **45**, 849–854.

2 C. F. Macrae, I. J. Bruno, J. A. Chisholm, P. R. Edgington, P. McCabe, E. Pidcock, L. Rodriguez-Monge, R. Taylor, J. van de Streek and P. A. Wood, *J. Appl. Crystallogr.*, 2008, **41**, 466–470.

3 V. Rodríguez, J. M. Gutiérrez-Zorrilla, P. Vitoria, A. Luque, P. Román and M. Martínez-Ripoll, *Inorg. Chim. Acta*, 1999, **290**, 57–63.

4 X. You and Z. Wei, *Transit. Met. Chem.*, 2014, **39**, 675–680.